# Modeling of Chaotic Fluctuating Channels for Signal Detection

Cory Myers

June 1995

U.S. Army Research Office

Contract Number DAAL03–91–C–0052

Sanders, A Lockheed Martin Company
P.O. Box 868
Nashua, NH 03061

# DISCLAIMER NOTICE


**THIS DOCUMENT IS BEST QUALITY AVAILABLE. THE COPY FURNISHED TO DTIC CONTAINED A SIGNIFICANT NUMBER OF PAGES WHICH DO NOT REPRODUCE LEGIBLY.**

# Modeling of Chaotic Fluctuating Channels for Signal Detection

Cory Myers

June 1995

U.S. Army Research Office

Contract Number DAAL03–91–C–0052

Sanders, A Lockheed Martin Company
P.O. Box 868
Nashua, NH 03061

# REPORT DOCUMENTATION PAGE

Form Approved
OMB No. 0704-0188



| 1. AGENCY USE ONLY (Leave blank) | 2. REPORT DATE | 3. REPORT TYPE AND DATES COVERED |
|---|---|---|
| | June 1995 | Final 30 Sept 91 - 30 Apr 95 |

**4. TITLE AND SUBTITLE**

Modeling of Chaotic Fluctuating Channels for Signal Detection

**5. FUNDING NUMBERS**

DAAL03-91-C-0052

**6. AUTHOR(S)**

Cory Myers

**7. PERFORMING ORGANIZATION NAME(S) AND ADDRESS(ES)**

Sanders, A Lockheed Martin Company
P.O. Box 868
Nashua, NH 03061

**8. PERFORMING ORGANIZATION REPORT NUMBER**

**9. SPONSORING/MONITORING AGENCY NAME(S) AND ADDRESS(ES)**

U. S. Army Research Office
P. O. Box 12211
Research Triangle Park, NC 27709-2211

**10. SPONSORING/MONITORING AGENCY REPORT NUMBER**

ARO 29212.10-PH

**11. SUPPLEMENTARY NOTES**

The view, opinions and/or findings contained in this report are those of the author(s) and should not be construed as an official Department of the Army position, policy, or decision, unless so designated by other documentation.

**12a. DISTRIBUTION/AVAILABILITY STATEMENT**

Approved for public release; distribution unlimited.

**12b. DISTRIBUTION CODE**

**13. ABSTRACT** *(Maximum 200 words)*

This report summarizes the work performed under contract DAAL03-91-C-0052, "Modeling of Chaotic Fluctuating Channels for Signal Detection." In this work we developed algorithms for the modeling and analysis of nonlinear systems; we developed algorithms for the separation of signals from nonlinear systems from noise; we performed an acoustics propagation experiment; and we analyzed several datasets and identified the opportunity to collect some signifcant new data. During this work we published over sixty documents. A complete list of publications is included.

**14. SUBJECT TERMS**

Chaos, Nonlinear Systems

**15. NUMBER OF PAGES**

110

**16. PRICE CODE**

| 17. SECURITY CLASSIFICATION OF REPORT | 18. SECURITY CLASSIFICATION OF THIS PAGE | 19. SECURITY CLASSIFICATION OF ABSTRACT | 20. LIMITATION OF ABSTRACT |
|---|---|---|---|
| UNCLASSIFIED | UNCLASSIFIED | UNCLASSIFIED | UL |

# Table of Contents

# 1.0 Problem Statement

This report summarizes the work performed under the contract DAAL03–91–C–0052, "Modeling of Chaotic Fluctuating Channels for Signal Detection." This work was performed from July 1991 to April 1995.

The detection of signals propagated through a fluctuating medium is a significantly challenging problem and is of significant practical interest. The objective of this research was to investigate the tools and techniques used to model fluctuating propagation as nonlinear systems and to analyze propagation data in the context of a nonlinear systems model.

The objectives of this program were as follows:

- Develop signal processing algorithms and software applicable to the modeling and analysis of nonlinear system. We were to develop tools and techniques which had applicability to a range of nonlinear processing problems and to apply them both to the problem at hand, propagation of signals through a fluctuating medium, as well as to other problem which seemed to be amenable to these techniques.
- Develop signal detection algorithms which are well suited to the exploitation of nonlinear propagation and interference phenomenon. We were to develop signal processing algorithms which would allow us to exploit the nonlinear description of systems to extract information about signals of interest.
- Perform analyses of acoustic signals propagated through the atmosphere to determine if the propagation effects can be well modeled as a nonlinear system. We were to design a propagation experiment to collect air acoustics data to determine if propagation of signals in the real world could be modeled as the response of a nonlinear system.
- Identify new opportunities for the application of nonlinear processing to additional areas of interest. We were to investigate datasets of interest to identify new opportunities for the application of nonlinear modeling and processing.

# 2.0 Summary of Significant Results

During the course of this project we achieved significant progress against the four main objectives. Most of this work has been documented in published material and will be only summarized here.

## 2.1 Algorithms and Software for the Modeling and Analysis of Nonlinear Systems

As part of our contract work we have developed a wide range of algorithms for the analysis and modeling of nonlinear systems [3, 4, 8, 11, 12, 14, 22, 24, 41]. These tools include algorithms for the following:

- establishing the proper method data selection for modeling a data stream as the output of a nonlinear system;

- determining the proper embedding dimension of data for analysis as the output of a nonlinear system;
- quantitatively differentiating between the output of low dimensional nonlinear system and "noise";
- determining invariant characteristics, e.g. Lyapunov exponents, of a nonlinear system from its outputs; and
- building a predictive model of a nonlinear system which can be used for data extrapolation or for control of a nonlinear system.

The software for these algorithms has been made available to researchers worldwide through the University of California, San Diego and is being incorporated into "toolboxes" for use in standard signal processing packages such as Matlab.

## 2.2 Signal Detection Algorithms

As part of the contract work we developed algorithms for the separation of signals produced by low dimensional nonlinear systems from signal produced by noise sources [1, 2, 22, 24]. This work resulting in the development of algorithms which successfully merged classical signal processing techniques, such as the Cramer–Rao lower bound and the Viterbi algorithm, with nonlinear systems. With this work we developed the following significant results:

- Demonstration that the noise reduction potential for nonlinear systems is globally the same as the noise reduction potential for linear systems but the local properties of noise reduction in nonlinear systems is drastically different.
- The signal structure of a chaotic signal can be exploited by a signal detection algorithm which has been trained to the chaotic system of interest to provide a significant processing gain compared to a conventional colored noise detection system.

## 2.3 Analysis of the Propagation of Acoustic Signals

As part of our contract work we collected and analyzed acoustic propagation data from a real-world environment. The data collection experiment took place at the US Army White Sands Missile Range in White Sands, New Mexico in December 1992. In preparation for this experiment we defined a wide range of signals of interest for propagation through the atmosphere; we determined the proper sensor locations; we defined the data collection hardware and software that would be used; we coordinated with the Atmospherics Sciences Laboratory at White Sands to use some of their equipment; and we coordinated with another Sanders contract, this one to ARDEC, to jointly collect data (Appendix A).

The data was collected at White Sands over a period of three day in the morning, at midday, and in the evening for a total of ten separate data collections. Each collection contained sixteen channels of recorded data with each recording lasting between ten and thirty minutes. The sensor locations included an array of microphones on the ground as well as microphones placed on a tower at various elevations off the ground.

The collected data was analyzed through a number of nonlinear processing techniques to determine if any significant nonlinear structure could be found in the data (Appendix B). We were not able to identify any significant low dimensional nonlinear behavior in the data. Additionally, classical signal processing techniques were used to analyze the data and these demonstrated that the data was best modeled as simple direct path channel with random fluctuations on the propagation. The data is dominated by acoustic interfere due to acoustic sources in the area over which we had no control and by wind noise which significantly interferes with the measurement of the propagated signals.

## 2.4 Identification of Other Applications for Nonlinear Processing

Because of the lack of significant nonlinear behavior in the White Sands data, we expanded our data analysis work to include additional datasets. In this portion of the work we:

- examined wind tunnel data collected on a jeep at the NASA Langley wind tunnel;
- examined data collected by the Navy on a buoyant test vehicle [19];
- analyzed various climatic, laser, and fluidized bed data [various]; and
- developed an experimental plan to provide high quality air acoustic flow noise data [46].

The results of the wind tunnel data indicated that, at least for some sensors on the vehicle at some wind speeds, that nonlinear behavior was observed. Unfortunately the data analyzed here was collected under conditions which were not completely defined by the data we received. The buoyant vehicle experiment was much better instrumented and controlled. The results of the buoyant test vehicle experiment data clearly showed the transition from laminar to turbulent flow and regions of low dimensional behavior were observed. We took the work done here and extrapolated to define an experiment that could be performed for the propagation of air over a surface in a controlled environment and with a high resolution data acquisition system to develop a high quality data set which will demonstrate the transition from laminar to turbulent flow in air propagation and which may lead to insight into the mechanisms by which acoustical noise is generated by the wind.

# 3.0 List of Publications and Technical Reports

During the duration of this contract over sixty documents were prepared. The following documents were published under this contract:

[1] Myers, C., Singer, A., Shin, F., and Church, E., "Modeling Chaotic Systems with Hidden Markov Models", *Proc. ICASSP 1992.*

[2] Myers, C., Kay, S., and Richard, M. "Signal Separattion for Nonlinear Dynamical Systems," *Proc. ICASSP 1992.*

[3] Abarbanel, H. D. I., R. Brown, and M. B. Kennel, "Lyapunov Exponents in Chaotic Systems: Their Interpretation and their Evaluation using Observed Data", *International Journal of Modern Physics* **B5**, 1347-1375 (1991).

[4] Abarbanel, H. D. I., R. Brown, and M. B. Kennel, "Local Lyapunov Exponents from Observed Data", *Journal of Nonlinear Science* **2**, 343-365 (1992).

[5] Abarbanel, H. D. I. and A. Rouhi, "Symmetric Truncations of the Shallow Water Equations", *Physical Review E* **48**, 3643-3655 (1993).

[6] Abarbanel, H. D. I. and A. Rouhi, "Symmetry Preserving Truncations of Equations in Geophysical Fluid Dynamics", *Proc. of the Hawaiian Winter 'Aha Huliko'a Workshop*, (1991)

[7] Abarbanel, H. D. I., E. Church, D. Mook, and C. Myers, "Nonlinear Dynamical Descriptions of Flow Noise", Submitted Talk at the IUTAM *Symposium of Interpretation of Time Series from Mechanical Systems*, University of Warwick, England. August 25-30, 1991.

[8] Kennel, M. B., R. Brown, and H. D. I. Abarbanel "Determining Embedding Dimension for Phase Space Reconstruction Using a Geometrical Method", *Phys. Rev. A* **45**, 3403 (1992).

[9] Abarbanel, H. D. I. and K. Lindenberg, "The Making of an Institute: The INLS at UC-San Diego", *Nonlinear Science Today* **2**, 14-18, 23 (1992).

[10] Abarbanel, H. D. I. "Chaotic Signals and Physical Systems", Invited (and refereed) paper at the International Conference on Acoustics Speech and Signal Processing, March, 1992

[11] Abarbanel, H. D. I. and M. M. Sushchik, "True Lyapunov Exponents and Models of Chaotic Data", *Int. J. Bif. and Chaos*, **3**, 543-550 (1993).

[12] Abarbanel, H. D. I., R. Brown, J. J. ("Sid") Sidorowich, and Lev Sh. Tsimring, "The Analysis of Observed Chaotic Data in Physical Systems", *Reviews of Modern Physics* **65**, 1331-1392 (1993).

[13] Lam, B., H. D. I. Abarbanel, etc. "Observation of Chaotic Instabilities in the Active Mode-Locking of a Semiconductor Laser", *J. Optical Soc. America, B* **10**, 2065-2070 (1993).

[14] Abarbanel, H. D. I. and M. B. Kennel, "Local False Nearest Neighbors and Dynamical Dimensions from Observed Chaotic Data", *Phys. Rev. E*, **47**, 3057-3068 (1993).

[15] Abarbanel, H. D. I., Y. Boneh, M. Chu, J. Goldberg, and S. Koonin, "Dynamical Analysis of the Behavior of a Small Climate Model", to be submitted to *J. Atmos. Sci.*, Summer, 1993.

[16] Abarbanel, H. D. I., M. I. Rabinovich, and M. M. Sushchik, *Lectures in Nonlinear Dynamics for Undergraduate Physics Students*, published by **World Scientific Press**, June, 1993.

[17] Abarbanel, H. D. I., M. I. Rabinovich, N. Rul'kov, and A. Volkovskii, **Dynamical Chaotic Masking of Information Bearing Signals**, Patent applied for in March, 1993.

[18] Abarbanel, H. D. I., and Paul S. Linsay, "Secure Communications and Unstable Periodic Orbits of Strange Attractors", *IEEE Transactions on Circuits and Systems* **40**, 643-645 (1993).

[19] Abarbanel, H. D. I., J. Cembrola, T. Frison, T. Galib, and R. Katz, "Analysis of High Reynolds Number Flows over a Buoyant Axisymmetric Body", *Physical Review E* **49** 4003-4018 (1994).

[20] Abarbanel, H. D. I., J. Cembrola, T. Frison, T. Galib, and R. Katz, "Boundary Layer Chaos", *Physical Review Letters*, **72** 2383-2386 (1994).

[21] Abarbanel, H. D. I. "Analyzing and Utilizing Time Series Observations from Chaotic Systems", Invited General Lecture at the IUTAM Symposium on **Nonlinearity and Chaos in Engineering Dynamics**, London, July 19-23, 1993. John Wiley and Sons, *Nonlinearity and Chaos in Engineering Dynamics* 1993, pp 379-392.

[22] Abarbanel, H. D. I., T. Carroll, L. M. Pecora, J. J. Sidorowich, and L. Sh. Tsimring, "Predicting Physical Variables in Time Delay Embedding", *Physical Review E*, **49** 1840-1853 (1994).

[23] Abarbanel, H. D. I., "Nonlinearity and Chaos at Work", *Nature* **364**, 672-673 (1993). Invited Conference Review for the IUTAM Symposium on **Nonlinearity and Chaos in Engineering Dynamics**, London, July 19-23, 1993.

[24] Abarbanel, H. D. I., "Tools for Analyzing Observed Data", in *Stability, Vibration and Control of Structures*, ed. A. Guran and D. J. Inman. Kluwer Academic Publishers, Dordrecht, Netherlands. Invited Review Article, to appear Winter, 1995.

[25] Abarbanel, H. D. I., "Nonlinear Systems", *Encyclopedia of Applied Physics*, ed. G. L. Trigg, published by VCH Publishers in collaboration with the American Institute of Physics, the German Physical Society, the Japan Society of Applied Physics, and the Physical Society of Japan. **Volume II**, 417-439; November, 1994.

[26] Abarbanel, H. D. I., Invited Book Review for *Chaotic and Fractal Dynamics: An Introduction for Engineers and Applied Scientists* by F. C. Moon. To appear in *Foundations of Physics*, Winter, 1994.

[27] Lam, B., H. D. I. Abarbanel, etc. "Three Frequency Route to Chaos in a Mode Locked Laser", submitted to *J. Opt. Soc. Am. B*, Fall, 1993.

[28] Abarbanel, H. D. I., C. S. Daw, and W. F. Lawkins, "An Analysis of Fluidized Bed Data Using Techniques Based on Chaotic Nonlinear Dynamics Principles", to be submitted to *Phys. Rev. E*, Fall, 1994

[29] Kennel, M. B., H. D. I. Abarbanel, and J. J. ("Sid") Sidorowich "Prediction Errors and Local Lyapunov Exponents", submitted to *Physical Review E*, February, 1994.

[30] Abarbanel, H. D. I., J. M. Cembrola, R. A. Katz, and T. W. Frison, "Application of Nonlinear/Chaotic Processing of Signals-of-Interest", *Journal of Underwater Acoustics*, April, 1994

[31] Abarbanel, H. D. I., A. Garrett Lisi, A. Rouhi, and J. A. Wright, "Vortex Filament Stability and Boundary Layer Dynamics", *Physical Review E*, **50** 1206-1218 (1994).

[32] Rul'kov, N. F., L. Sh. Tsimring, and H. D. I. Abarbanel, "Tracking Unstable Orbits in Chaos Using Dissipative Feedback Control", *Physical Review E*, **50** 314-324 (1994)

[33] Abarbanel, H. D. I., M. I. Rabinovich, and Lev Sh. Tsimring, "`Crystals' and `Quasi-crystals' in Nonequilibrium Media", *Applied Nonlinear Dynamics* **2**, 5-23 (1994)--in Russian.

[34] Abarbanel, H. D. I., M. I. Rabinovich, and L. Sh. Tsimring, "Chaotic Fields: Chaos in Time and Space", submitted to *Physical Review E*, Fall, 1994

[35] Abarbanel, H. D. I., U. Lall, and T. Sangoyomi, "Nonlinear Dynamics of the Great Salt Lake: Nonparametric Short Term Forecasting", submitted to *Water Resources Journal*, June, 1994.

[36] Abarbanel, H. D. I., U. Lall, and T. Sangoyomi, "Nonlinear Dynamics of the Great Salt Lake: System Identification and Prediction", Fall, 1994.

[37] Abarbanel, H. D. I., N. F. Rul'kov, M. M. Sushchik and L. Sh. Tsimring, "Generalized Synchronization of Chaos in Directionally Coupled Chaotic Systems", to appear in *Physical Review E* **51**, February, 1995.

[38] Abarbanel, H. D. I., C. Liu, Z. Gills, and R. Roy, "Intrinsic Quantum Fluctuations in Chaotic Laser Dynamics", submitted to *Phys. Rev. Letters*, July, 1994.

[39] Abarbanel, H. D. I., Z. Gills, R. Roy, and C. Liu, "Quantum Fluctuations in the Operation of a Chaotic Laser", submitted to *Physical Review E*, January, 1995.

[40] Abarbanel, H. D. I., P. F. Rowat, and A. I. Selverston, "Nonlinear Dynamics of the Lobster Gastric Mill Central Pattern Generator", to be submitted Fall, 1994.

[41] Kennel, M. B. and H. D. I. Abarbanel, "False Strands and False Neighbors", to be submitted to *Physical Review E*, Winter, 1995.

[42] Abarbanel, H. D. I., N. F. Rul'kov, and M. M. Sushchik, "Blending Chaotic Attractors Using Chaotic Synchronization", submitted to *Physical Review Letters*, October, 1994.

[43] Abarbanel, H. D. I., T. Frison, and L. Sh. Tsimring, "Chaotic Methods for Image Processing", ICASSP, Detroit, MI, May, 1995.

[44] Abarbanel, H. D. I., T. Frison, R. Katz, and J. Cembrola, "Nonlinear Analysis of Environmental Distortions of Continuous Wave Signals in the Ocean", submitted to *J. Acoust. Soc. Am.*, November, 1994.

[45] Abarbanel, H. D. I. and Upmanu Lall, "Nonlinear Dynamics of the Great Salt Lake: System Identification and Prediction", submitted to *J. of Climate*, November, 1994.

The following material represents unpublished reports developed under this contract:

[46] Dingus, P., Lang, S., Myers, C., Nation, R., Abarbanel, H., "Basic Physics and Applications of Nonlinear Dynamics," submitted to ARO, April 1995.

[47] Abarbanel, H. D. I., "Eikonal approximation techniques in elastic scattering and production processes", Lecture Notes in Physics: Strong Interaction Physics, (Summer School Lectures at the Canadian School of Physics) (1973).

[48] Abarbanel, H. D. I., Gribov, V.N., and Kanchelli, O.V., "Couplings of the vacuum trajectory."

[49] Abarbanel, H. D. I., "Strongly mixed stationary turbulence", LBL Report (1979).

[50] Abarbanel, H. D. I., Grebogi C., and Kaufman, A., "Statistical analysis of a deterministic orbit", *Proc. Intl. Conf. on Plasma Physics* (1980).

[51] Abarbanel, H. D. I., Grebogi, C., and Kaufman, A. "Statistical analysis of a deterministic mapping", Report to the Plasma Physics Division of the APS, (1980).

[52] Abarbanel, H. D. I., Grebogi, C., and Kaufman, A., "Resonance diffusion in an eikonal field", Report to the Plasma Physics Division of the APS, (1980).

[53] Abarbanel, H. D. I., "Irreversibility and transport equations in nonlinear deterministic dynamics", Seventh West Coast Statistical Mechanics Conference, LBL-12683, (1981).

[54] Abarbanel, H. D. I., and Crawford, J.D., "Bifurcation theory and plasma instabilities", Report to the Plasma Physics Division of the American Physical Society (1982).

[55] Abarbanel, H. D. I., Brown, R., and Yang, Y.M., "Equations of State with Maximum Symmetry in Inviscid Fluids", (October, 1987).

[56] Abarbanel, H. D. I., Brown, R., and Yang, Y.M., "Symmetries and Conserved Quantities for Inviscid, Compressible Fluids in Two and Three Space Dimensions".

[57] Abarbanel, H. D. I., Brown, R., and Yang, Y.M., "Symmetries and Conserved Quantities for Inviscid, Compressible Fluids in One Space Dimension".

[58] Abarbanel, H. D. I. and Hjorth, P., "Surface Instability of a Driven Non-Newtonian Film Flow".

[59] Abarbanel, H. D. I. and J. B. Kadtke, "Information Theoretic Methods for Determining the Minimum Embedding Dimension for Strange Attractors".

The following represent material which is still under preparation but which was begun under this contract:

[60] Abarbanel, H. D. I., *Analysis of Observed Chaotic Data*, to be published by Springer-Verlag, Summer, 1995.

[61] Abarbanel, H. D. I., M. I. Rabinovich, and Lev Sh. Tsimring, *Spatio-temporal Chaos: Structures and Experimental Analysis* to be published by Springer-Verlag.

[62] Richard, M. D. and H. D. I. Abarbanel, "Estimating in Chaos: Cramer-Rao Bounds for Chaotic Time Series", UCSD/MIT Preprint, Spring, 1993. To be submitted to *Journal of Nonlinear Science*.

## 4.0 List of Participating Scientific Personnel

The work reported on in this contract was performed in cooperation of Sanders, under the direction of Dr. Cory Myers and at the University of California, San Diego under the direction of Professor Henry Abarbanel.

The following personnel from Sanders participated on this project:

Dr. Cory Myers
Dr. Steven Lang
Mr. Edward Real
Ms. Frances Shin
Mr. Andrew Singer (summer student from MIT)
Mr. Jeffery Ludwig (summer student from MIT)

The following personnel from the University of California, San Diego participated on this project:

Professor Henry Abarbanel
Dr. Matt Kennel (received his Ph.D. during the course of this project)
Dr. J. J. ("Sid") Sidorowich
Dr. L. Sh. Tsimring
Dr. Reggie Brown
Dr. Mischa Sushchik (will receive his Ph.D. this fall)

## 5.0 Inventions

No inventions were patented under this contract.

## 6.0 Bibliography

See the list of publications and technical reports in section 2.

## 7.0 Appendices

Enclosed are copies of material which was developed under this contract but which has not been previously published or submitted.

Appendix A – Experimental Plans – Documents describing the experimental setup for the White Sands data collection of December 1992. Included here is the associated data collection plan for the ARDEC data collection which shared facilities and equipment with our data collection.

Appendix B – Sanders Internal Data Analysis Reports – A collection of data analysis reports relating to the analysis of the White Sands data and to the NASA wind tunnel data.

# Appendix A

# Modeling of Chaotic Fluctuating Channels for Signal Detection

# Experiment Description

## 1 Objective

The objective of the proposed data collection is to provide high quality data sets that can be analyzed in our work for ARO under contract DAAL03-91-C-0052. The objective of the program is to apply recent developments in the area of nonlinear systems to the problem of detecting acoustic signals that have been propagated through the atmosphere. Our objectives are to extend our understanding of nonlinear systems, to apply the theory of nonlinear systems to the modeling of fluctuations in the atmosphere and their effects on the propagation of signals, and to develop processing approaches for the improved detection of signals as propagated through fluctuating channels.

The program is been performed jointly by the Signal Processing Center of Technology (SPCOT) at Lockheed Sanders, Inc. and the Institute for Nonlinear Science (INLS) at the University of California, San Diego (UCSD). SPCOT has extensive experience in the processing of acoustic signals, particularly for detection and classification. INLS has extensive experience in the theory of nonlinear systems and in applying these models to physical systems.

The particular objectives of the experiment are to provide high quality acoustic propagation data sets. We desire data that can be used to characterize the fluctuations in the atmosphere, how these fluctuations propagate, and how the transmission of signals are affected by these fluctuations.

## 2 Approach

We will transmit a number of waveforms from a speaker and measure the received waveforms at a number of locations. The types of waveforms that we will use include the following:

1. Tonals, i.e., waveforms consisting of a single frequency. We expect to use between five and ten different tonals in the frequency range from 20 Hz to 1 KHz. These waveforms will be used to characterize the time-varying behavior of the channel both in terms of amplitude and phase fluctuations.
2. Multi-tonals, i.e., waveforms consisting of multiple frequencies. We will combine the single tone waveforms to generate the multi-tone waveforms. These waveforms will be used to characterize the time-varying behavior of the channel and how fluctuations in at one frequency can be related to fluctuations at a different frequency.
3. Pulse trains. These waveforms will be used to simulate sources of potential interest. We will use both single period pulse trains and multiple period pulse trains. The fundamental frequency of the pulse trains will be between 10 Hz and 100 Hz.
4. Broadband modulated waveforms. These waveforms will allow time-varying mea-

surement of the channel impulse response. We will use modulated signals with frequency ranges from 20 Hz up to 1000 Hz.

Each waveform will be approximately a minute in duration and will be preceded with a standard header to mark it.

Measurements will be made at a number of ranges using both single microphones and microphone arrays. Most measurements will be made at ground level but additional measurements will be made using a microphone mounted on a tower. Measurements will be made morning, noon, and evening each of the days of the experiment. Most measurements will be made with a 500 Hz anti-aliasing filter and a 12 bit A/D convertor running at 2083.33 samples per second. A selected subset of measurements will be performed with a significantly higher sampling rate but using only a selected subset of the sensors.

In addition to measurements of the propagated signals we will take advantage of the setup to also record both background noise and wind noise. ASL will be collecting meteorological data, e.g., wind speed and direction, temperature, relative humidity, air pressure, and solar radiation, with one minute, five minute, and twenty four hour averages during the experiment.

## 3 Test Plan

Attachment A (ASSCE Test Plan: Acoustic Self Location) is the formal test plan for this data collection. This data collecting will be performed in conjunction with work performed under contract No. DAAA21-90-C-0017 for ARDEC. The work for ARDEC is to investigate acoustic self location and orientation using propane cannon sources. Our experiment will share the recording and data analysis equipment with the ARDEC work. We will use a speaker provided by ASL to provide calibrated waveforms, rather than the propane cannons.

The schedule for the experiment is as follows:

| Activity | Start Date | End Date |
|---|---|---|
| Arrive | Nov 30 | Nov 30 |
| Setup Equipment | Dec 1 | Dec 4 |
| Collect Data | Dec 7 | Dec 10 |
| Pack Equipment | Dec 11 | Dec 11 |

**Table 1: Test plan schedule.**

The speaker for the waveforms will be placed on the South Tower (page 4 of Attachment A) and sensors will placed at ranges of 500 feet, 1.5 km, 2 km, and 3 km. A circular array of eight sensors will be placed at 1 km, near the North Tower and microphone will be placed on the North Tower.

## 4 Planned Analysis

We will analyze the received data both in the field and in the laboratory. Analysis in the field will be to verify data quality and to allow a quick look. In the field we will perform the following analyses:

1. Signal to noise ratio analysis to verify data quality.
2. Spectral analysis to quantify basic signal propagation characteristics.
3. Channel impulse response extraction to get a quick look at the channel characteristics.

Laboratory analysis will focus on the use of nonlinear systems modeling techniques, including:

1. Mutual information analysis to determine the proper time delay for subsequent analysis.
2. Time-delay embedding and state space reconstruction. These techniques are used to determine if the data can be modeled as a low dimensional nonlinear system. Measurements of the time-varying amplitude and phase response of the channel and of the time-varying impulse response will be used.
3. Hidden Markov Models as a method for signal detection in fluctuating channels. We will train signal detectors based on observed characteristics and test these detectors to determine their ability to enhance signal detectability.

Analyses will be correlated with environmental conditions with direction of arrival (for the circular array) and with distance from the source.

# Modifications to ASSCE Test Plan

## 1 Sensor Locations

The specifications in the ASSCE test plan call for two circular arrays and eight ground sensors. The following modifications are made to the ASSCE Test plan regarding the location of sensors for the ARO data collection:

- The circular array located near the North Tower will be used.
- The eight ground based sensors will be used.
- The circular array located near the South Tower will be used but is only of secondary interest. If the circular array at the North Tower fails then the circular array from the South Tower can be used as a replacement.
- Three microphones will be placed on the North Tower at heights of approximately 30, 60, and 90 feet. These microphones will be mounted inside styrofoam to reduce wind noise.

## 2 DAPS Channel Assignments

During the recording of the ARO datasets the channel assignments on the North Tower DAPS will be changed as follows:

| Channel | Group 1 Sensor | Group 2 Sensor |
|---|---|---|
| 0 | 8 foot array 0 | remote 0 - 3 km |
| 1 | 8 foot array 1 | remote 1 - 2 km |
| 2 | 8 foot array 2 | remote 2 - 1.5 km |
| 3 | 8 foot array 3 | remote 3 - 1 km |
| 4 | 8 foot array 4 | remote 4 - 500 ft |
| 5 | 8 foot array 5 | tower 0 - 30 feet |
| 6 | 8 foot array 6 | tower 1 - 60 feet |
| 7 | 8 foot array 7 | tower 2 - 90 feet |

**Table 1: DAPS channel assignments.**

This change implies that channels 5, 6, and 7 of Group 2 will be changed from remote 5, 6, and 7, used in the self-localization tests to tower microphones used in the propagation tests.

## 3 Test Setup

In addition to the test setup specified in the ASSCE plan we will make the following additions:

- Day 2 - test ASL speaker connections and playback

- Day 3 (after DAPS) setup - test propagation. A special test setup tape will be prepared and the recorded DAPS waveforms will be examined in the field and FedEx to Lockheed Sanders for analysis.

## 4 Recording Conditions

The default recording conditions will be with a 500 Hz low pass filter (eight order Butterworth) and a sampling rate of 2083 Hz (same as for the self-localization experiments). If a selectable low pass filter is made available in time for the test then alternative selections will be specified according to the capabilities of the filters.

## 5 List of Waveforms

Each waveform to be transmitted will consist of the following format:

| Description | Center Frequency (Hz) | Duration (seconds) |
|---|---|---|
| 13 chip Barker code | 100 | 0.1 |
| 13 chip Barker code | 200 | 0.1 |
| 13 chip Barker code | 300 | 0.1 |
| 13 chip Barker code | 400 | 0.1 |
| Silence | 0 | 0.5 |
| 13 chip Barker code | 250 | 0.1 |
| Five bit waveform id | 250 | 0.5 |
| 13 chip Barker code | 250 | 0.1 |
| Silence | 0 | 1.0 |
| Data | variable | variable |
| Silence | 0 | 10.0 |

**Table 2: Basic waveform formating.**

The first four Barker codes are used to generate a timing mark. The total bandwidth of the signal used for the timing mark is approximately 500 Hz so the timing resolution will be approximately 0.002 seconds. The waveform id sequence will consist of five, 0.1 second duration segments, each of which will either contain a 13 chip Barker code or silence. This id capability will provide for up to 32 distinct waveforms. The total duration of the header and the silence segments is 12.6 seconds. The data sequences are as follows:

| ID | Class | Description | Duration (seconds) |
|---|---|---|---|
| 0 | Silence | Silence | 60 |
| 1 | Tone | 20 Hz | 60 |

**Table 3: Waveform descriptions.**

| ID | Class | Description | Duration (seconds) |
|---|---|---|---|
| 2 | Tone | 40 Hz | 60 |
| 3 | Tone | 60 Hz | 60 |
| 4 | Tone | 80 Hz | 60 |
| 5 | Tone | 100 Hz | 60 |
| 6 | Tone | 150 Hz | 60 |
| 7 | Tone | 200 Hz | 60 |
| 8 | Tone | 300 Hz | 60 |
| 9 | Tone | 400 Hz | 60 |
| 10 | Tone | 500 Hz | 60 |
| 11 | Multi-tone | 20 Hz and 40 Hz | 60 |
| 12 | Multi-tone | 20 Hz and 80 Hz | 60 |
| 13 | Multi-tone | 40 Hz and 80 Hz | 60 |
| 14 | Multi-tone | 100 Hz and 150 Hz | 60 |
| 15 | Multi-tone | 100 Hz and 200 Hz | 60 |
| 16 | Multi-tone | 100 Hz and 300 Hz | 60 |
| 17 | Multi-tone | 100 Hz and 400 Hz | 60 |
| 18 | Multi-tone | 100 Hz and 500 Hz | 60 |
| 19 | Pulse Train | Fundamental = 15 Hz | 60 |
| 20 | Pulse Train | Fundamental = 30 Hz | 60 |
| 21 | Pulse Train | Fundamental = 65 Hz | 60 |
| 22 | Multi-Pulse Train | Fundamentals = 15 Hz and 65 Hz | 60 |
| 23 | Multi-Pulse Train | Fundamentals = 30 Hz and 65 Hz | 60 |
| 24 | QPSK Modulation | Baud Rate = 50 Hz, Center Frequency = 250 Hz | 60 |
| 25 | QPSK Modulation | Baud Rate = 100 Hz, Center Frequency = 250 Hz | 60 |
| 26 | QPSK Modulation | Baud Rate = 250 Hz, Center Frequency = 250 Hz | 60 |
| 27 | QPSK Modulation | Baud Rate = 50 Hz, Center Frequency = 100 Hz | 60 |
| 28 | QPSK Modulation | Baud Rate = 100 Hz, Center Frequency = 100 Hz | 60 |
| 29 | QPSK Modulation | Baud Rate = 50 Hz, Center Frequency = 400 Hz | 60 |
| 30 | QPSK Modulation | Baud Rate = 100 Hz, Center Frequency = 400 Hz | 60 |

**Table 3: Waveform descriptions.**

All signals will be generated at a 2083.33 Hz sampling rate and low pass filtered with a 800 Hz

low pass filter prior to digitization.

The play list for data collection will be as follows:

| Segment Number | Waveform ID |
|---|---|
| 1 | 0 |
| 2 | 8 |
| 3 | 11 |
| 4 | 12 |
| 5 | 13 |
| 6 | 14 |
| 7 | 15 |
| 8 | 16 |
| 9 | 17 |
| 10 | 18 |
| 11 | 19 |
| 12 | 20 |
| 13 | 21 |
| 14 | 22 |
| 15 | 23 |
| 16 | 24 |
| 17 | 25 |
| 18 | 26 |
| 19 | 27 |
| 20 | 28 |
| 21 | 29 |
| 22 | 30 |
| 23 | 8 |
| 24 | 0 |

**Table 4: Data collection play list.**

The play list for the special test tape will be as follows:

| Segment Number | Waveform ID |
|---|---|
| 1 | 0 |

**Table 5: Test tape play list.**

| Segment Number | Waveform ID |
|---|---|
| 2 | 1 |
| 3 | 2 |
| 4 | 3 |
| 5 | 4 |
| 6 | 5 |
| 7 | 6 |
| 8 | 7 |
| 9 | 8 |
| 10 | 9 |
| 11 | 10 |
| 12 | 0 |

**Table 5: Test tape play list.**

CDRL A012

# ASSCE Test Plan:
# Acoustic Self-Location
Support of ARDEC at White Sands Missile Range


prepared by

M. Rollender

Lockheed Sanders

95 Canal Street
Nashua, New Hampshire 03061


for

US Army AMCCOM
Picatinny Arsenal, New Jersey

10 September 1992


Contract No. DAAA21-90-C-0017

## Abstract

This plan describes the objectives, procedures, equipment, schedule, and level of effort needed to gather experimental data for investigating acoustic self-location and self-orientation using propane cannon sources. Another experiment that will be performed concurrently, is the ARO experiment which is designed to collect propagation data using speaker sources. The purpose of the ARO experiment is to generate practical models for the spatially and temporally varying acoustic channel in the desert environment. Raw data will be recorded in a field test environment near the DIRT Site at White Sands Missile Range. This data will be used to demonstrate self-location algorithms in the Lockheed-Sanders SPCOT laboratory at a later date.

# 1 Objective

The fundamental objective of this exercise, comprised of a field test, is to gather data to be used to demonstrate self-location algorithms which demonstrate the ability to eliminate the requirement for beamformer calibration, self-righting, north-seeking, and position location capabilities in each node of a distributed acoustic sensor system. The development of such a technique could impact systems such as WAM, netted mines, and distributed acoustic sensors, by reducing the size, weight, and cost of each node through the elimination of self-righting capability, compasses, and position electronics.

This self-location objective will be met by the following: Collection of data during a field experiment from both circular sensor arrays and remotely located sensors, including ambient noise levels and impulsive blasts with at least four impulsive cannons placed at different locations in the test area.

The objective of the ARO experiment will be met by the following: Collection of data at various times of the day that will consist of synthetic signals including harmonically related tones and broadband signals. These signals will be broadcast from the Servo-drive speaker/amplifier system that is mounted in the South Tower. The signals will be broadcast for no longer than 15 minute durations at intervals in the morning, midmorning, noon, and midafternoon.

Whenever possible, a Sun workstation will be used to perform analysis on the data and also to exercise the demo algorithms.

# 2 Approach

The data collection exercises will be performed outside in a field test situation. The test will be performed at the DIRT Site at the White Sands Missile Range, near the Orogrande Range Camp.

## 2.1 Field Test

The test will consist of recording a series of signature measurements made up of ambient noise and impulsive noise from cannons. Up to five single microphones (remote sensors) will be located along a straight line north and south of the DAPS located at the North tower. One of these single sensors will be placed near the circular array at the North tower site. Additionally, three remote sensors will also be located along a parallel line 2km to the west. All the sensors will be connected to the DAPS via field wire. This field wire will be supplied by ARDEC. Additionally, ARDEC will provide a field wire laying apparatus that is man portable and/or a field wire laying kit that attaches to the HMMWV. ARDEC will also provide a kit that enables the field wire to be rolled up at the conclusion of the test, if required. ASL wil provide a HMMWV and will investigate any permissions required to drive the vehicle both on and off road in the general area.

A speaker will be placed in the South tower for the ARO experiment. A second DAPS with a circular array will also be located at the South tower.

With respect to the ARO experiment, an acoustic source (loud speaker) will be placed on the South MET tower approximately 100 feet above ground. A series of acoustic sensors will be placed on the ground at varying distances along the direct path of the speaker: a single sensor at 500 ft, an eight channel array at 1km (near the North tower), and single sensors at 1.5km, 2km and 3km. All of the sensors for this part of the experiment will be connected to the DAPS at the North tower. Synthetic signals including harmonically related tones and broadband signals will be broadcast from the speaker, and recorded at each of the sensor locations. These data will then be verified on a portable workstation in the field.

### 2.1.1 Array Data Collection

The equipment for this part of the test will be arranged as in Figure 1. Each DAPS will support up to two groups, each consisting of eight channels divided up as appropriate between primary and remote microphone sensors. The Desert DAPS will be located at the North tower and will support a circular array and eight remote arrays. The TDOA DAPS will be located at the South tower and will support the circular array. In order to make future processing of data from a given DAPS easier, only sensors of one type (either high or low gain) will be used in the test.

### 2.1.2 Test Conduct

The test will be conducted at the White Sands Missile Range, NM during the time period November 30, 1992 to December 12, 1992. The test is scheduled to last for eleven days. The first day will be for equipment transportation to the field test site from the freight receiving area. The next four days will be for equipment setup and checkout. The following four days will be for data collection, and the last day will be for equipment tear-down and transportation back to the shipping location. The ARO experiment will be conducted at various times throughout the day as needed. The collected data will be checked for data integrity during the test with the assistance of the Sun workstation. The data will be sorted and annotated to maximize future usability. The following sections give detailed information on each of the stages of the field test.

**Test Equipment Transportation/Setup** This portion of the field test will be accomplished in five days. Day one will consist of transporting the equipment out to the test site. A U-Haul truck or another appropriate vehicle will be rented for a day to transport the material from the air freight terminal in El Paso to the test range. The day will be spent unpacking the equipment from the shipping containers, loading it onto the vehicle, driving out to White Sands, NM, and then unloading the equipment into the equipment/personnel trailer. A fork lift to unload the boxes from the truck will

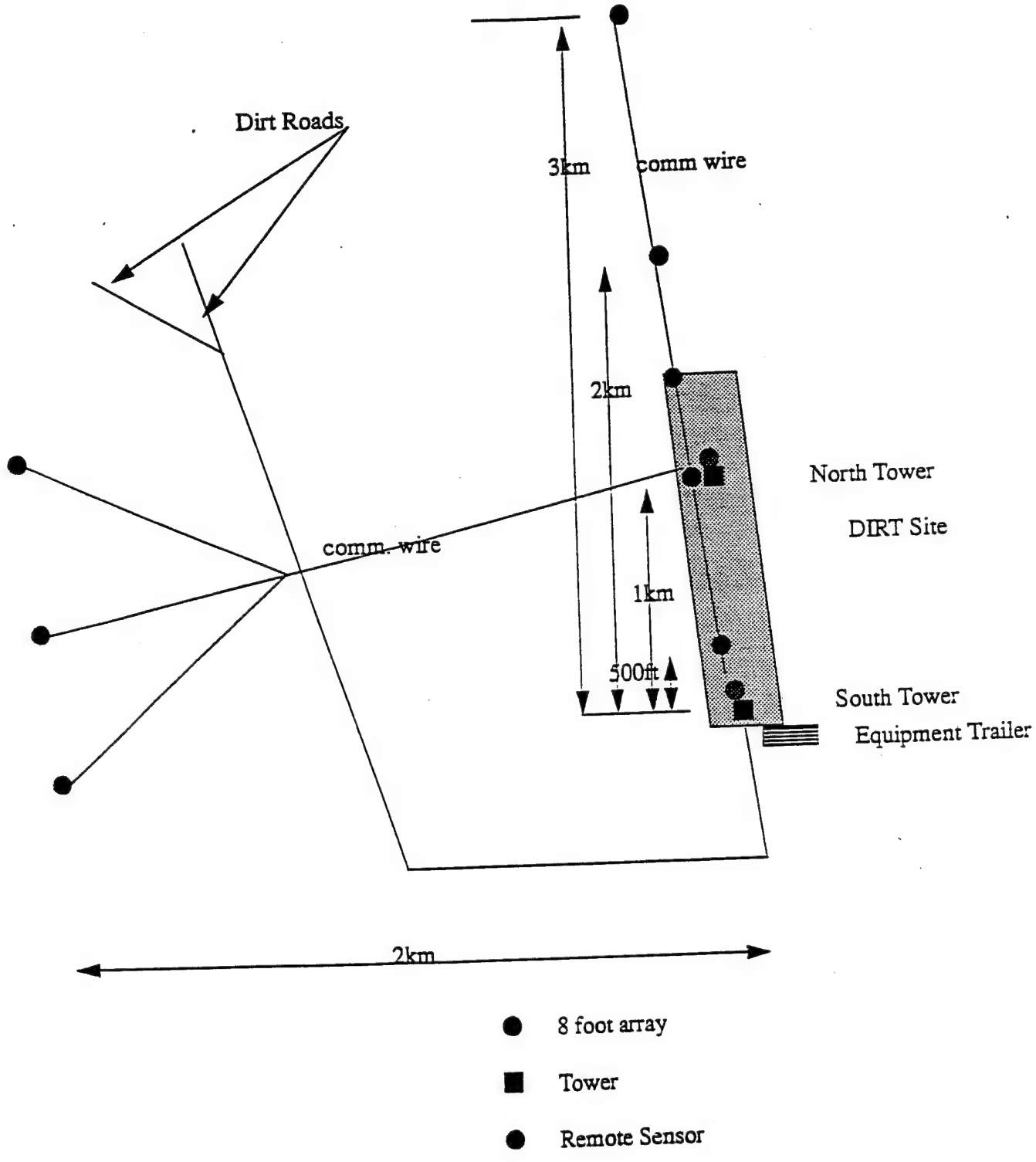


Figure 1: General Site Setup

be required during setup. One will also be required during teardown and shipment of material back to the freight terminal.

The following four days will be used to setup and checkout the equipment at the field test site. The workstation will be set up in the equipment trailer. Also, the circular arrays which will be located at the North and South Towers will be constructed. A significant task in terms of time will be that of laying out the remote sensor field wire. The ends of the field wire will be finished with XLR three conductor type connectors (if the connectors have not already been attached - plug on one end and a socket on the other end). The sensors that will be placed in the path of the speaker propagation (along the North/South Tower line) will be laid out next to the dirt road with the assistance of a vehicle. The remote sensor cables on the line located 2km away and parallel to the North/South Tower line will also be laid out with the assistance of a cross-country vehicle, if one is available. Trenche(s) will be dug in the dirt road where necessary to prevent damage to the field wire due to road traffic.

Also, during the setup stage both the remote and circular array sensor locations will be surveyed and recorded. This will be performed with the aid of a laser transit/range-finder and also a differential GPS. The speaker and amplifier system will be mounted up in the tower by ASL, along with the remote sensor that is to be positioned in the tower. Once setup is completed, a system check-out will be done, including verification of remote sensors, local sensors, DAPS, Sun workstation, speaker system, and propane cannons. See the Appendix for a more detailed schedule of the test setup and data collection.

The DAPS units will be stored in the test trailer at night and the arrays will be wrapped in weatherproof tarps and stored underneath the trailer. The remote sensors will be also be housed in the trailer at night as well, however, the field wire cabling will be left out for the duration of the experiment.

**Recording Assignments** Tables 1 and 2 give sensor position/DAPS recording assignments. These recording assignments may change due to circumstances of the test as required.

**Ambient Noise Data Collection** This portion of the test is designed to record a series of noise level measurements of the environment. The DAPS will be used as the recording device. The data will be collected to provide a baseline to verify proper operation of later portions of the experiment. Ambient noise measurements will be recorded throughout the test to provide data under various propagation conditions.

**Impulsive Event Data Collection** This portion of the test is designed to record a series of impulsive events from the orchard cannons. These cannons will be placed at locations within the test site and their locations will be determined via the laser range-finder and differential GPS. Acoustic recordings will be made with all of the cannons firing at a known average rate, but not synchronized in any way. This portion of the

Table 1: North Tower DAPS

| Group1 Channel # | Sensor |
|---|---|
| 0 | 8 foot array 0 |
| 1 | 8 foot array 1 |
| 2 | 8 foot array 2 |
| 3 | 8 foot array 3 |
| 4 | 8 foot array 4 |
| 5 | 8 foot array 5 |
| 6 | 8 foot array 6 |
| 7 | 8 foot array 7 |
| Group2 Channel # | Sensor |
| 0 | remote 0 3km |
| 1 | remote 1 2km |
| 2 | remote 2 1.5km |
| 3 | remote 3 1km |
| 4 | remote 4 500ft |
| 5 | remote 5 2km west |
| 6 | remote 6 2km west |
| 7 | remote 7 2km west |

Table 2: South Tower DAPS

| Group1 Channel # | Sensor |
|---|---|
| 0 | 8 foot array 0 |
| 1 | 8 foot array 1 |
| 2 | 8 foot array 2 |
| 3 | 8 foot array 3 |
| 4 | 8 foot array 4 |
| 5 | 8 foot array 5 |
| 6 | 8 foot array 6 |
| 7 | 8 foot array 7 |

Table 3: Test/Schedule Cross-Reference

| | |
|---|---|
| Test 1 | Baseline AM |
| Test 2 | Baseline PM |
| Test 3 | Angular Resolution AM |
| Test 4 | Angular Resolution PM |
| Test 5 | Ranging Resolution AM |
| Test 6 | Ranging Resolution PM |
| Test 7 | Small Constellation AM |
| Test 8 | Small Constellation PM |
| Test A | TBD |
| Test B | TBD |

experiment will take approximately four days. Daily maintenance will be performed on the remote power supplies as is needed.

A number of different configurations will be used as data collection scenarios. Data will be collected for as many of these scenarios as is possible. The initial configuration will serve as a baseline configuration and will utilize as many of the sensors as possible. Data will be collected in the baseline configuration over a several hour period. including morning and evening if possible, to provide comparisions on performance under various climactic conditions. Another configuration will be set up to test the resolving capabilities of the array for varied spacing between the sources. The sensor arrangement will be similar to the baseline test, but the sources will be placed at increasing distances. A similar test will be run to investigate ranging resolution of the system. The sources will be placed as increasing distances in a linear fashion outside of the sensor area and data will be gathered. If time permits, the non-collinear sensors will be moved closer together to investigate the effects of a closer constellation of sensor elements. For this experiment, the source arrangement from the angular resolution test will be utilized.

The baseline sensor/cannon arrangement is shown in Figure 2. The sensor/cannon angular resolution test arrangement is shown in Figure 3. The sensor/cannon setup for the ranging configuration is shown in Figure 4, and the setup for the small constellation is shown in Figure 5. Table 3 shows a cross-reference between the test configuration and the test scedule. Note that optional tests A and B will be determined during the test and will either be used to collect data in one of the previously mentioned configurations or will be used to collect data in a configuration which may be desirable due to particular topographical irregularities at the test site.

**ARO Data Collection** The ARO experiment, which will be performed concurrently, is designed to collect propagation data using a speaker source. The purpose of this experiment is to generate practical models for the spatially and temporally varying acoustic

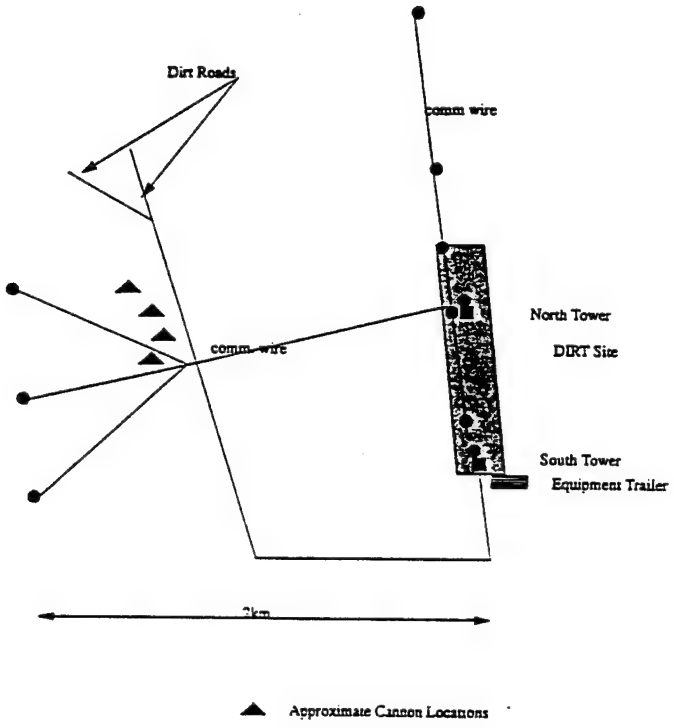


Figure 2: Baseline Configuration

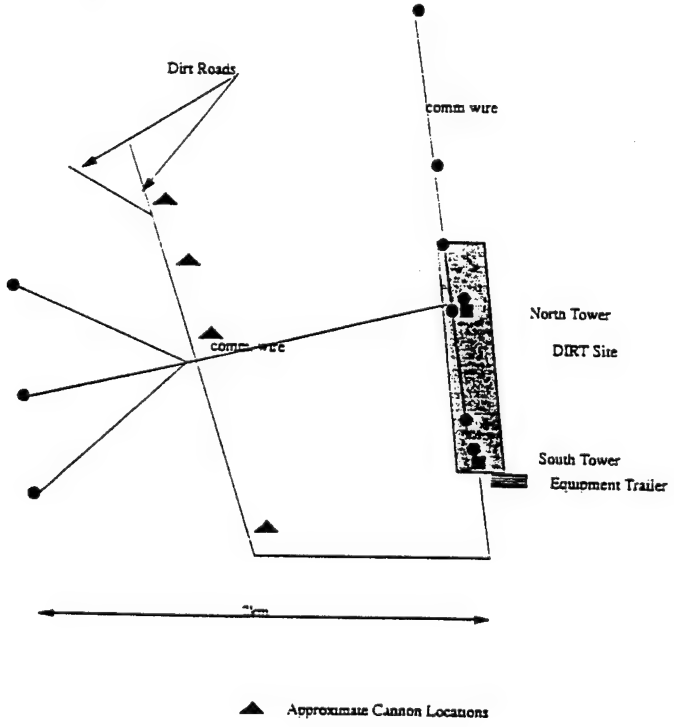


Figure 3: Angular Resolution Configuration

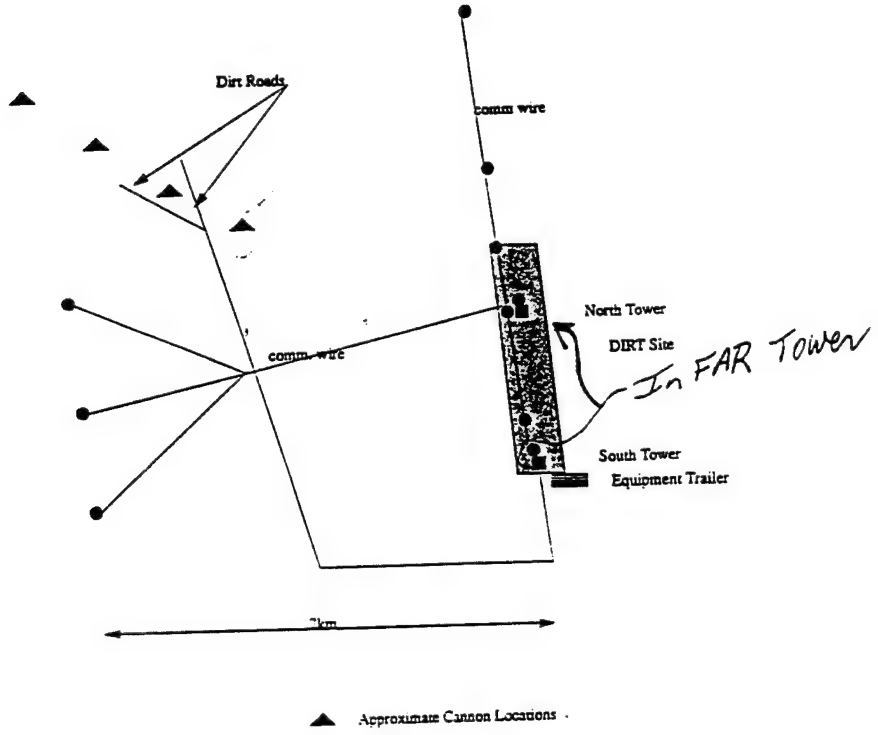


Figure 4: Ranging Resolution Configuration

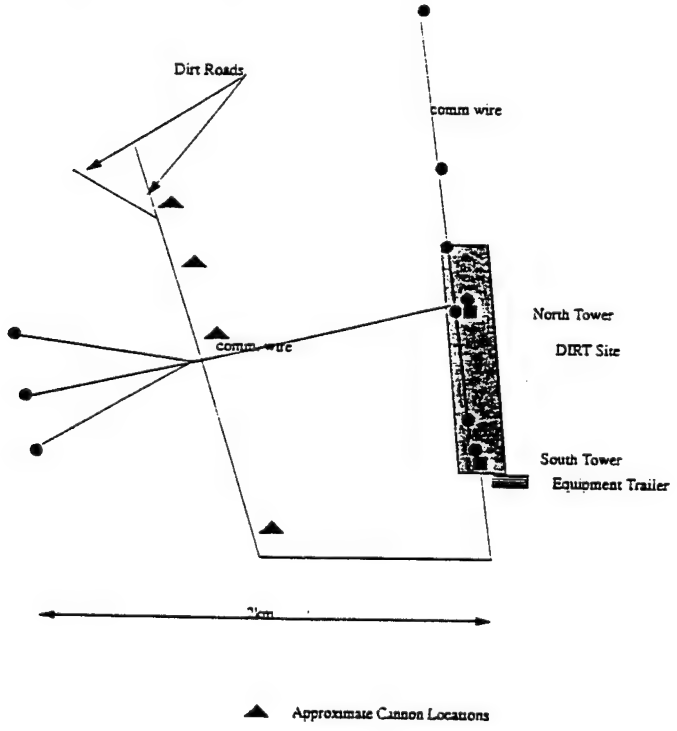


Figure 5: Small Constellation Configuration

channel in the desert environment.

Data will be collected at various times of the day and will consist of synthetic signals including harmonically related tones and broadband signals. These signals will be broadcast from the Servo-drive speaker/amplifier system that is mounted in the South Tower. The signals will be broadcast for no longer than 15 minute durations at intervals in the morning, midmorning, noon, and midafternoon. Time permitting, these scenarios will be recorded over the course of more than one day of the test. The propane cannons will need to be turned off/on during these propagation tests.

This experiment will run for the duration of the self-location test, and the time of day when the synthetic signals will be broadcast may be modified as appropriate to coincide with down-time of the other experiment. The sensor configuration to be used will be the same as the baseline sensor configuration used in the impulsive data collection exercises.

**Test Cleanup** This portion of the test will take approximately one day. The DAPS equipment, circular arrays, and remote sensors will be gathered up and returned to the site trailer. The equipment will then be boxed up and returned to the shipping site in El Paso. Again, a U-Haul type vehicle will be rented to transport the material to the air freight terminal.

### 2.1.3 Test Personnel

The following personnel are required to run the test. A brief description of their duties is listed below.

**Test Coordinator** Responsible for the overall implementation of this test plan and coordination of the various aspects of this test. Makes decisions as required for running the tests. Will also assist in data collection exercises as well as set-up and tear down.

**DAPS Equipment Operator/Scribe - 2** Responsible for the operation of the DAPS unit. Ensures that the unit is operating properly prior to start of the test, and maintains it during the test. Records the configuration of the system at test time (channels, sampling rates, etc). Makes sure that recording tapes are properly loaded and labeled. Makes sure system clock is properly synchronized and set. Records information in the log book including the following:

(a) *Impulse Times* - Records the time that the impulsive events were heard at the DAPS.

(b) *Interference* - Records when any interference (i.e. vehicles, planes, helos, etc.) are present in the test area.

(c) *Start/Stop Times* - Record the start and stop times of each portion of the experiment and any pertinent details associated with each data collection phase.

(d) *Location* - Record the location of all remote and local sensors.

(e) *Other* - Record any other pertinent information.

All personnel at the site will assist in setup and maintenance of the data collection and signal source equipment. This includes daily setup of the propane cannons, microphone arrays, recording units, remote microphone power supplies, etc. As time permits, the test personnel will perform analysis on the data that has been collected. This data analysis will be performed on the Sun workstation and will be used to provide feedback as to proper system operation and configuration.

# 3 Description of Equipment

## 3.1 DAPS

The main instrumentation recorder to be used in this test is Sanders' Digital Acquisition and Processing System (DAPS) developed by the NCTR lab. Two DAPS units will be used, a 24Vdc "desert DAPS" configuration and a DAPS in the TDOA configuration. In the field test, the Desert Daps will be connected to the remote sensors and an eight element circular array located at the North tower. The TDOA DAPS will be connected to an eight element circular array located at the South tower.

Two analog modules (housed in the VME chassis) provide the anti-aliasing filters for each channel prior to digitization by the DAPS. The DAPS is controlled by a Motorola 68020 CPU and is able to store up to 2 Gbytes of signal information at a rate of 200 Kbytes/second. The storage medium is 8 mm video cassette tape.

The DAPS records a time stamp on the data from its own time of day clock. Since the microphones are on different groups but are recorded with the same DAPS, a 0.5 second ambiguity in synchronization may exist. Written data will provide annotation of the tests. An oscilloscope may be used to check the integrity of the sensor data in the field.

## 3.2 Signal Sources

For generation of the impulsive noise signals, up to five artillery noise-makers will be used. Four of these systems will be provided by the Signal Processing Center of Technology, Lockheed-Sanders. ASL will provide units as necessary to function as additional impulsive noise sources and also to serve as replacement units in the event that spares are needed.

For generation of the synthetic harmonically related tones and broadband signals, a high power speaker system will be used in conjunction with a tape deck. ASL will supply the Servo-drive speaker and the high power amplifier, while Lockheed-Sanders will provide the tape deck and pre-recorded synthetic signals. ASL will provide the harness for mounting the speaker in the tower as well as assistance mounting the speaker

system in the South Tower. Lockheed-Sanders will need access to the speaker system at various times throughout the test.

## 3.3 Radio Communications

Lockheed-Sanders will bring two hand-held radios to the DIRT site area for communications both during site setup and during test exercises (11/30/92 to 12/11/92). These radios operate at 158.280MHz and 153.395MHz and are Licensed by the FCC for operation in the US. The emission designator for these radios is 20K0F3E. The call letters for these radios are WNMU754 and WRP698, respectively.

## 3.4 Surveying Tools

ASL will provide a Laser Transit for surveying the sensor locations and the cannon locations. ASL will also provide assistance in surveying these points during setup as well as well as any intermediate survey points required, if the Laser Transit's effective survey range is shorter than the distance from the reference point to the sensor and/or cannon locations. If additional points need to be surveyed during the data collection portion of the experiment, either ASL personnel or Lockheed-Sanders personnel will perform the site survey with the Laser Transit. Up to twelve cannon locations and twelve sensor location will need to be surveyed.

Lockheed-Sanders will provide 2 portable GPS systems to survey points in a pseudo-differential GPS mode. This surveying will be done independently from the surveying that is performed with the Laser Transit and is intended to verify the survey points of the Laser Transit.

## Appendix A: Equipment list

(1) 24Vdc Digital Acquisition and Processing System (Desert DAPS)
(1) 24Vdc Digital Acquisition and Processing System (TDOA)
(1) Power Supply for TDOA
(4) 12 Volt Deep Cycle Marine Batteries
(2) Portable GPS
(4) M-4 Single Detonation Cannon
(1) RF Modem
(1) Set Battery Connectors
(2) Exabyte Tape Drive in External Shoebox
(1) Exabyte Tape Drive (spare)
(2) Random Console terminal with charging cable
(1) Compass
(1) Sensor Calibration Kit
(1) Tape Deck to play synthetic signals
(2) Servodrive speaker and associated amplifier (Gov't. Supplied)
(1) Speaker Harness for tower mounting
(1) South Tower
(30) Countryman Microphones
(25) Single Sensor Windscreens
(2) 1'x.5'x.25' styrafoam squares (wind screen for tower mounted microphone)
(2) 2' Velcro mounting straps (for tower mounted microphone)
(2) 3"(approx) pipe clamps (for tower mounted microphone)
(1) 120' DAPS-microphone cable (for tower mounted microphone)
(2) 8' Circular Arrays and construction hardware
(4) Junction Boxes
(8) Remote Sensor Phantom-Power Supplies
(150) 9 Volt Batteries for Remote Sensor Power Supplies
(3) 2km Rolls of Field Wire
(2) 1km Rolls of Field Wire
(1) 1.5km Roll of Field Wire (ARO)
(1) 2km Roll of Field Wire (ARO)
(1) 3km Roll of Field Wire (ARO)
(2) 0.5km Rolls of Field Wire
(1) 150' Roll of Field Wire
(1) Field Wire Repair Kit
(1) Cable Laying Apparatus
(3) Boxes 8mm Data Tapes
(1) Battery Recharger
(12) Propane Tanks
(2) Pairs earmuffs
(1) Adjustable Ladder

(5) Weatherproof Tarpaulins
(1) SparcStation SLC with 8mm tape drive and external hard disk
(2) P-100 Hand-Held Radios and rechargers
(1) Oscilloscope
Duct tape, elastic cords, cabling, spikes, mallet
Dust Shields for DAPS and Exabyte Tape Drive
(1) Electroline Duct Seal
Assorted small tools (screwdrivers, etc), power cords, etc

## Appendix B: Test Schedule

### Week 1

Day 1
- 1/2 day - transport material out to test site, begin unpacking

Day 2
- 1/4 day - quick site survey
- 3/4 day - begin laying field wire, attaching connectors

Day 3
- 1/2 day - laying remaining field wire
- 1/2 day - begin surveying sensor locations

Day 4
- entire day to survey remaining sensor locations and start surveying cannon locations

Day 5
- 1/2 day - survey remaining cannon locations
- 1/2 day - debug/repair as necessary

### Week 2

Day 1
- 1/2 day - Test 1
- 1/2 day - Test 2

Day 2
- 1/2 day - Test 3
- 1/2 day - Test 4

Day 3
- 1/2 day - Test 5
- 1/2 day - Test 6

Day 4
- 1/2 day - Test 7
- 1/2 day - Test 8

Day 5
- 1/2 day - Optional Test A
- 1/2 day - Optional Test B
- OR
- entire day to pack and ship material back to Air Freight terminal

Day 6
- entire day to pack and ship material back to Air Freight terminal if not done prior day

# Appendix B

SPCOT
Edward C. Real
PTP2-A001
885-5147
FAX 885-0631

MEMO: August 25, 1993

TO: C. Myers

FROM: E. Real

RE: Elimination of interfering signals from acoustic data.

CC:

This is a summary report on my efforts to date to remove the interfering signals from the ARO data set. The basic operational parameters for this work are outlined in the following table.

| Parameter | Value | Comments |
|---|---|---|
| Sample Rate | 2083.33 Hz | As given in the ARO test plan. |
| Data Acquisition Date | Dec. 7, 1992 | As given on data tape label. |
| Time | 1 to 1:10 pm | ibid. |
| Location | North Tower, WSMR | ibid. |
| Tape # That Data Is On | 2 | ibid. |
| Channel Used | 3 | Relatively clean data. |
| Group # Used | 1 | There are 2 groups on this tape. |

**Table 1: Basic Operational Parameters**

For this study the following signal types were extracted by hand from the data file identified in table 1.

| Signal ID | Class | Description |
|---|---|---|
| 0 | Silence | No intentional signals emitted. |
| 18 | Multi-tone | 100 and 500 Hz. |
| 19 | Impulse Train | Impulses emitted at a 15 Hz rate. |
| 20 | Impulse Train | Impulses emitted at a 30 Hz rate. |
| 21 | Impulse Train | Impulses emitted at a 65 Hz rate. |
| 22 | Multi-Impulse Train | Impulses emitted at 15 and 65 Hz rates. |
| 23 | Multi-Impulse Train | Impulses emitted at 30 and 65 Hz rates. |
| 24 | QPSK | Center frequency at 250 Hz. Baud Rate is 50 Hz. |
| 25 | QPSK | Center frequency at 250 Hz. Baud Rate is 100 Hz. |

**Table 2: Signal Types Used In This Study**

## Preliminaries - The Sounds Of Silence.

The goal of this study is to remove unwanted signals from the environment without 1) disturbing the signals of interest and/or 2) changing the character of the data in such a was as to distort any subsequent measurements of the acoustic channel. For the most part, the unwanted signals are tones generated by nearby machinery; although this is not necessarily the (only) form of the interference. An example of the tonal interfering signals is shown in figure 1.

Figure 1 is a time/frequency (spectrogram) plot of a bracketed segment of silence taken from the beginning of the data file outlined in table 1. The time origin is relative to the beginning of the plot, and intensity (magnitude in dB) is identified by grey scale. Darker regions indicate greater amplitude. Several features of this silence segment are readily visible, and warrant further discussion.

The first set of features we consider are the broad band signals with a bandwidth of about 400 Hz ranging between approximately 200 to 600 Hz. These are evident in the time segments between 7 and 10 seconds, and again between 80 and 83 seconds. These signals are timing marks which were emitted to bracket the silence segment which lies in between (~10 to 80 seconds).

Another prominent feature is the 300 Hz tone evident from about 83 to 90 seconds. This is the beginning of signal 8 which immediately follows signal 0 on the play list.

These features aside, the rest of figure one should represent silence. Clearly, this is not the case. There remain several distinct tonal artifacts from nearby machinery. These tonals appear to be harmonically related, with a frequency spacing of a little over 100 Hz. A properly centered comb filter with this spacing and an appropriate set of gain values for the teeth might suffice to eliminate these tones, but other artifacts in the noise would then require separate processing; assuming they could be identified. There is also the additional problem of new interferers whose spectral characteristics vary over time. For these rea-

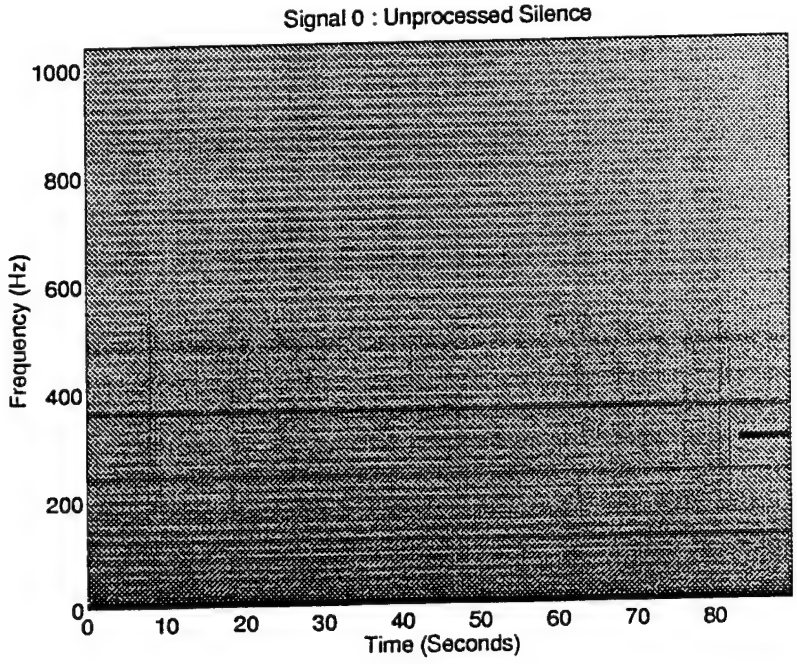


**Figure 1: Spectrogram of unprocessed silence.**

sons, it is more convenient to have a technique which adapts to the data at hand than a set of rigid filters.

### A Projected Solution

The three major requirements on the interference removal technique are then 1) minimum impact on the signals of interest, 2) minimum distortion of any acoustic channel measurements and 3) data adaptability. These three requirements by no means uniquely identify a particular technique to use. There are many techniques which could make a claim at achieving these goals. However, one technique which recommends itself is the technique of null space projection.

We begin by assuming that the interferers are stationary over a long enough period of time that a segment of the data containing the interferers alone may be characterized via a projection operator constructed out of the data itself. That is, let $x_i$ be a segment of the data containing only the interfering signal(s). Obtain a set of n such data segments $\{x_i\}$ (possibly overlapping) and use these segments as a basis set to characterize the interferers. The assumption is that these data segments $\{x\}$ are linearly independent, so it is important that overlapping data segments preserve this assumption. This requirement is not hard to fulfill in practice. Any other data segment (vector) $x_j$ may be projected into this space via the projection operator

$$P = A\,[A^H A]^{-1} A^H \tag{1}$$

where H indicates complex conjugate transpose (Hermitian), and the matrix A is constructed from the n element data set $\{x_i\}$ as.

$$A = \begin{bmatrix} | & | & & | \\ x_1 & x_2 & \cdots & x_n \\ | & | & & | \end{bmatrix} \tag{2}$$

where the columns of A are made up of elements of the data set $\{x_i\}$. The projected data vector $x_k$ is given by

$$x_k = P x_j \tag{3}$$

A refinement to this technique is to apply a reduced rank approximation to (2) in order to select only those components of A which contribute the most to the projection. The rationale behind this approach is that 1) the strongest contributors to the projection operator are the interferers and 2) we want to distort the data relating to the acoustic channel as little as possible, so we only identify that which we don't want. With this goal we reformulate (1) in terms of its singular vectors.

The Moore-Penrose inverse of A is given by

$$A^+ = [A^H A]\,A^H \tag{4}$$

The SVD of A is given by

$$A = U \Sigma V^T \tag{5}$$

In terms of the SVD of A then, the Moore-Penrose inverse is given by

$$A^+ = V\Sigma^+ U^T \tag{6}$$

Combining (1), (4), (5) and (6) the projection operator P can now be cast in terms of the singular vectors of A as

$$P = AA^+ = UU^T \tag{7}$$

The singular vectors which make up the columns of U are an orthonormal basis set which span the range of A. However, not all of the singular vectors are equally important in the reconstruction (projection) process. Those associated with the largest singular values are the most important, in the sense that excluding them would increase the mean square error between any projected data vector $x_k$ and the original data vector $x_j$ by the largest amount. Conversely, excluding the singular values associated with the smallest singular values would have the smallest impact on the mean square error. Since it is assumed that it is the interferers which contribute the most to the structure of the data, the singular values associated with their presence should be the largest. Therefore we construct P only out of the singular vectors in U which are associated with the largest singular values.

Figure 2 shows a power spectral density plot of signal 0 constructed from 2048 samples (approximately 1 second of data) taken form a starting position near the 15 second point of figure 1. The presence of the interfering tones is clearly visible, and it is noted that they are not all harmonically related. Note also that the bulk of the noise floor lies below about -65 dB and that the interferers lie primarily in that region.

Figure 3 shows the singular values of a data matrix A constructed from a set of 121 sample vectors $\{x_i\}$ taken from signal 0. Each sample vector was 2048 sample points in length, and there was a 50 percent data overlap between adjacent vectors. We can see that the power of the associated singular vectors extends down to about where we would like to

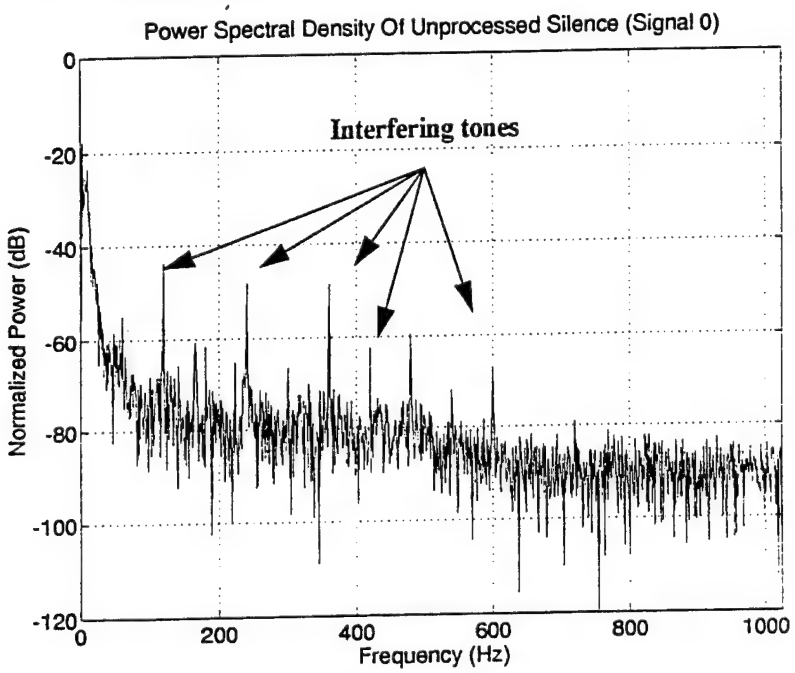


**Figure 2: Power spectral density of signal 0.**

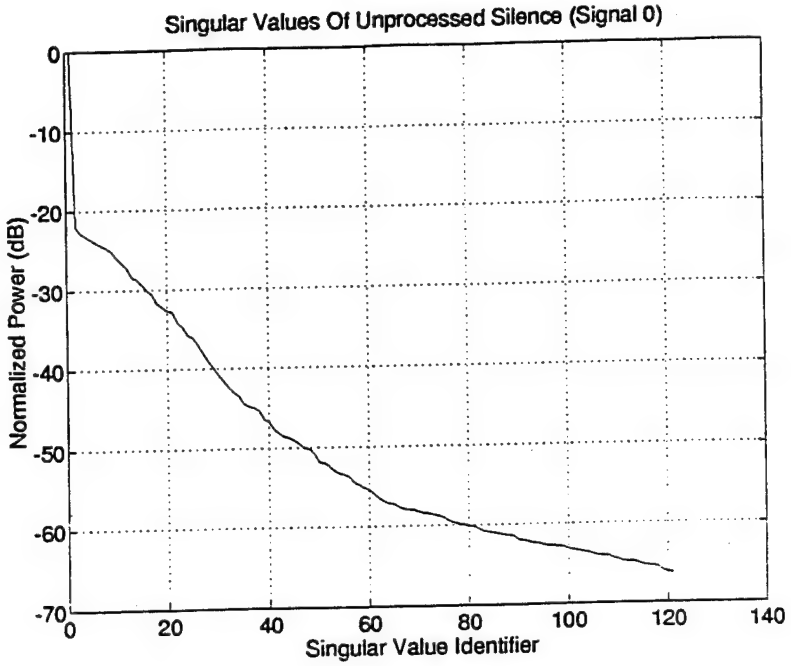


**Figure 3: Singular values of signal 0.**

go, so we will use all of the singular values (the A matrix is of rank 121) to compute the projector P from (7).

However, it is not the projection of the interferers which we want, it is their elimination. To do this we construct the null space projector $P^{\perp}$. This projector projects a given vector into the null space of A. In the case of a raw data vector $x_j$ extracted from signal 0, the result of the projection $x_k = P^{\perp}x_j$ will be the noise (silence) only, since the interferers are in the range of A. The null space projector $P^{\perp}$ is given by

$$P^{\perp} = I - P \tag{8}$$

where I is the identity matrix.

Figure 4 shows the spectrogram resulting from the null space projection of the data graphed in figure 1. Note that the absolute difference in grey scale is not as important as the relative difference. Comparison of figure 4 with the original spectrogram of figure 1 shows that the strongest interferers have been suppressed the most while the timing marks and the short segment of signal 8 (300 Hz tone) above 80 seconds have been retained since they are in the null space of A.

Figure 5 shows the corresponding power spectral density plot. The power in figure 5 is not normalized, however the range is the same in order to facilitate direct comparison with figure 2. Note that the interfering tones are gone, except for those which were approximately 60 dB down from the peak power (0 dB) in figure 2. Note also that apart from the suppression of the frequencies near DC, the overall shape of the noise floor has been preserved. The suppression of the low frequency terms is a consequence of using all of the largest 121 singular vectors to construct the projector matrix, rather than being more selective. Future work will address this issue. There is, for example, a marked knee in the curve of figure 3 after the first singular value. This implies that the first singular value is related to the DC and/or lower frequency terms in figure 2. Using the singular vector corresponding

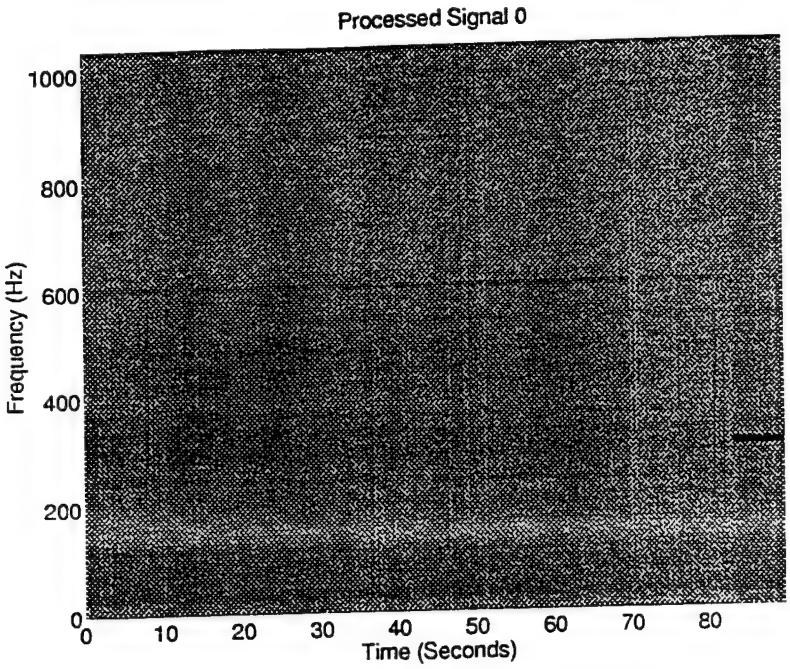


**Figure 4: Spectrogram of processed silence.**

to this term in the construction of the projection operator P in future studies may prevent the suppression of the lower frequencies.

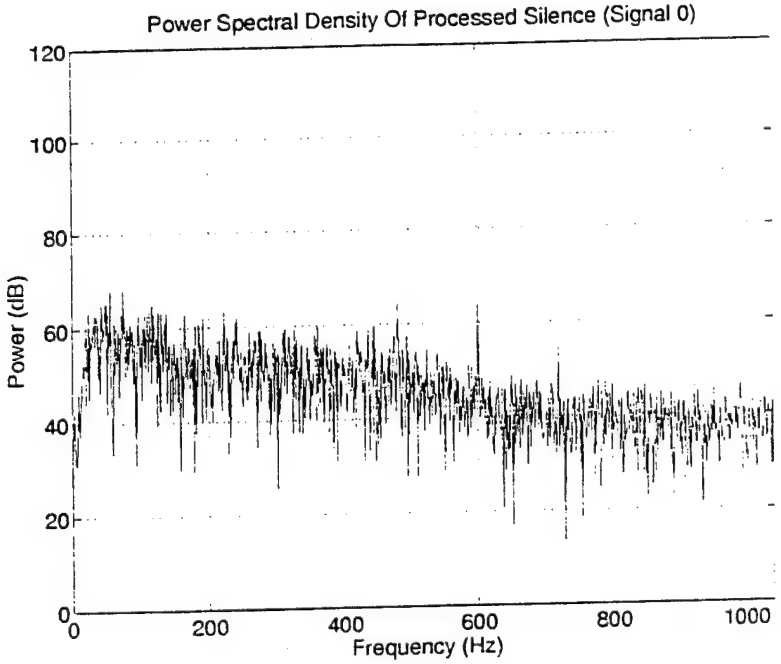


**Figure 5: Power spectral density of processed signal 0.**

## Test Results

This sections outlines the test results to date. The null space projector of the previous section is used to eliminate the interferers from the signal list shown in table 2. Each of these cases will be considered separately. In each case, a spectrogram and power spectral density plot of the original signal will be shown, followed by similar plots for the processed signal.

**Signal 18 - A multi-tone signal consisting of 100 and 500 Hz tones.**

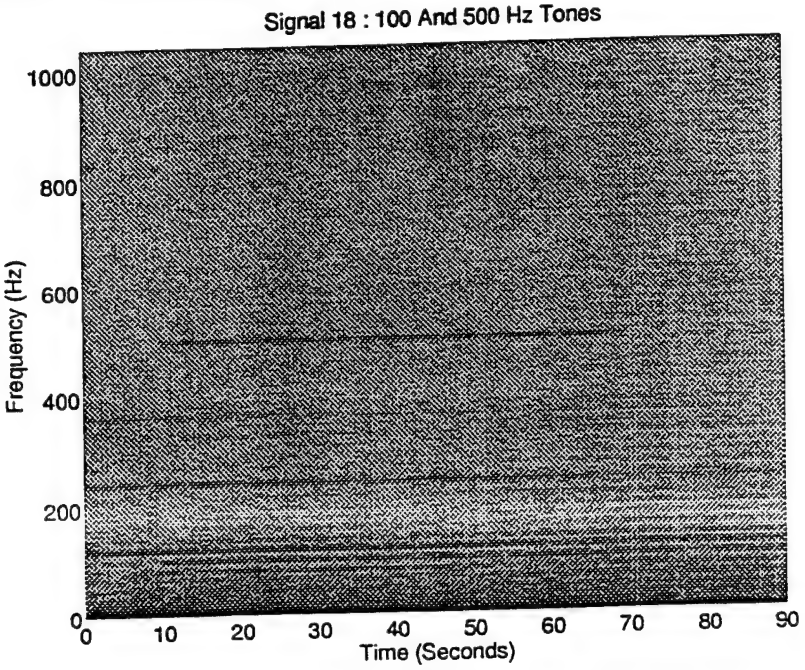


**Figure 6: Spectrogram of unprocessed signal 18**

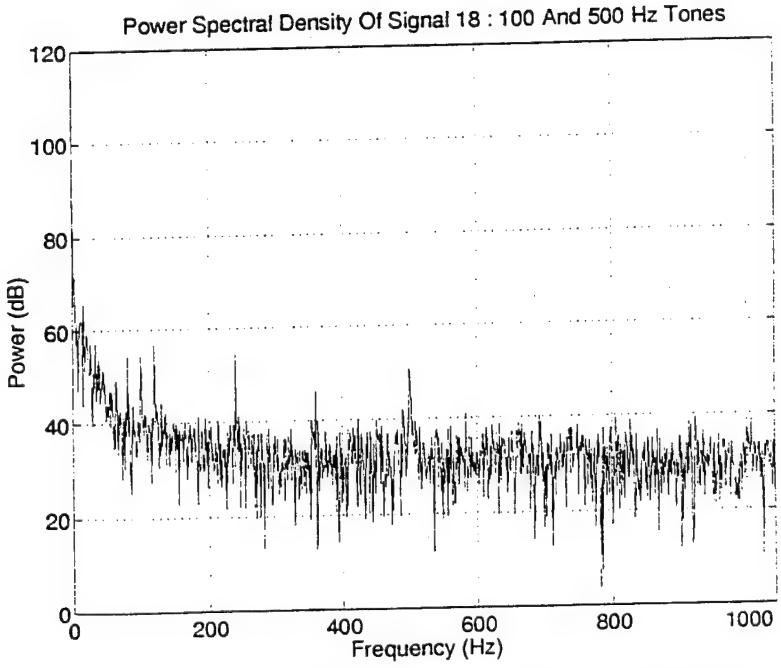


**Figure 7: Power spectral density of unprocessed signal 18**

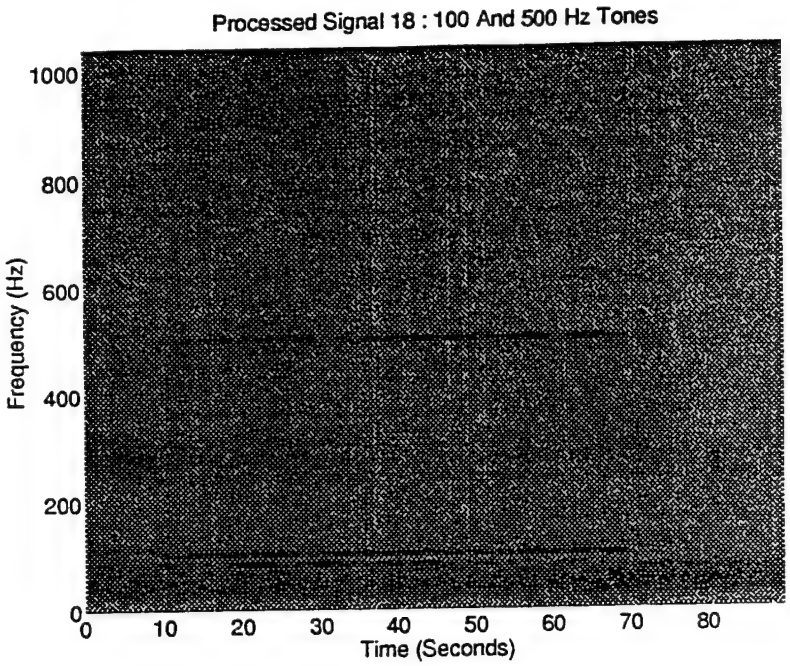


Figure 8: Spectrogram of processed signal 18

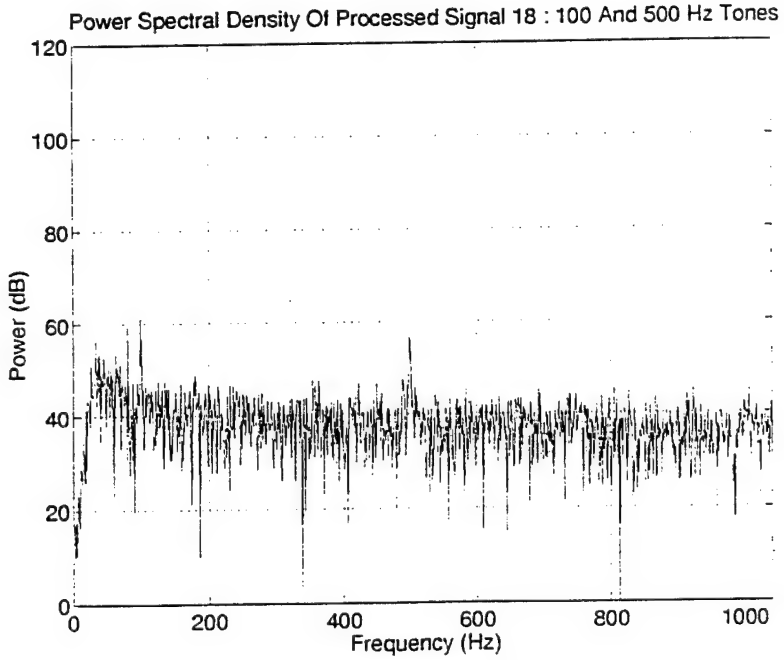


Figure 9: Power spectral density of processed signal 18

**Signal 19 - An impulse train with a 15 Hz repetition rate.**

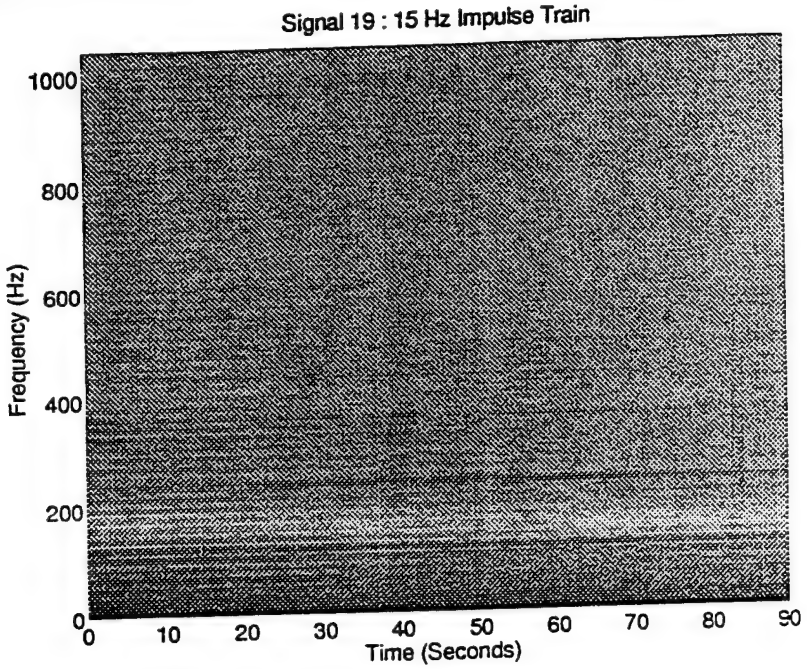


**Figure 10: Spectrogram of unprocessed signal 19**

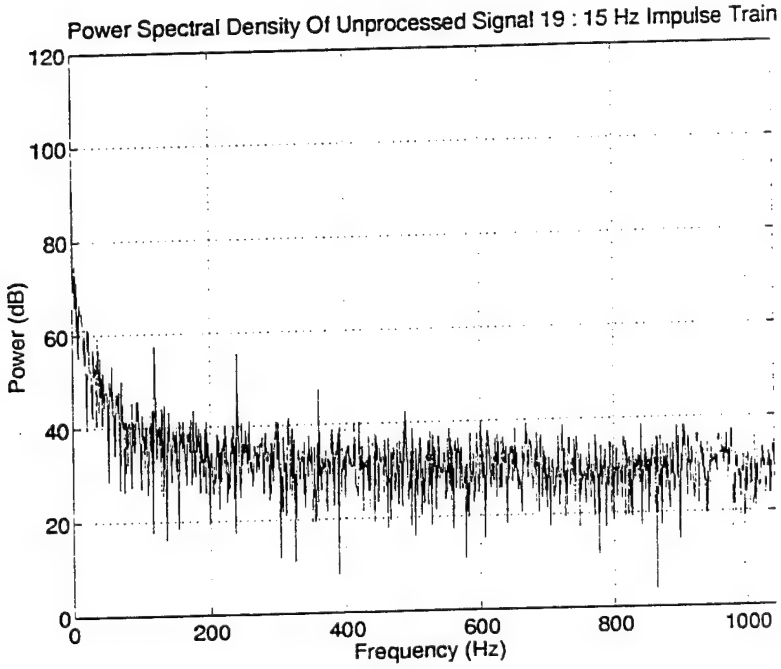


**Figure 11: Power spectral density of unprocessed signal 19**

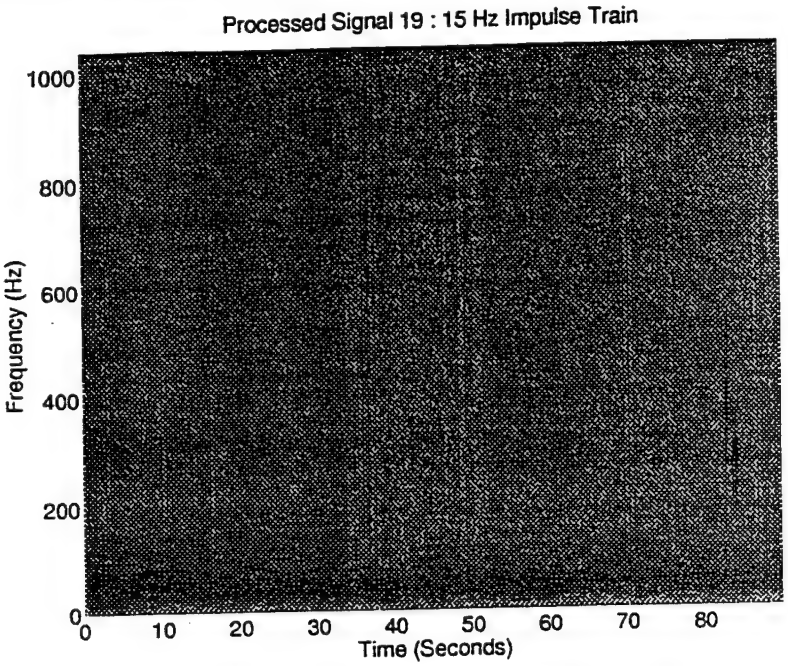


**Figure 12: Spectrogram of processed signal 19**

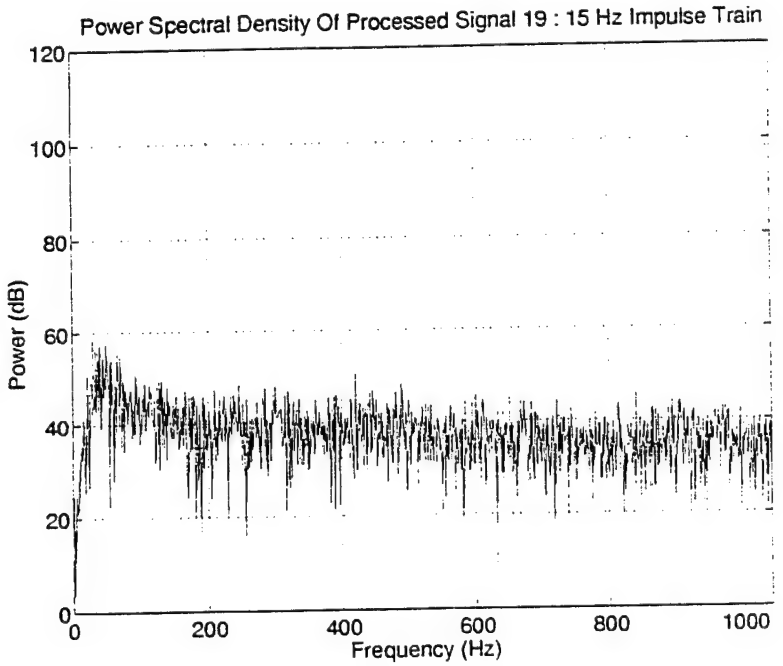


**Figure 13: Power spectral density of processed signal 19**

**Signal 20 - An impulse train with a 30 Hz repetition rate.**

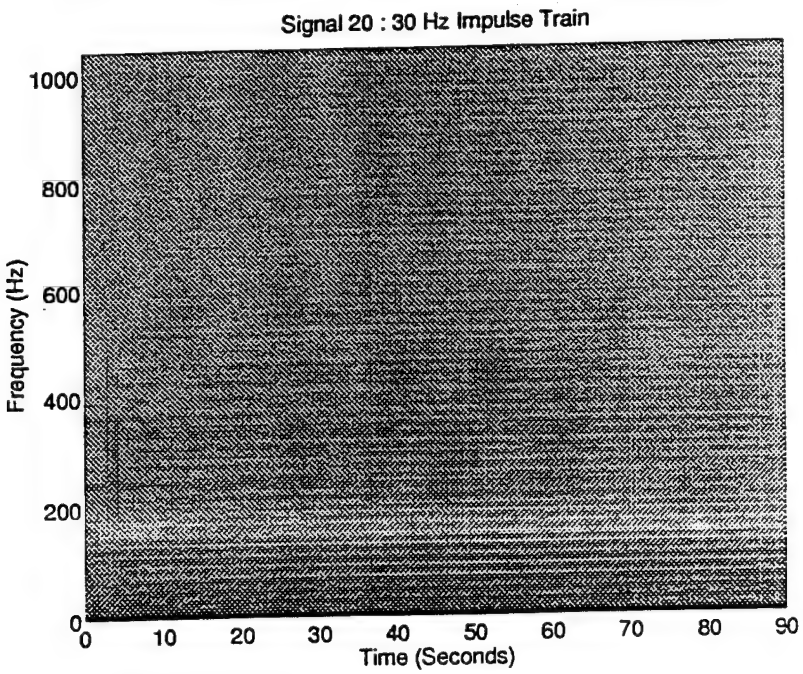


**Figure 14: Spectrogram of unprocessed signal 20**

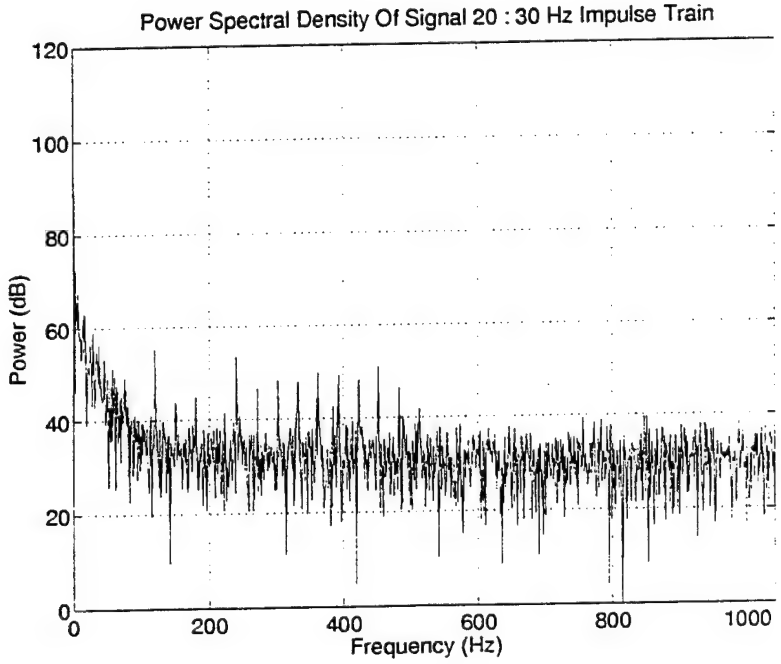


**Figure 15: Power spectral density of unprocessed signal 20**

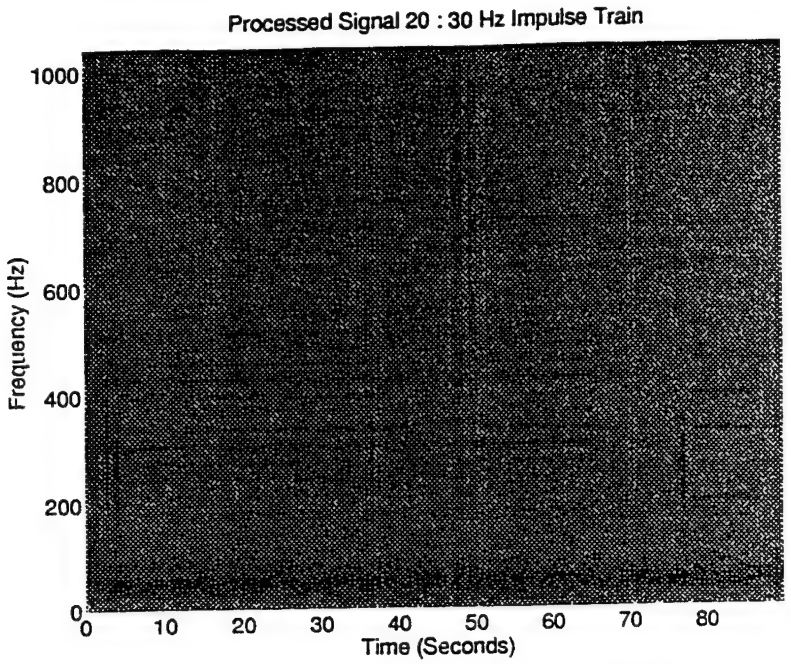


**Figure 16: Spectrogram of processed signal 20**

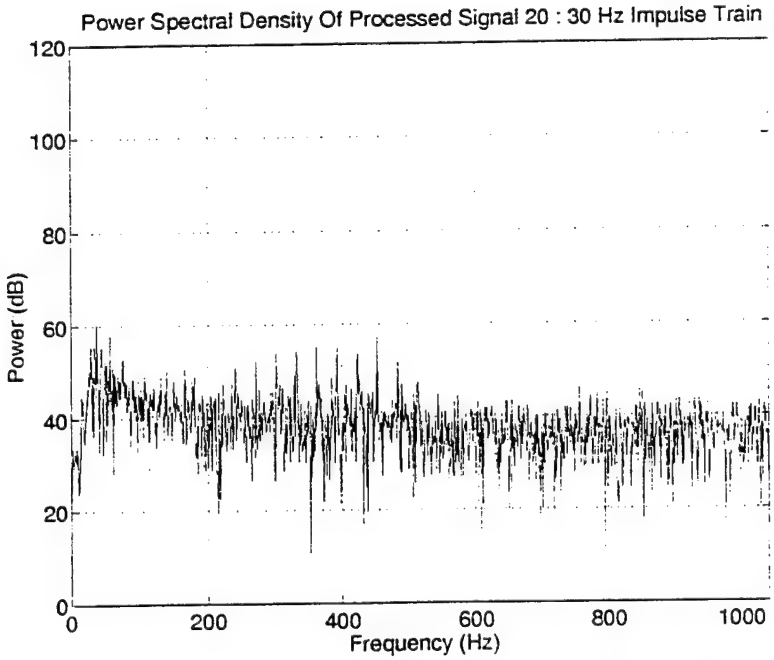


**Figure 17: Power spectral density of processed signal 20**

**Signal 21 - An impulse train with a 65 Hz repetition rate.**

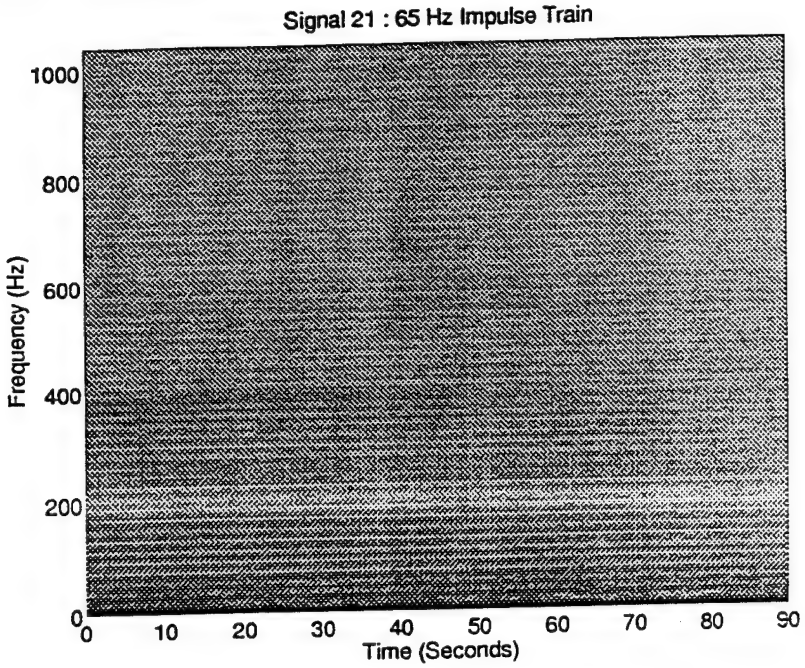


**Figure 18: Spectrogram of unprocessed signal 21**

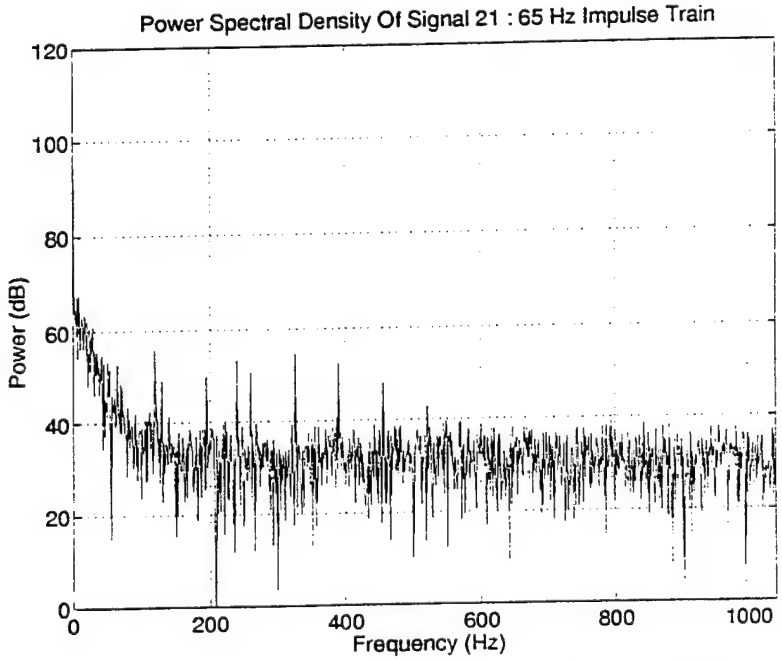


**Figure 19: Power spectral density of unprocessed signal 21**

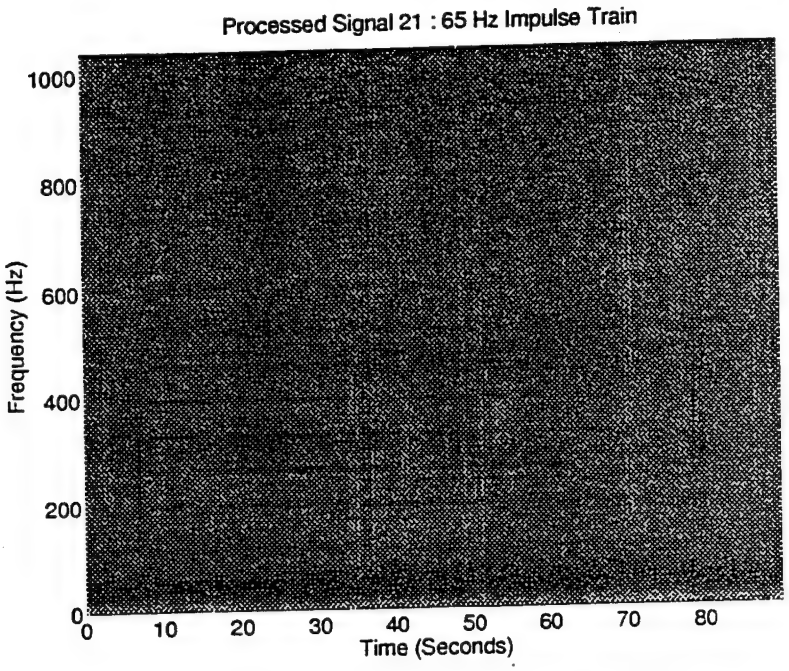


Figure 21: Spectrogram of processed signal 21

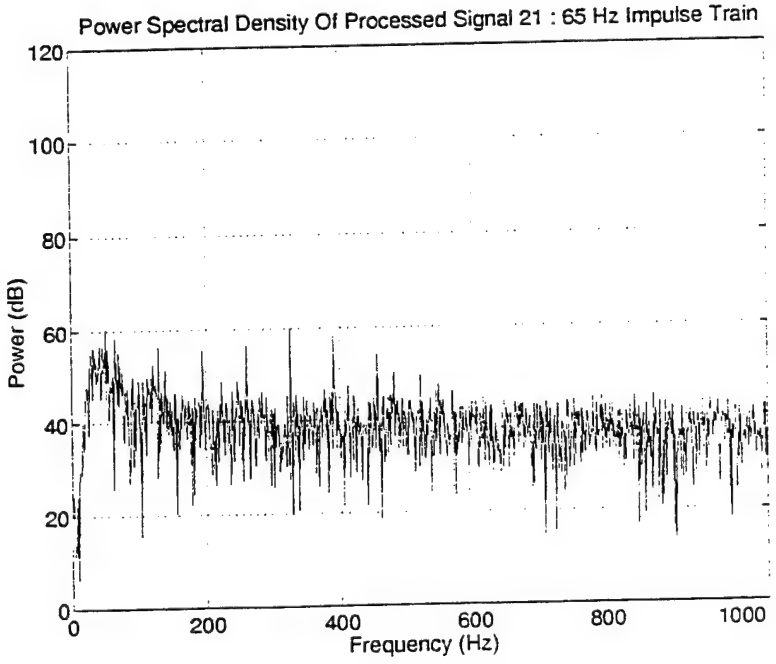


Figure 22: Power spectral density of processed signal 21

**Signal 22 - An multi-impulse train with a 15 and 65 Hz repetition rate.**

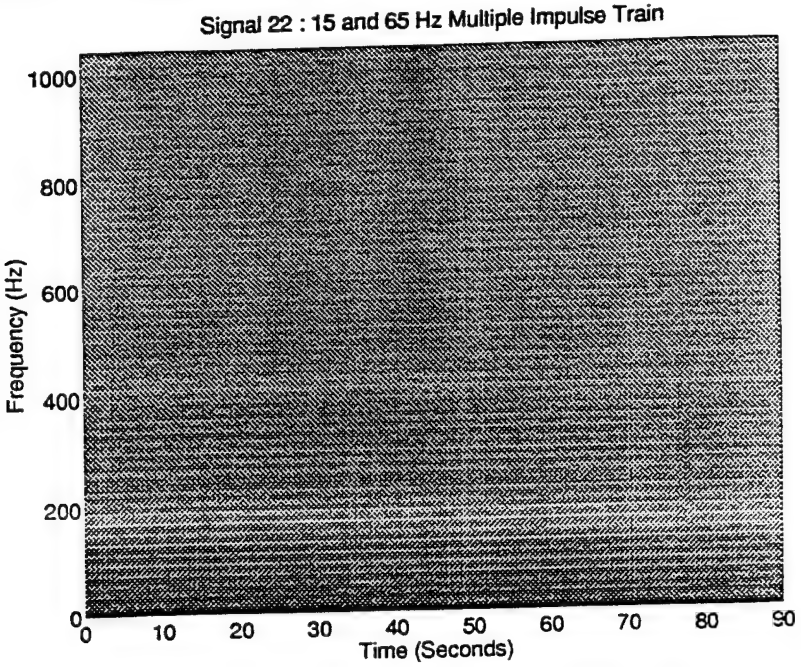


**Figure 23: Spectrogram of unprocessed signal 22**

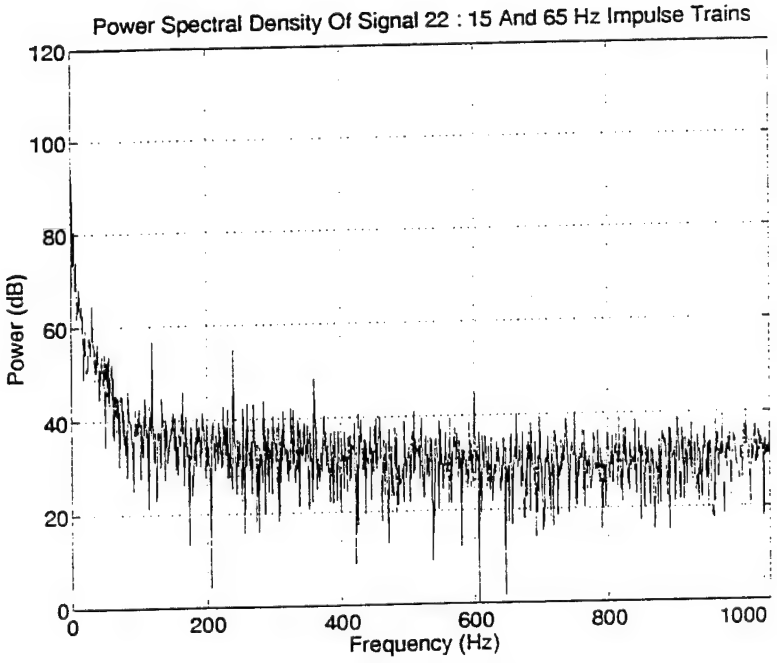


**Figure 24: Power spectral density of unprocessed signal 22**

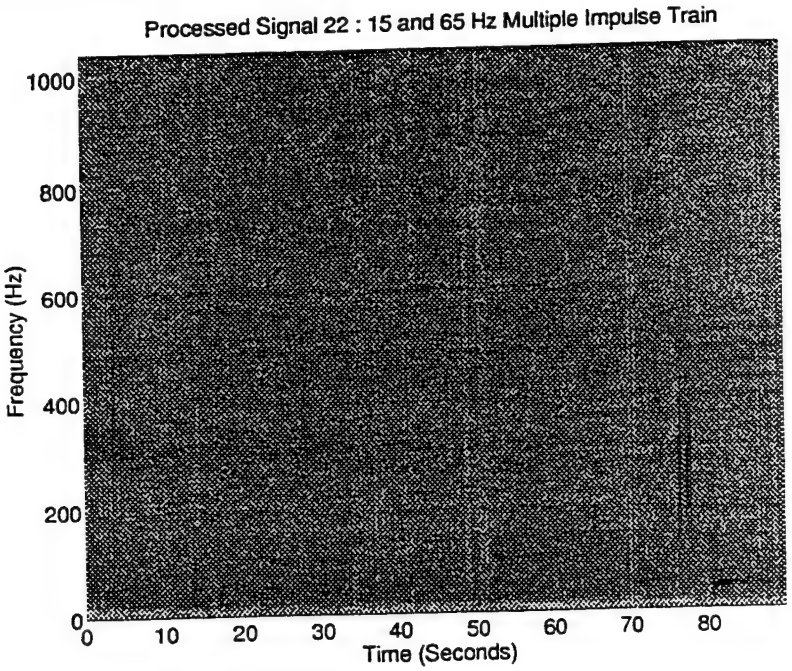


Figure 25: Spectrogram of processed signal 22

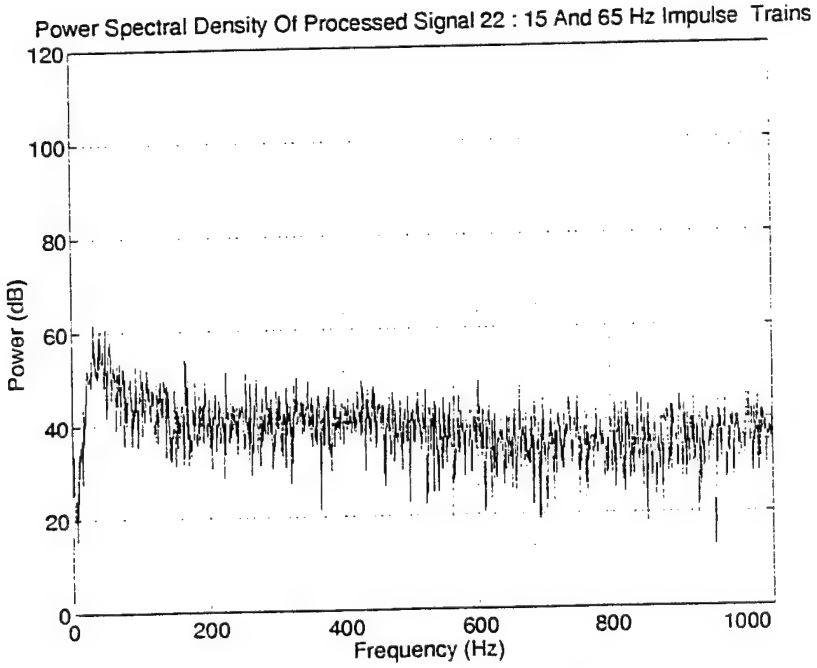


Figure 26: Power spectral density of processed signal 22

**Signal 23 - An multi-impulse train with a 30 and 65 Hz repetition rate.**

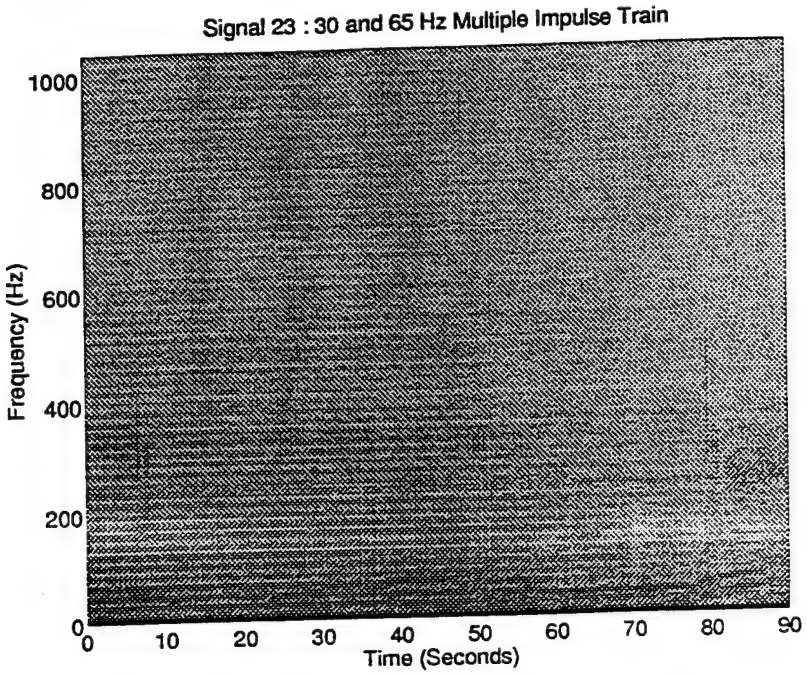


**Figure 27: Spectrogram of unprocessed signal 23**

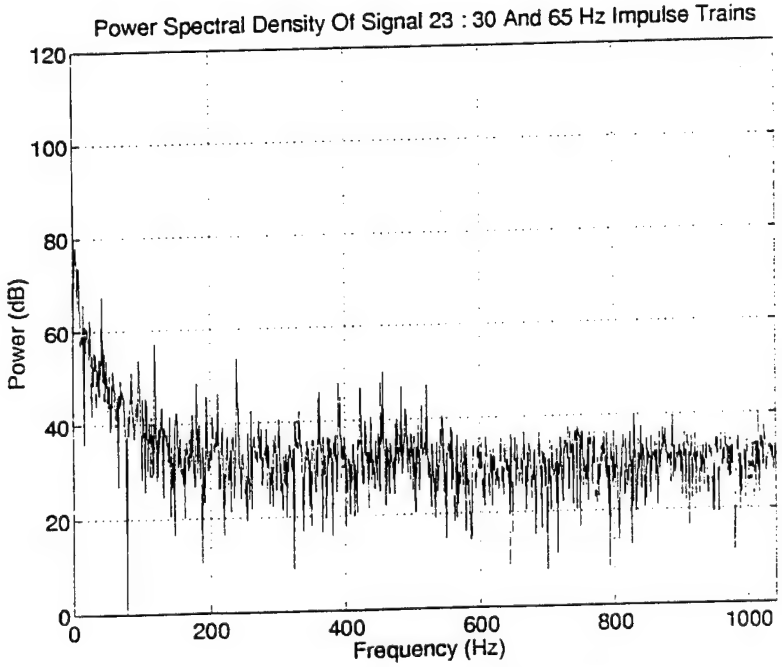


**Figure 28: Power spectral density of unprocessed signal 23**

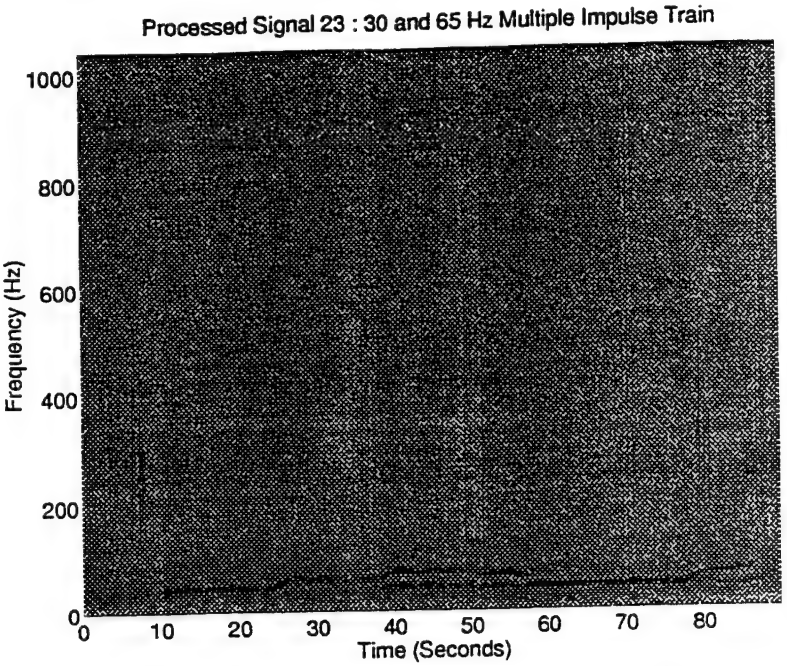


**Figure 29: Spectrogram of processed signal 23**

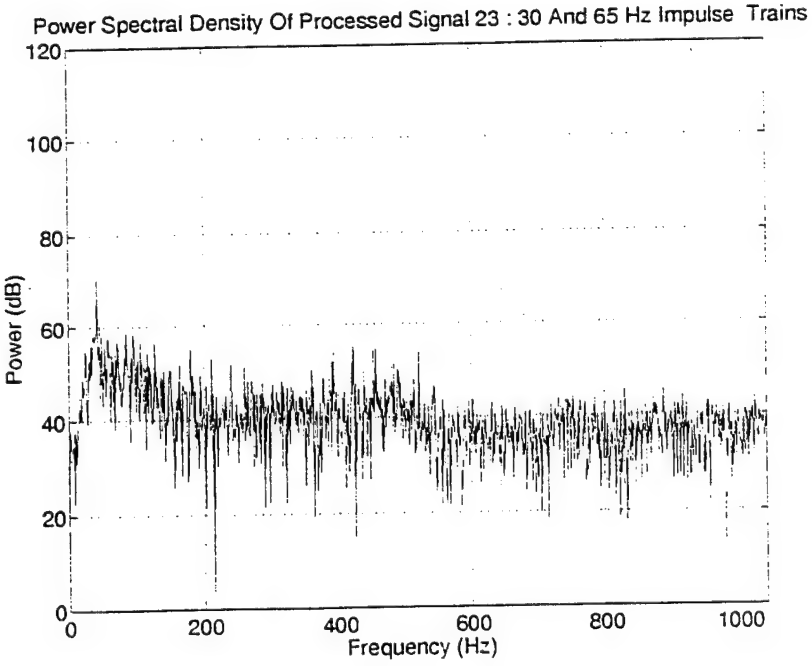


**Figure 30: Power spectral density of processed signal 23**

**Signal 24 - A QPSK signal with a baud. rate of 50 Hz centered on 250 Hz**

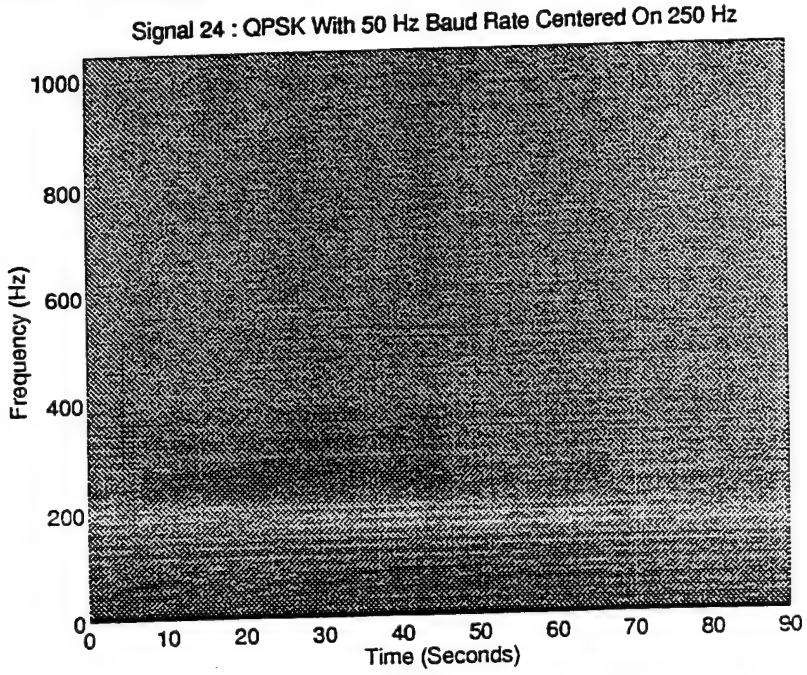


**Figure 31: Spectrogram of unprocessed signal 24**

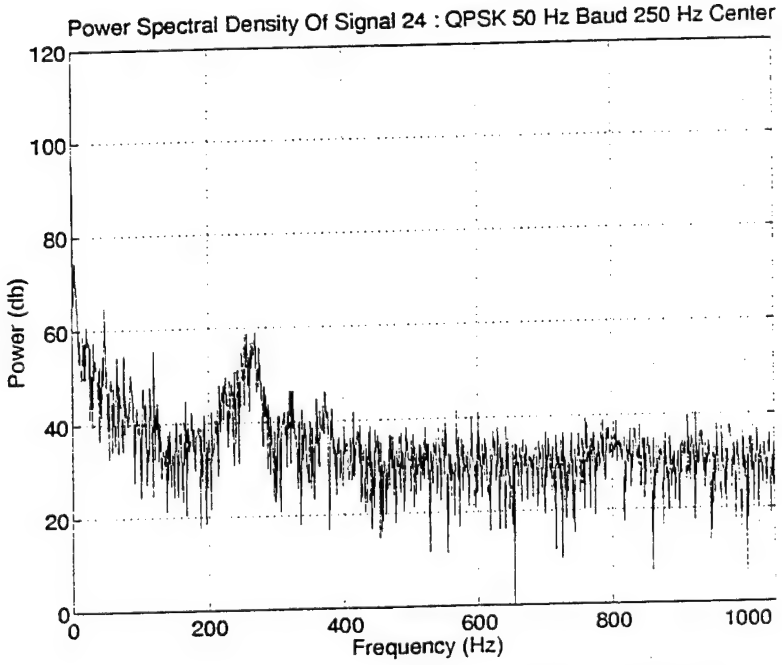


**Figure 32: Power spectral density of unprocessed signal 24**

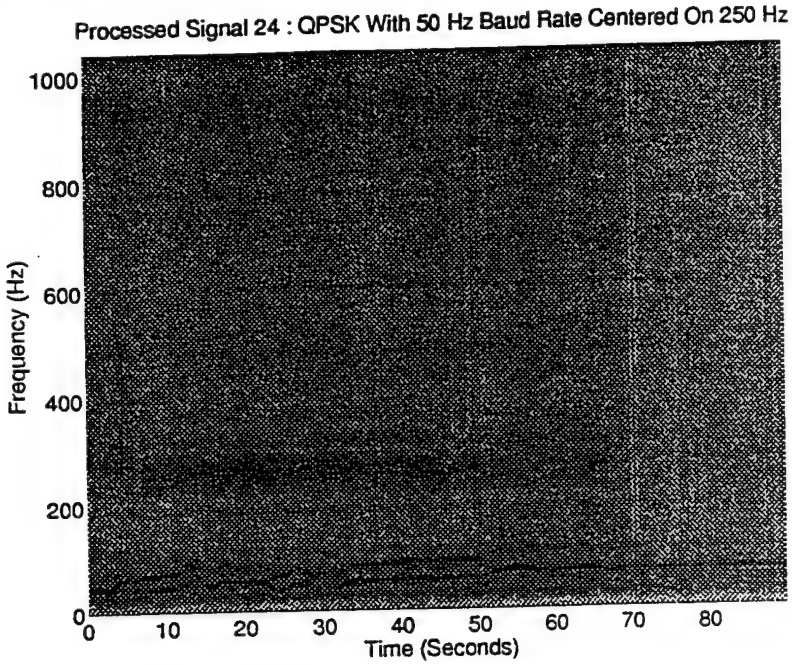


Figure 33: Spectrogram of processed signal 24

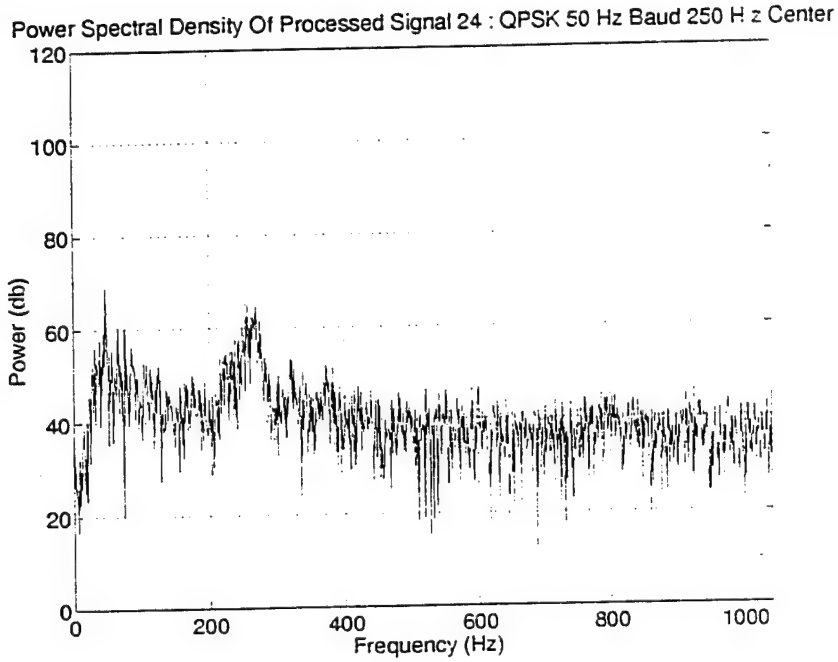


Figure 34: Power spectral density of processed signal 24

**Signal 25 - A QPSK signal with a baud. rate of 100 Hz centered on 250 Hz**

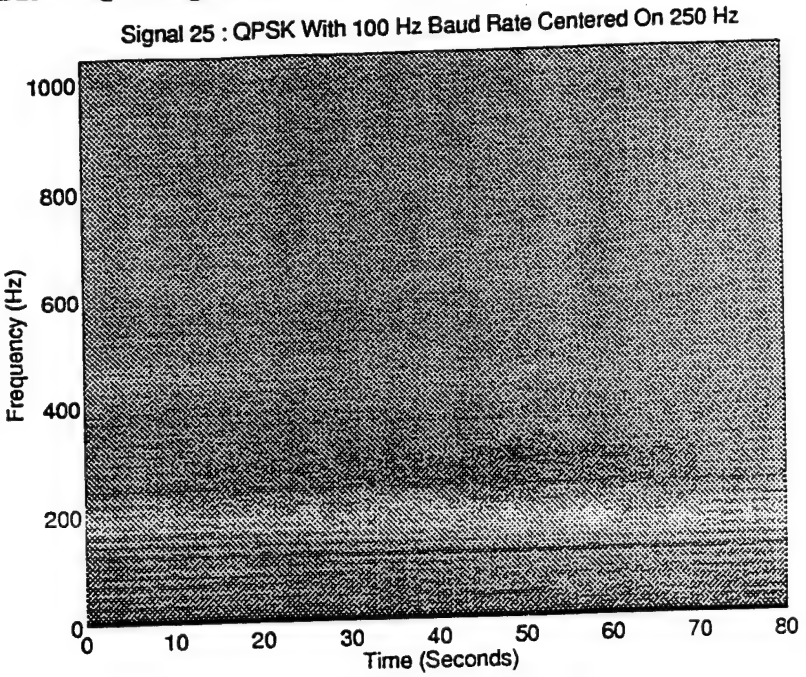


**Figure 35: Spectrogram of unprocessed signal 25**

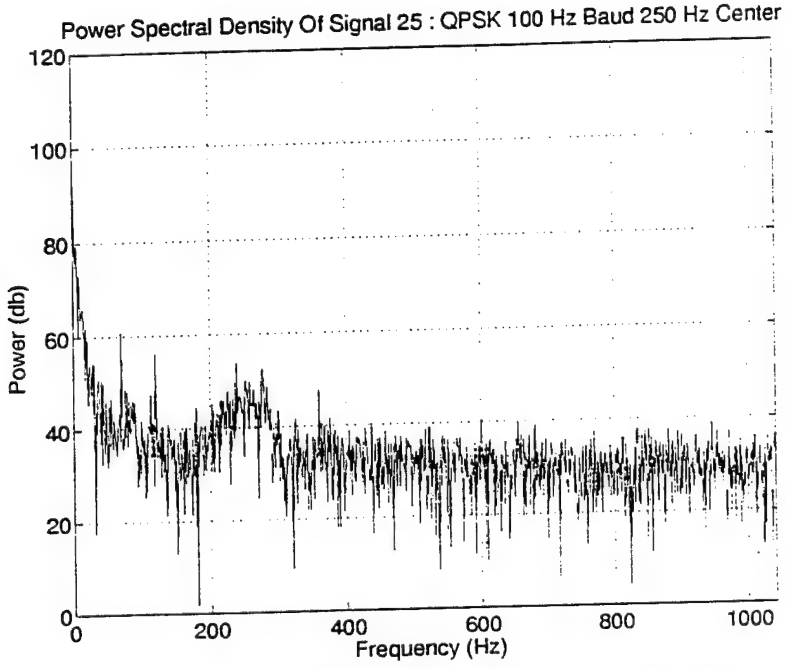


**Figure 36: Power spectral density of unprocessed signal 25**

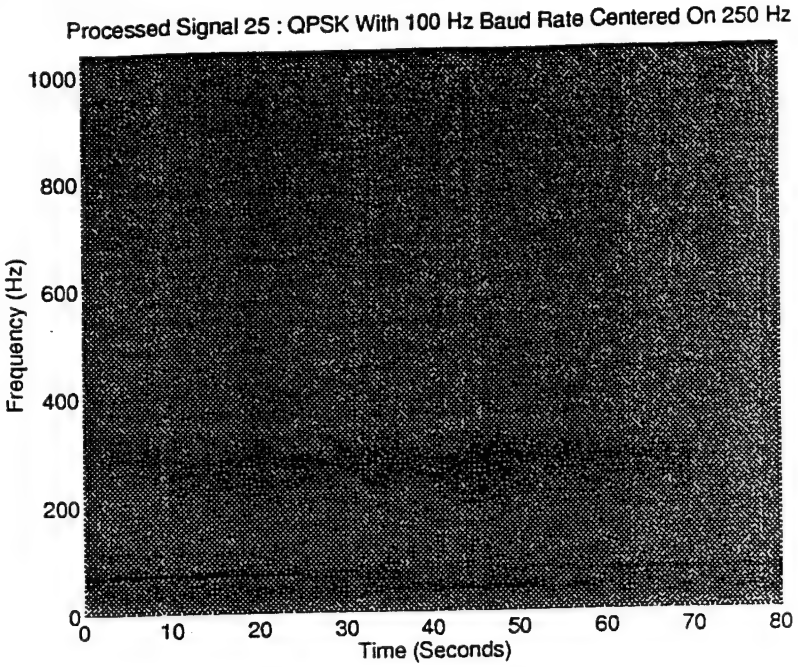


Figure 37: Spectrogram of processed signal 25

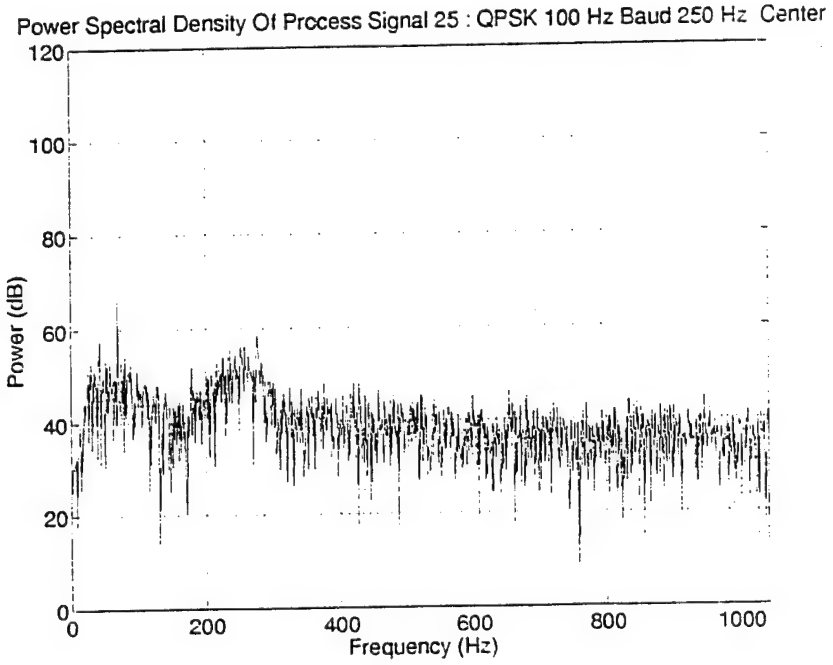


Figure 38: Power spectral density of processed signal 25

SPCOT
Edward C. Real
PTP2-A001
885-5147
FAX 885-0631

MEMO: September 1, 1993

TO: C. Myers

FROM: E. Real

RE: Elimination of interfering signals from acoustic data using LMS.

CC:

This report outlines the ability of the LMS algorithm to capture signals taken from the ARO data set. The basic operational parameters for this work are outlined in the following table.

| Parameter | Value | Comments |
|---|---|---|
| Sample Rate | 2083.33 Hz | As given in the ARO test plan. |
| Data Acquisition Date | Dec. 7, 1992 | As given on data tape label. |
| Time | 1 to 1:10 pm | ibid. |
| Location | North Tower, WSMR | ibid. |
| Tape # That Data Is On | 2 | ibid. |
| Channel Used | 3 | Relatively clean data. |
| Group # Used | 1 | There are 2 groups on this tape. |

**Table 1: Basic operational parameters**

For this study the signal extracted (by hand) from this data was signal 0 (silence). The LMS algorithm was taken from "Adaptive Filters" by C.F.N. Cowan and P.M. Grant, Prentice-Hall Signal Processing Series, Alan V. Oppenheim, Series Editor, 1985. The parameters used for the LMS algorithm are given in table 1.

| Parameter | Value | Comments |
|---|---|---|
| Number Of Taps | 15 | As directed. |
| Learning Constant (u) | 3.7509e-11 | Initial estimate. Equal to $\frac{1}{3\lambda_{max}}$ where $\lambda_{max}$ is the largest eigenvalue of a data matrix composed of 121 sample vectors of 2048 points each with 50 percent overlap, taken from a segment of the signal. This value was adjusted upwards as is shown below. See above reference for rational for choosing u this way. |

**Table 2: Parameters of the LMS algorithm**

## Preliminaries - The LMS Algorithm

The update scheme for the N element coefficient vector $\vec{h}$ obtained via the adaptive LMS algorithm is given in the above reference and is repeated here for convenience.

$$\vec{h}(n) = \vec{h}(n-1) + 2ue_{\vec{h}(n-1)}\vec{\Phi}(n) \tag{1}$$

where $n$ is the iteration number, $u$ is the learning constant mentioned above, $e_{\vec{h}(n)}$ is the error term for the $n^{th}$ iteration given as

$$e_{\vec{h}(n)}(n) = y(n) - \vec{\Phi}^T(n)\vec{h}(n) \tag{2}$$

and where $y(n)$ is the $n^{th}$ data point and $\vec{\Phi}(n)$ is an N element data vector consisting of the following data points

$$\vec{\Phi}(n) = \begin{bmatrix} y(n-1) \\ y(n-2) \\ \vdots \\ y(n-N) \end{bmatrix} \tag{3}$$

## Results

Employing this algorithm, and training on 10 seconds of silence with a learning constant $u$ of 3.7509e-11 resulted in the error curve shown in figure 1. Figure 2 shows the corresponding coefficient vector $\vec{h}$.

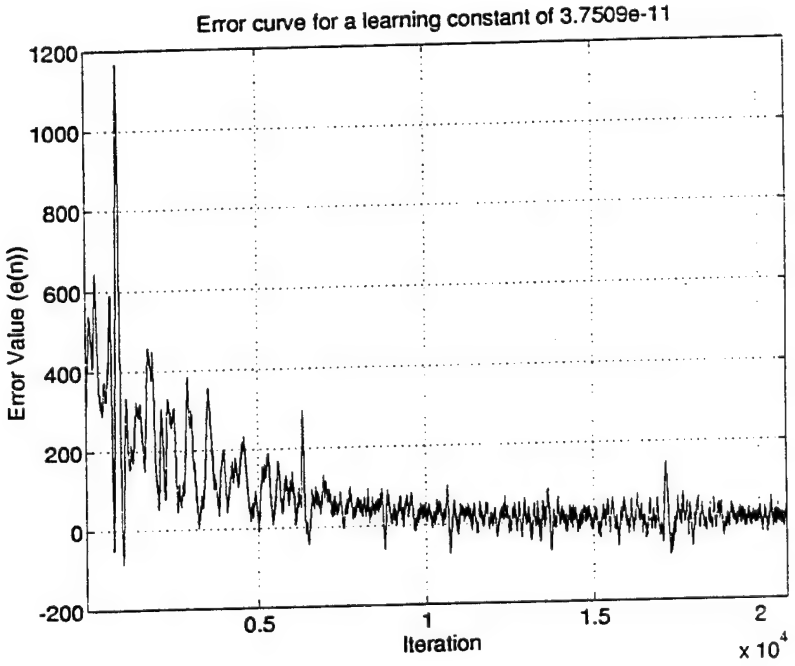


**Figure 1: Error curve for a learning constant of 3.7509e-11**

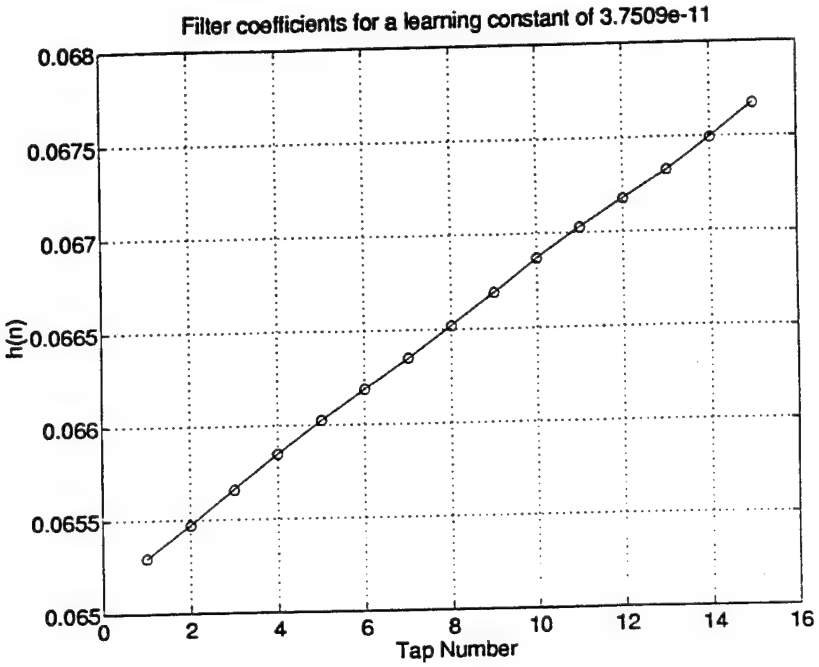


**Figure 2: Coefficient vector for a learning constant of 3.7509e-11.**

Figures 3 and 4 show similar graphs for a learning constant of 1.2003e-9 (32 * u) while figures 5 and 6 show graphs for a learning constant of 4.8011e-9 (128 * u). For clarity, figure 7 shows a blow up of the error curve plot of figure 5.

Figures 8 and 9 shows graphs for a learning constant of 9.6022e-09 (256 * u), note the change in scale on figure 8.

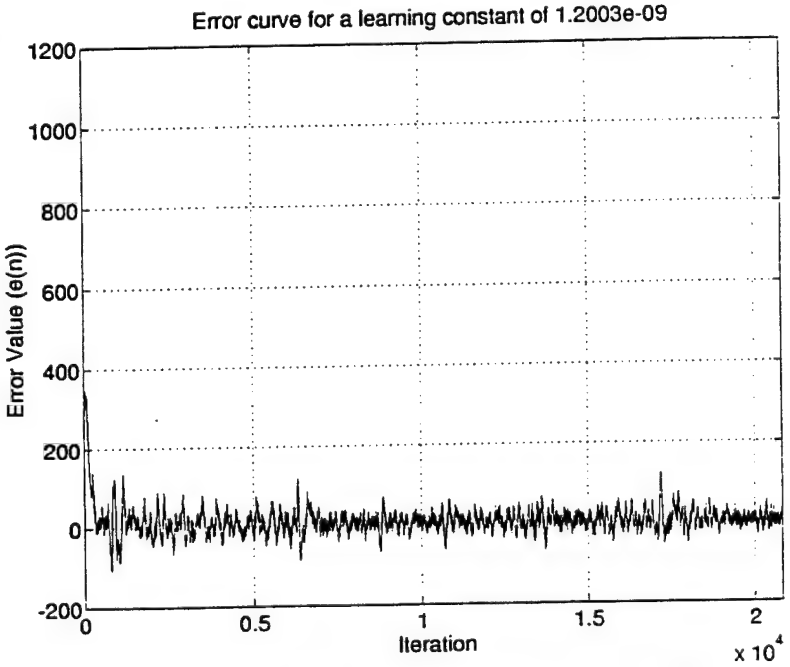


**Figure 3: Error curve for a learning constant of 1.2003e-9**

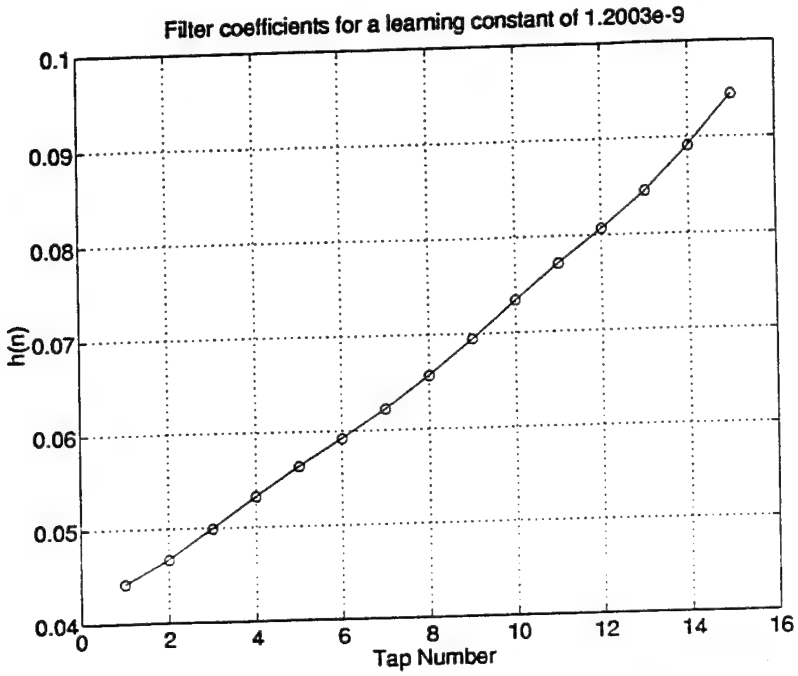


**Figure 4: Coefficient vector for a learning constant of 1.2003e-9**

Figures 10 and 11 show the graphs for a learning constant of 1.9204e-08 (512 * u).

Figures 12 and 13 are for a learning constant of 3.8409e-08 (1024 * u). Note that at this point the learning constant is driving the algorithm into instability. Figure 14 shows a blow up of figure 12.

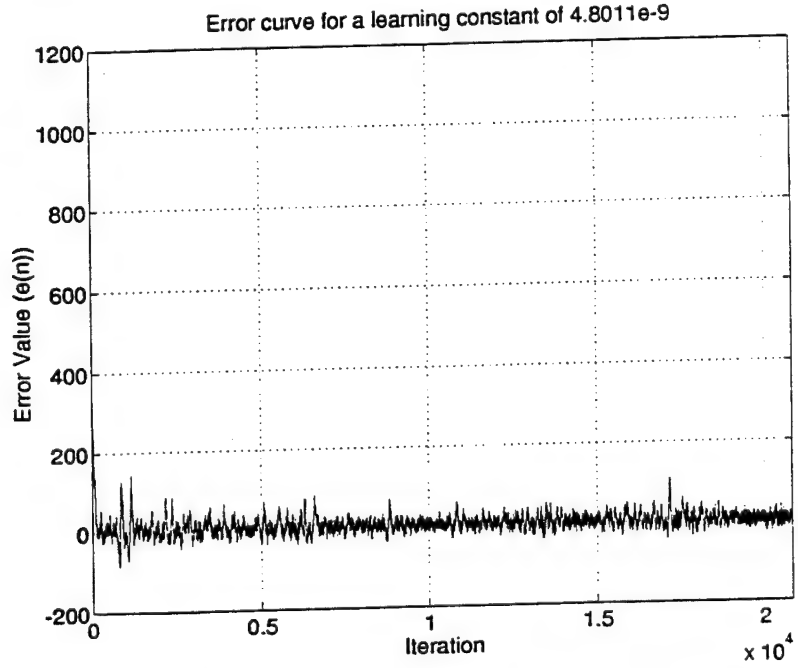


**Figure 5: Error curve for a learning constant of 4.8011e-9**

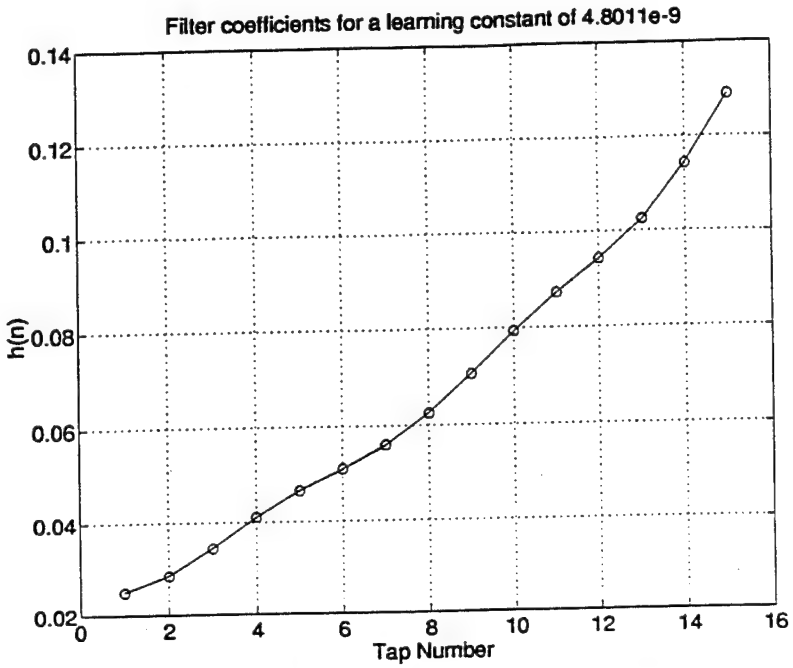


**Figure 6: Coefficient vector for a learning constant of 4.8011e-9**

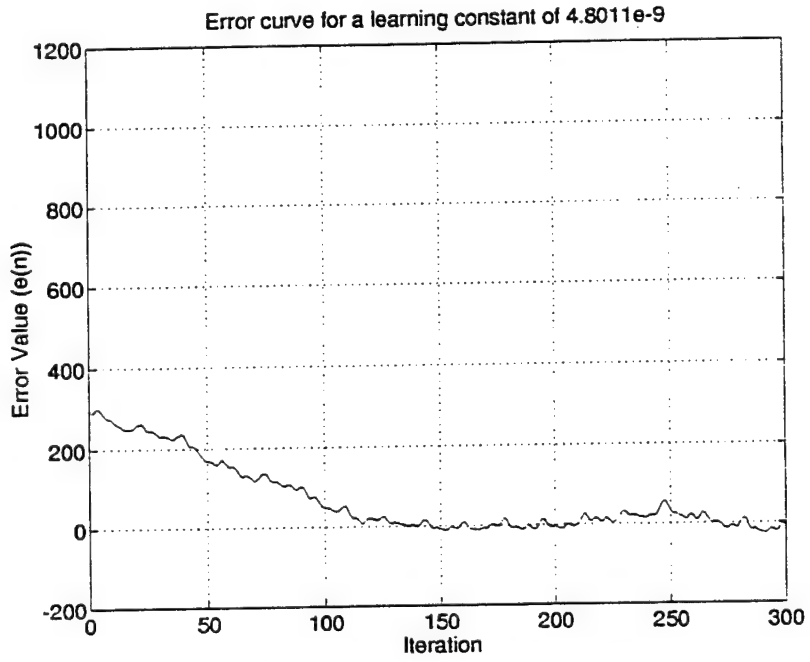


**Figure 7: Expanded error curve plot of figure 5.**

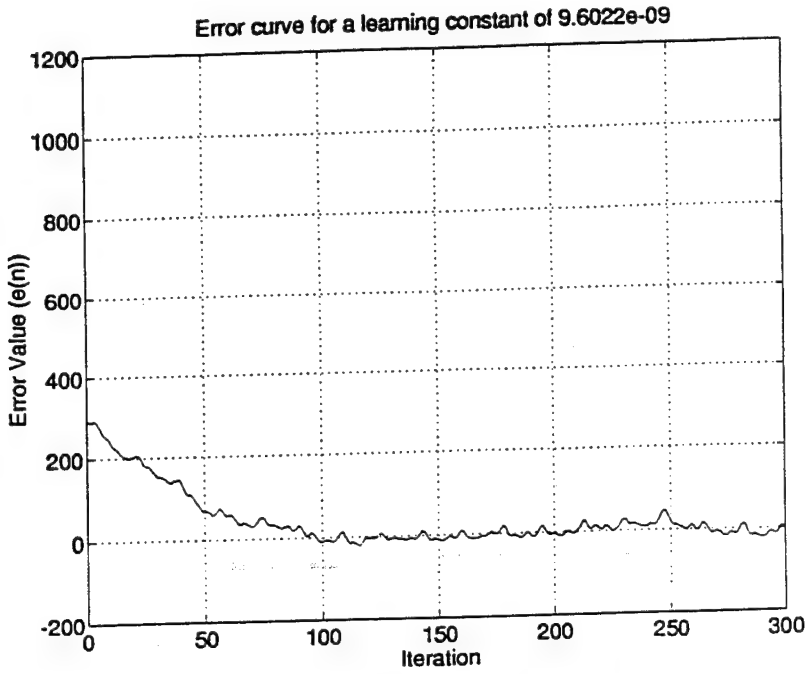


**Figure 8: Error curve for a learning constant of 9.6022e-9**

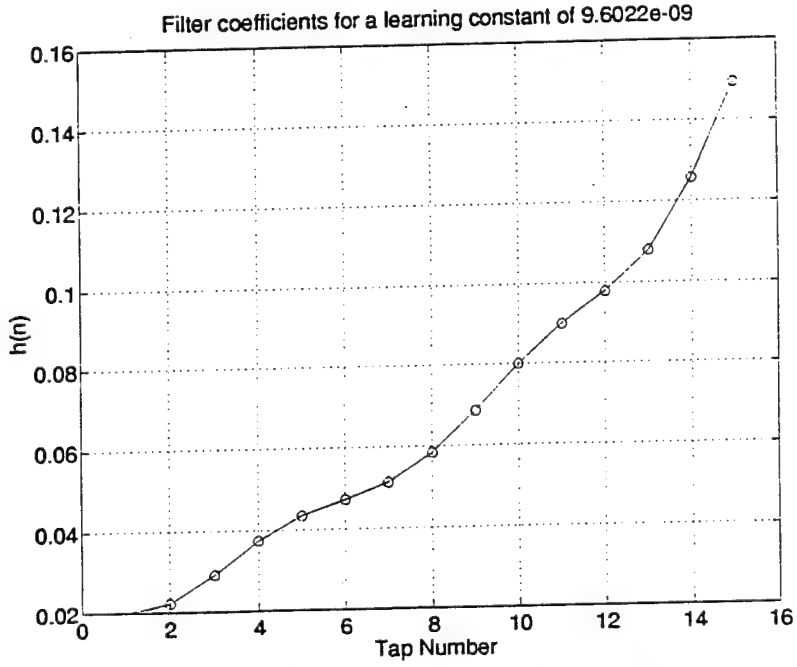


**Figure 9: Coefficient vector for a learning constant of 9.6022e-9**

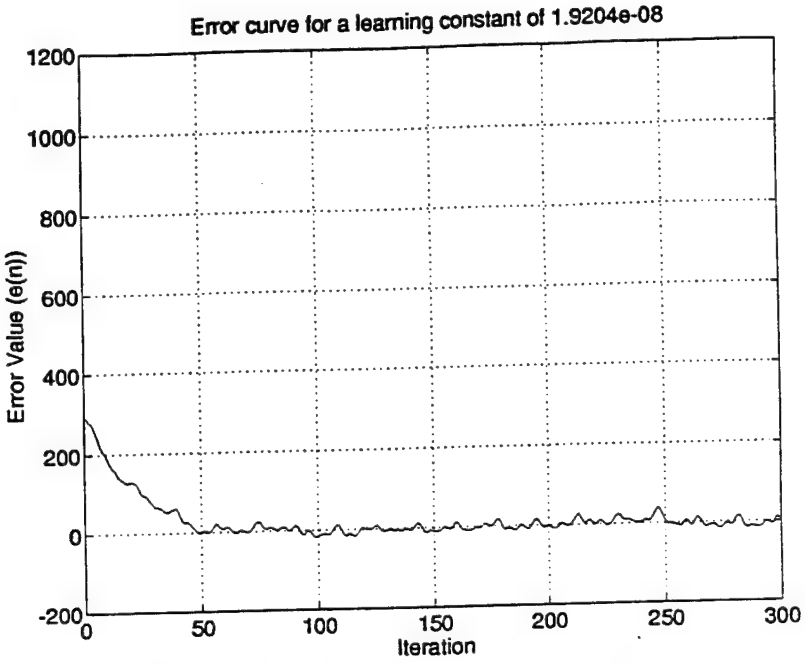


**Figure 10: Error curve for a learning constant of 1.9204e-08**

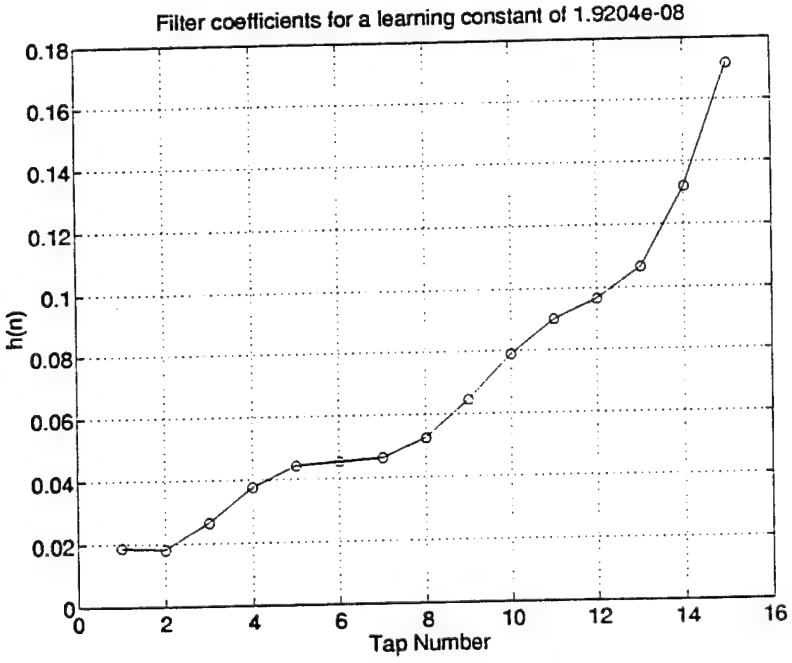


**Figure 11: Coefficient vector for a learning constant of 1.9204e-08**

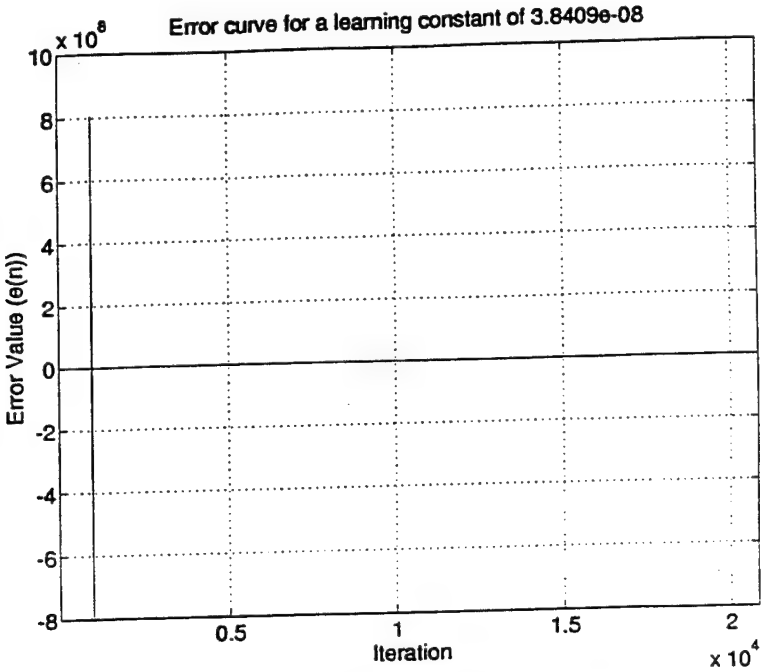


**Figure 12: Error curve for a learning constant of 3.8409e-08**

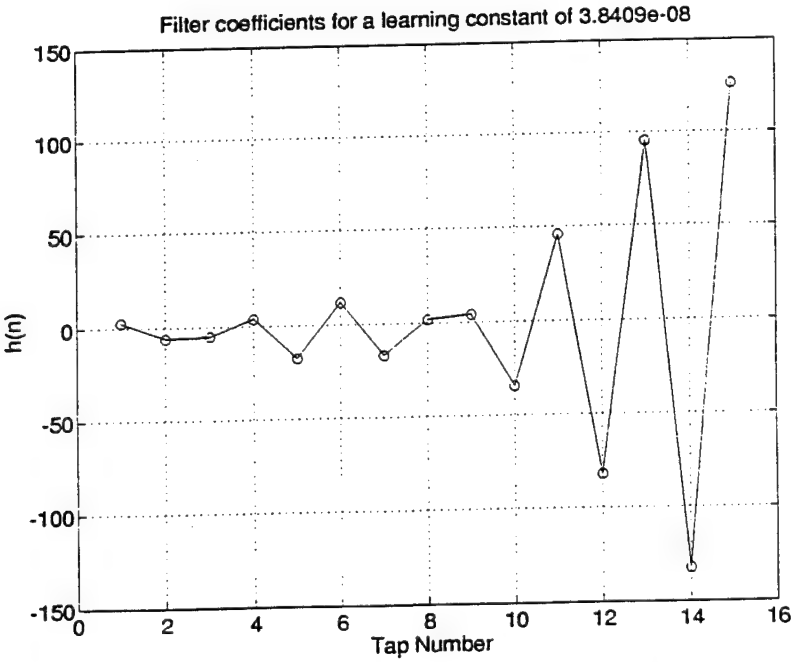


**Figure 13: Coefficient vector for a learning constant of 3.8409e-08**

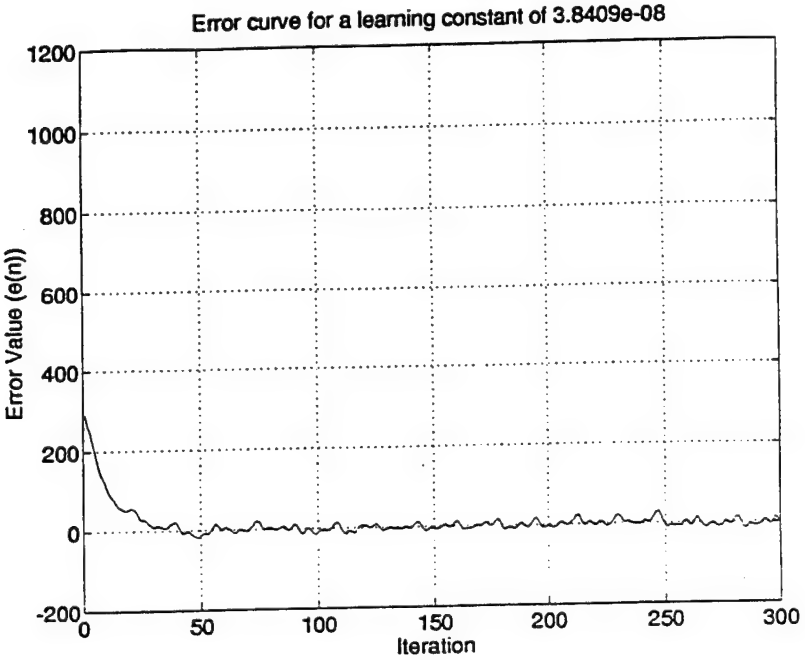


**Figure 14: Expanded error curve plot of figure 12.**

**SPCOT**

Edward C. Real

PTP2-A001

885-5147

FAX 885-0631

MEMO: September 17, 1993

TO: C. Myers

FROM: E. Real

RE: Plots from file 10.05.00.g1 of the NASA wind tunnel data.

CC: S. Lang

This memo contains the requested plots from the NASA wind tunnel data outlined in the September 15 fax to Doug Mook from Henry Abarbanel of UC San Diego. The specifics of the data plotted are contained in the table below.

| Parameter | Value | Comments |
|---|---|---|
| Sample Rate | 2083.33 Hz | As given in the fax mentioned above. |
| File Name | 10.05.00.g1 | From NASA wind tunnel data accompanying above fax. |
| Data Creation Date | July 9, 1993 | As specified in the extracted tar file date stamp. |
| Data Creation Time | 15:26 | ibid. |
| Location Of Sensor Array | Front center of canopy | 6" diameter circular sensor array (see fax). |
| Sensor Number Within Array | 4 | As specified by C. Myers. There are 8 sensors total. |
| Channel Used For Sensor Output | 3 | ibid. There are 8 channels total. |
| Group # Used | 1 | ibid. |

**Table 1: Data Specifics**

Figure 1 is a spectrogram of the entire data stream outlined in table 1. Figure 2 is a power spectral density plot of the same data over its entire length (125952 point DFT).

Ed.

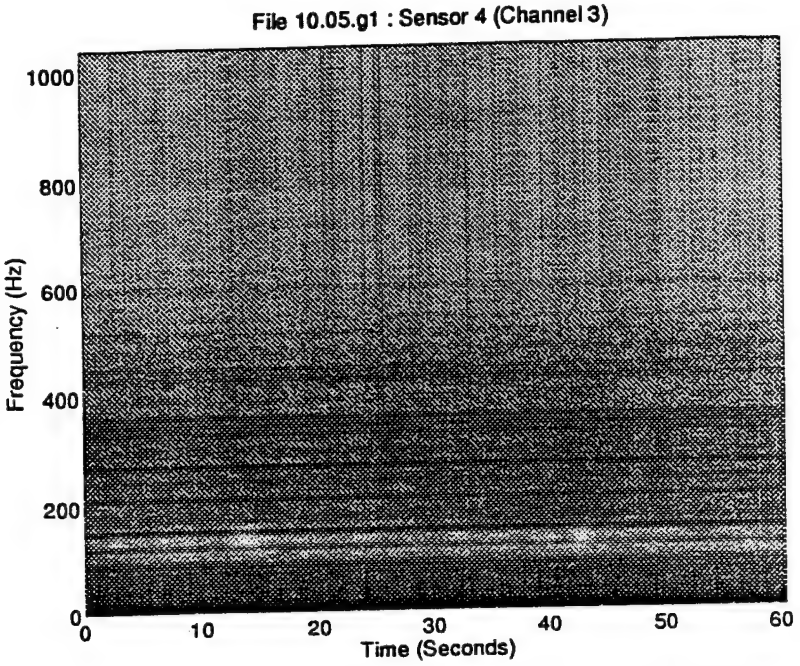


**Figure 1: Spectrogram of channel 3 of data file 10.05.00.g1**

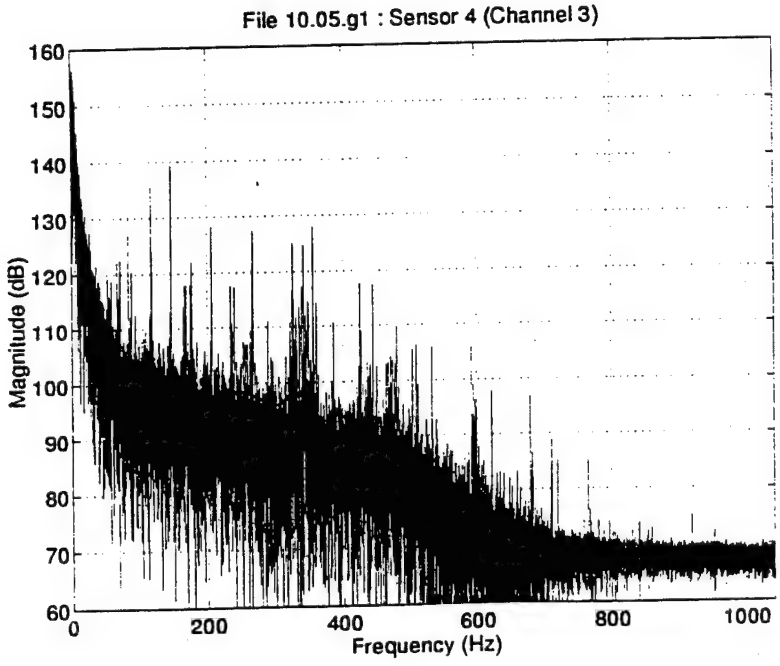


**Figure 2: PSD plot of channel 3 of data file 10.05.00.g1**

SPCOT

Edward C. Real

PTP2-A001

885-5147

FAX 885-0631

MEMO: September 19, 1993

TO: C. Myers

FROM: E. Real

RE: Plots from file 10.05.00.g1 of the NASA wind tunnel data - all channels.

CC: S. Lang

This memo contains the requested plots from all channels of the NASA wind tunnel data outlined in the September 15 fax to Doug Mook from Henry Abarbanel of UC San Diego. The specifics of the data plotted are contained in the table below.

| Parameter | Value | Comments |
|---|---|---|
| Sample Rate | 2083.33 Hz | As given in the fax mentioned above. |
| File Name | 10.05.00.g1 | From NASA wind tunnel data accompanying above fax. |
| Data Creation Date | July 9, 1993 | As specified in the extracted tar file date stamp. |
| Data Creation Time | 15:26 | ibid. |
| Location Of Sensor Array | Front center of canopy | 6" diameter circular sensor array (see fax). |
| Channels Used For Sensor Output | all | As specified by C. Myers. There are 8 channels total. |
| Group # Used | 1 | ibid. |

**Table 1: Data Specifics**

Figure 1, 3, 5, 7, 9, 11, 13, and 15 are spectrograms of the entire data streams for each of the channels outlined in table 1. Figure 2, 4, 6, 8, 10, 12, 14, and 16 are the corresponding power spectral density plots of the same data (over the entire data length - 125952 point DFTs).

Ed.

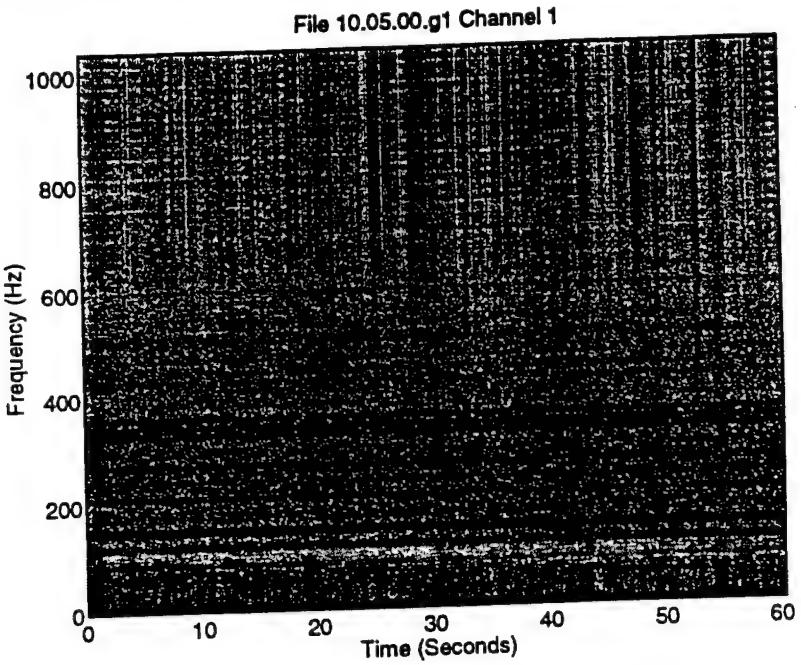


**Figure 1: Spectrogram of channel 1 of file 10.05.00.g1**

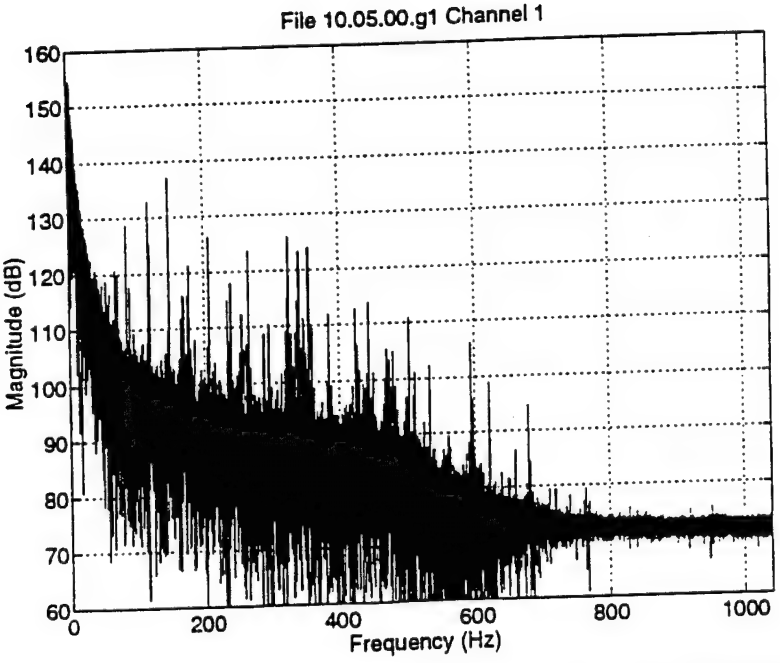


**Figure 2: Power spectral density plot of channel 1 of file 10.05.00.g1**

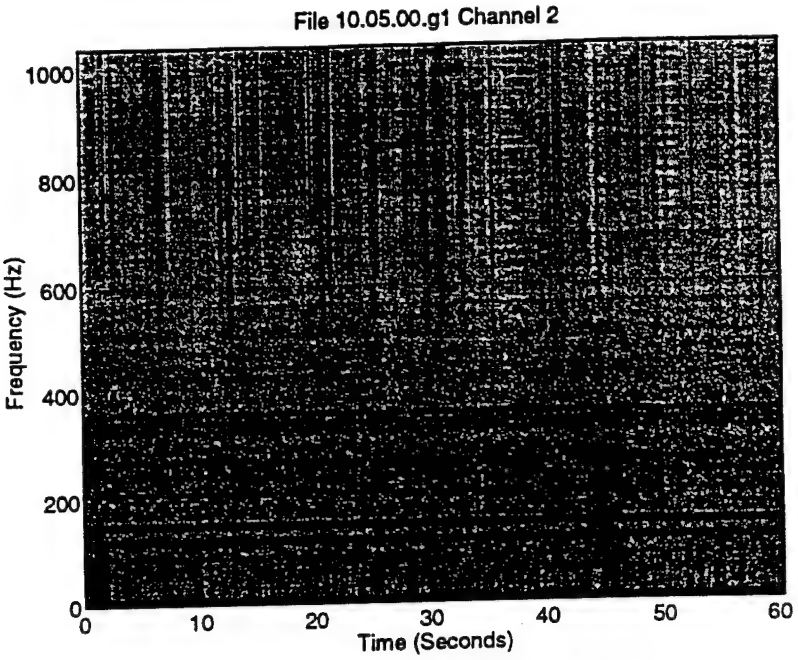


**Figure 3: Spectrogram of channel 2 of file 10.05.00.g1**

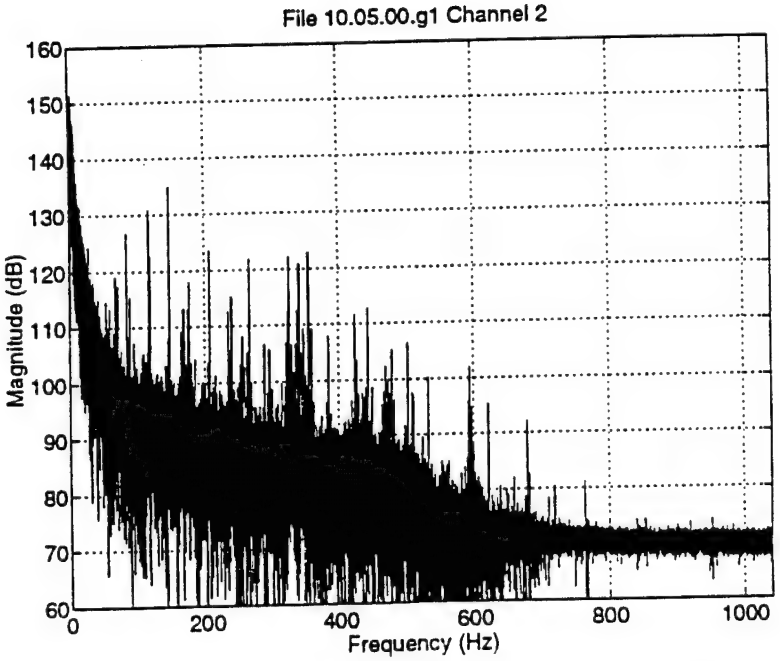


**Figure 4: Power spectral density plot of channel 2 of file 10.05.00.g1**

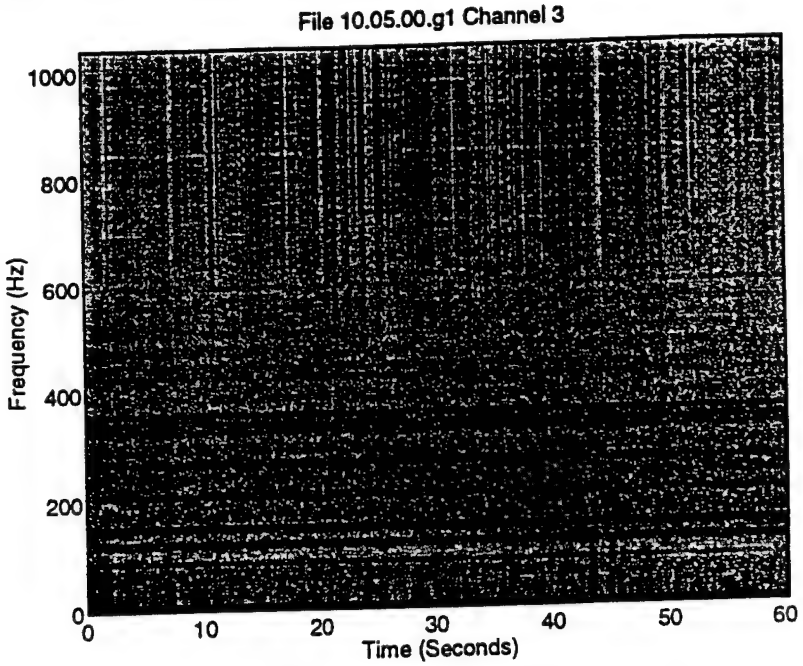


**Figure 5: Spectrogram of channel 3 of file 10.05.00.g1**

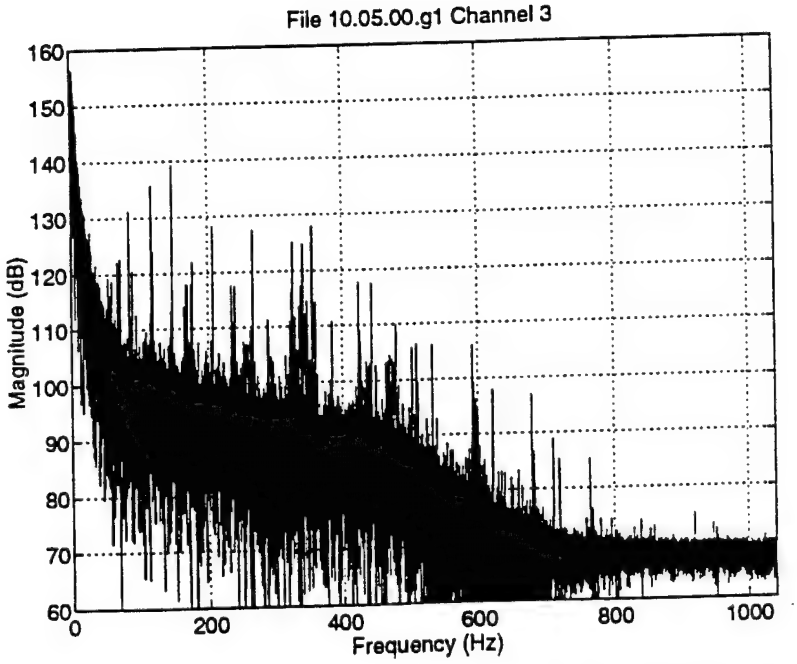


**Figure 6: Power spectral density plot of channel 3 of file 10.05.00.g1**

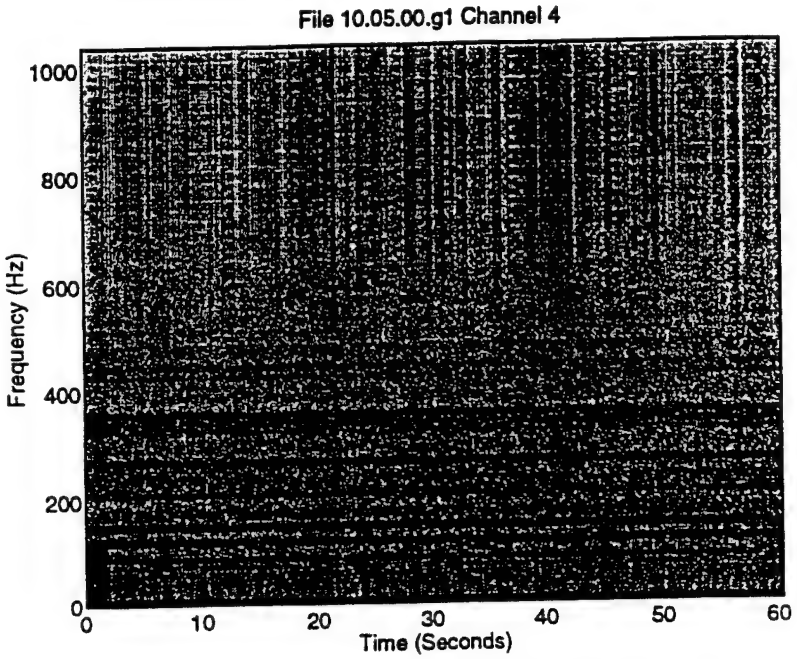


**Figure 7: Spectrogram of channel 4 of file 10.05.00.g1**

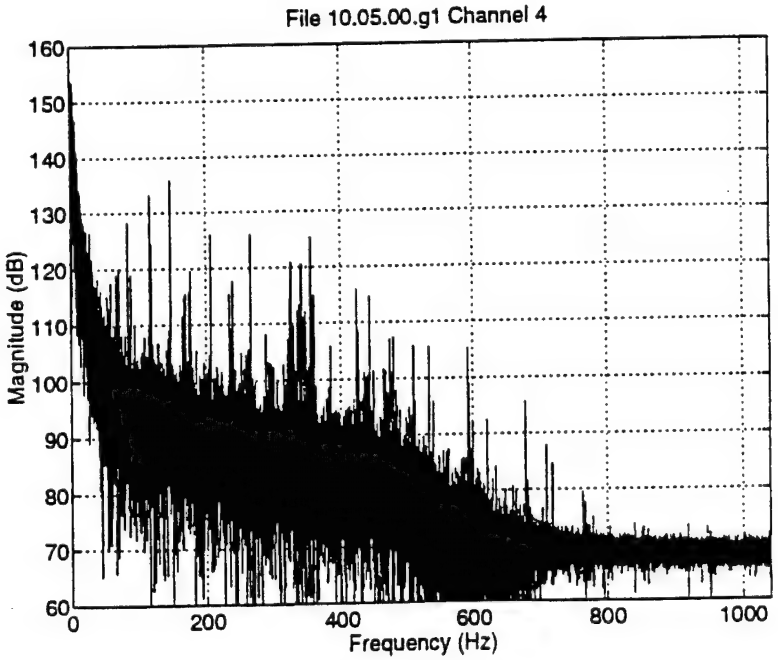


**Figure 8: Power spectral density plot of channel 4 of file 10.05.00.g1**

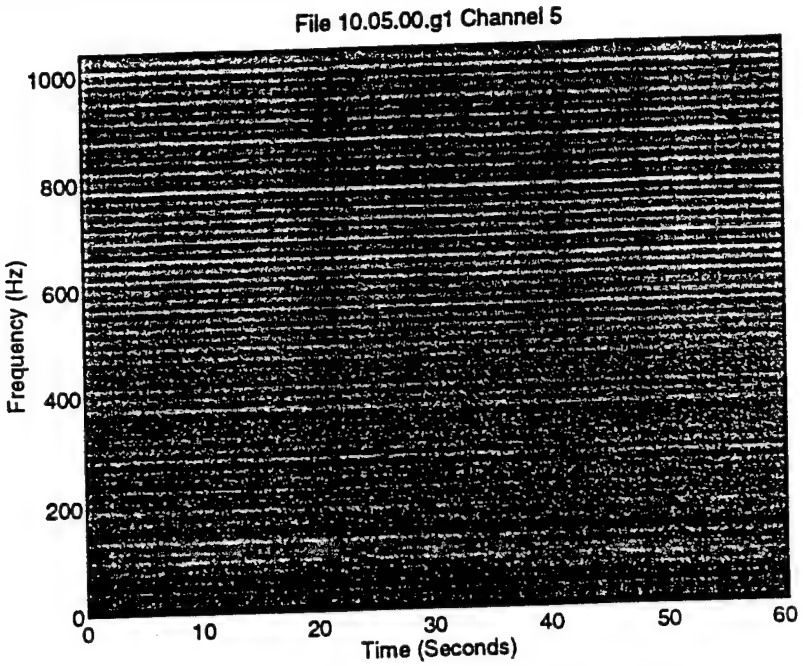


**Figure 9: Spectrogram of channel 5 of file 10.05.00.g1**

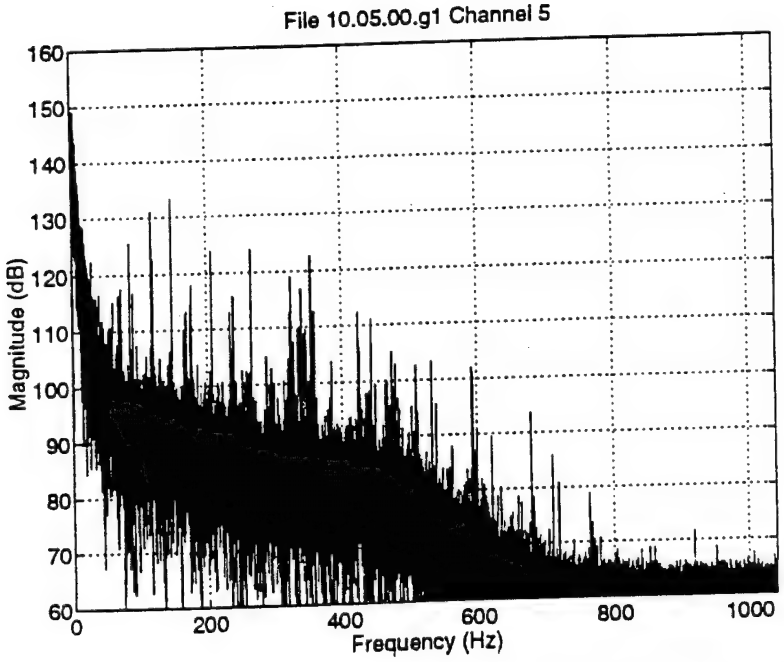


**Figure 10: Power spectral density plot of channel 5 of file 10.05.00.g1**

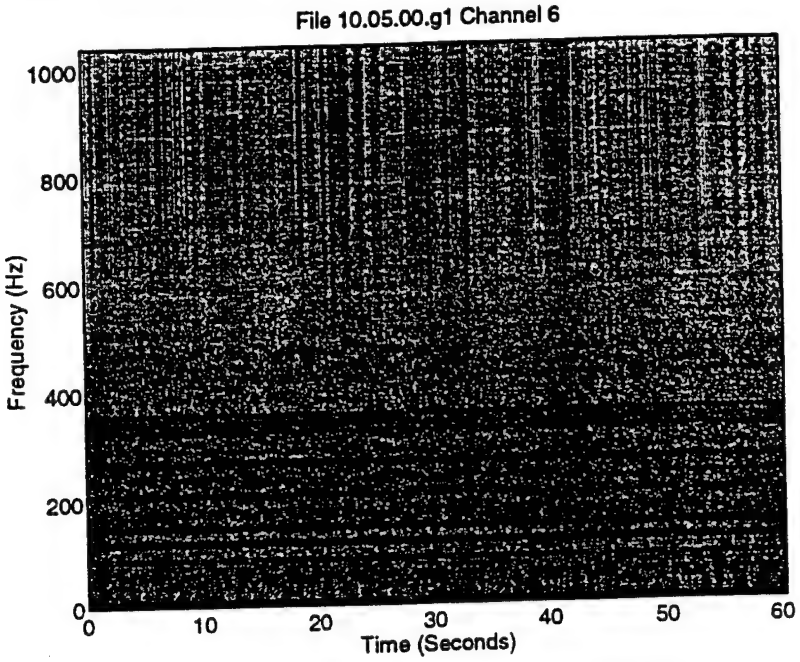


**Figure 11: Spectrogram of channel 6 of file 10.05.00.g1**

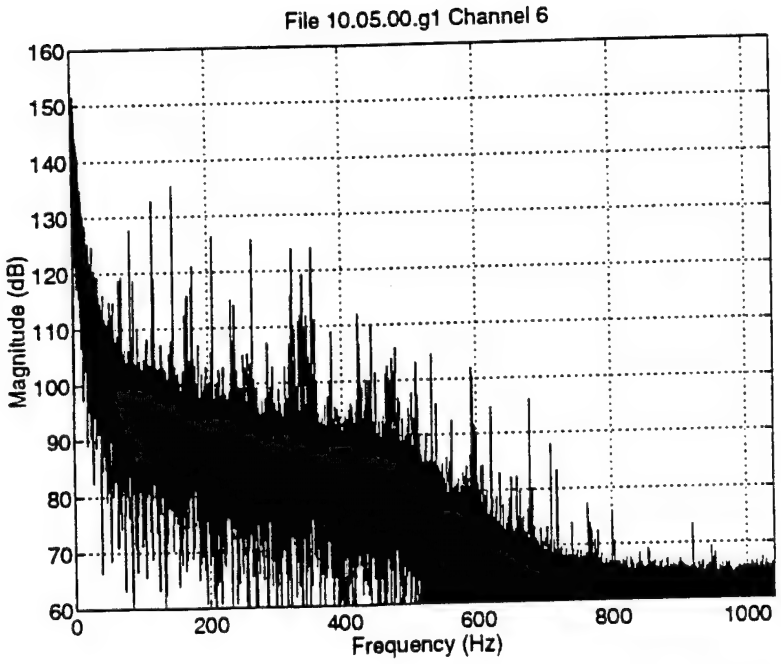


**Figure 12: Power spectral density plot of channel 6 of file 10.05.00.g1**

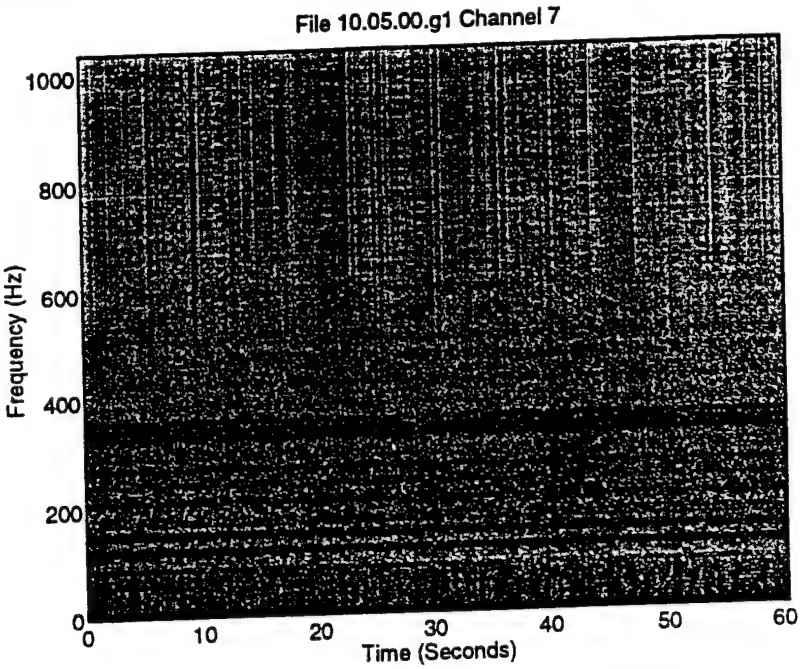


**Figure 13: Spectrogram of channel 7 of file 10.05.00.g1**

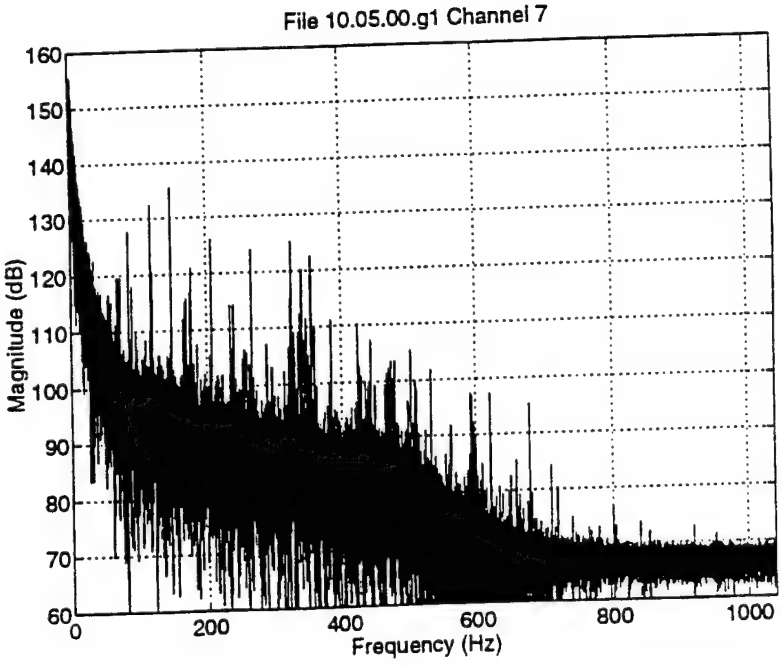


**Figure 14: Power spectral density plot of channel 7 of file 10.05.00.g1**

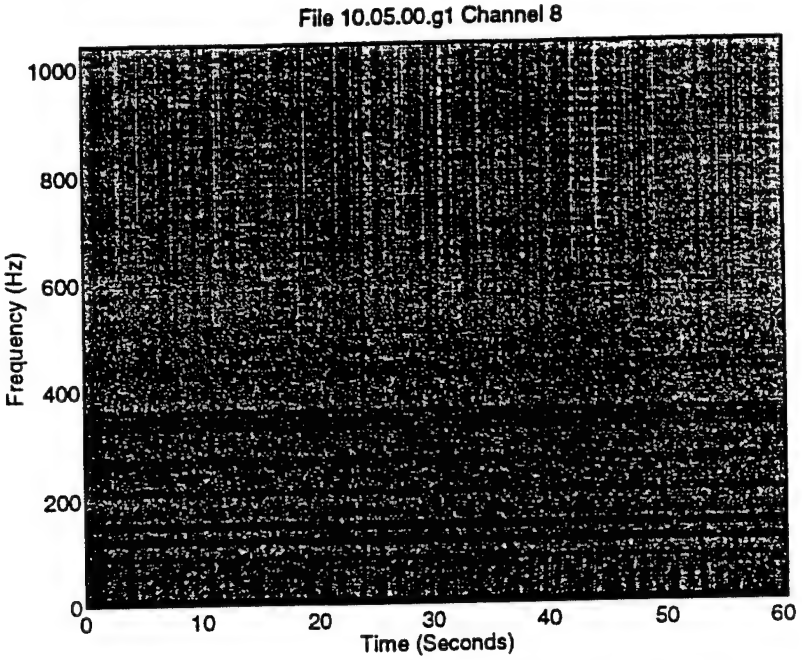


**Figure 15: Spectrogram of channel 8 of file 10.05.00.g1**

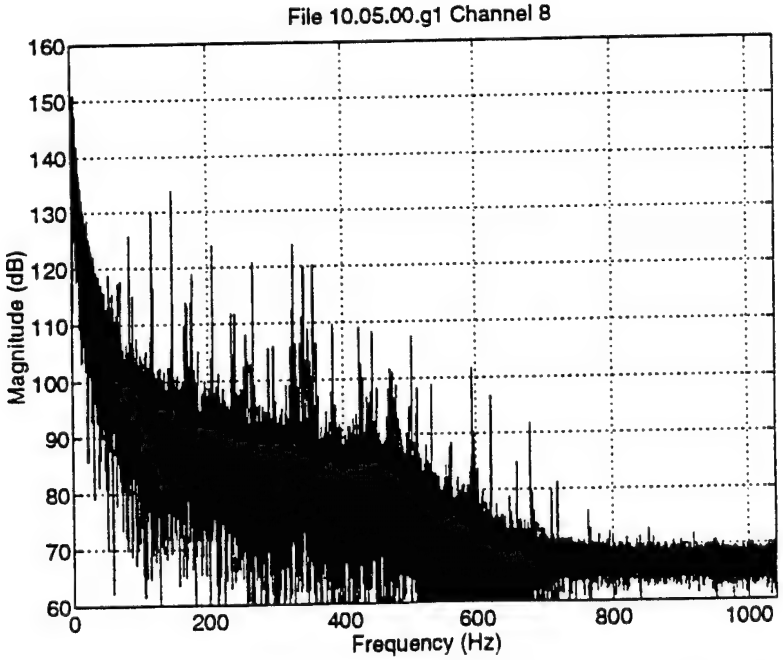


**Figure 16: Power spectral density plot of channel 8 of file 10.05.00.g1**

SPCOT

Edward C. Real

PTP2-A001

885-5147

FAX 885-0631

MEMO: October 1, 1993

TO: C. Myers

FROM: E. Real

RE: Plots from file 10.05.00.g1 of the NASA wind tunnel data - Channel 7

CC: S. Lang

This memo contains PSD plots from channel 7 of the NASA wind tunnel data outlined in the September 15 fax to Doug Mook from Henry Abarbanel of UC San Diego. The specifics of the data plotted are contained in the table below.

| Parameter | Value | Comments |
|---|---|---|
| File Name | 10.05.00.g1 | From NASA wind tunnel data accompanying above fax. |
| Data Creation Date | July 9, 1993 | As specified in the extracted tar file date stamp. |
| Data Creation Time | 15:26 | ibid. |
| Location Of Sensor Array | Front center of canopy | 6" diameter circular sensor array (see fax). |
| Channel Used For Sensor Output | 7 | As specified by C. Myers. There are 8 channels total. |
| Group # Used | 1 | ibid. |
| Sample Rate | 2083.33 Hz | As given in the fax mentioned above. |
| FFT size used in PSD computation | 2048 | Approximately 1 Hz resolution, and approximately 1 second of data. |
| Starting Data Point | 1 | Beginning of data set. |
| FIR filter order used | 15 | All prediction error plots. |

**Table 1: Data Specifics**

**Overview:**

A 15 tap FIR LS predictor filter was created in matlab (file lsfilter.m) and used to process the channel data for a variety of vector (d) and predictor (k) shifts. These values are outlined in table 2.

| Vector Shift (d) | Predictor Shift (k) |
|---|---|
| 1 | 1 |
| 130 | 130 |

**Table 2: Data Shifting Parameters**

The meaning of these parameters is defined in the following discussion.

The normal equations for the LS predictor are defined in equation 1.

$$\underbrace{\begin{bmatrix} x(n) & x(n-d) & \dots & x(n-(L-1)d) \\ x(n-1) & x(n-d-1) & \dots & x(n-(L-1)d-1) \\ x(n-2) & x(n-d-2) & \dots & x(n-(L-1)d-2) \\ \vdots & \vdots & \vdots & \vdots \end{bmatrix}}_{X} \underbrace{\begin{bmatrix} a_1 \\ a_2 \\ a_3 \\ \vdots \end{bmatrix}}_{a} = \underbrace{\begin{bmatrix} x(n+k) \\ x(n+k-1) \\ x(n+k-2) \\ \vdots \end{bmatrix}}_{x} \quad (1)$$

Where $x(n)$ is the n-th data point, $d$ is the vector shift parameter (defines the time shift between column vectors in $X$), $L$ is the number of taps in the FIR filter (15 in the cases presented here), $a$ is the tap coefficient vector, and $k$ is the predictor shift parameter (defines how far into the future that the prediction is to be made). The LS coefficients of the filter ($a$) are calculated via the Moore-Penrose inverse as in equation 2.

$$a = (X^H X)^{-1} X^H x \quad (2)$$

The error ($\varepsilon$) is then calculated as in equation 3

$$\varepsilon = x - Xa \quad (3)$$

## Case 1 - Original PSD:

The plot presented here is the (unweighted) power spectral density (PSD) of the first 2048 points of the data from channel 7. This was done to supply a basis for comparison with the other plots.

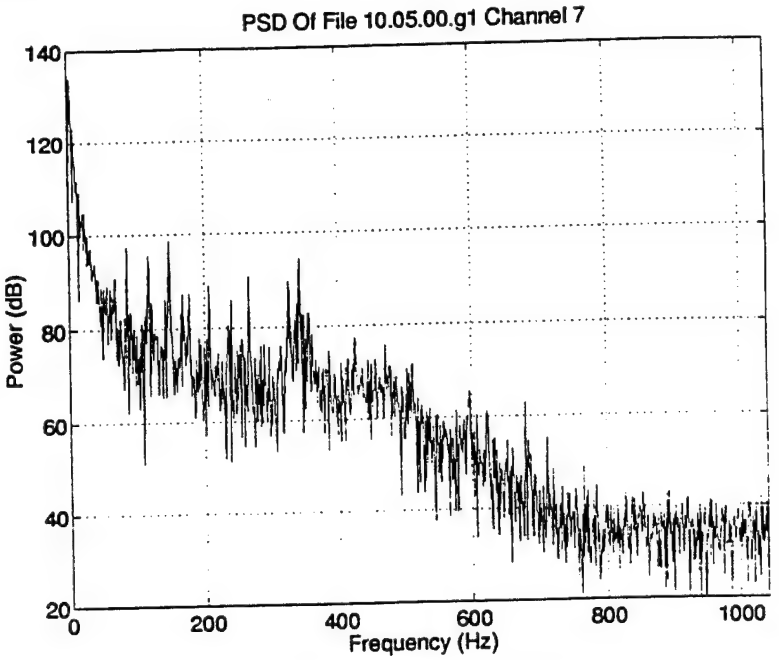


**Figure 1: PSD of first 2048 data points of channel 7 of file 10.05.00.g1**

**Case 2 - d = 1, k = 1:**

For this case a vector shift (d) and a predictor shift (k) of one were used. The plot here, and for all subsequent cases, represents the PSD of the first 2048 data points of the resulting error function (equation 3). The length of the column vectors of $X$ (number of rows) was 60,000 samples in all cases.

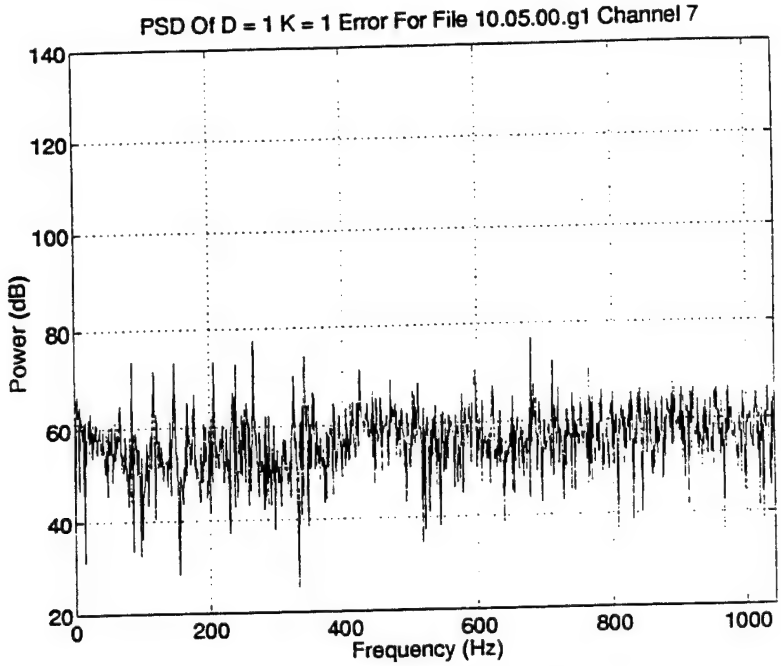


**Figure 2: PSD of error curve for parameters d = 1, k = 1.**

Case 3 - d = 1, k = 130

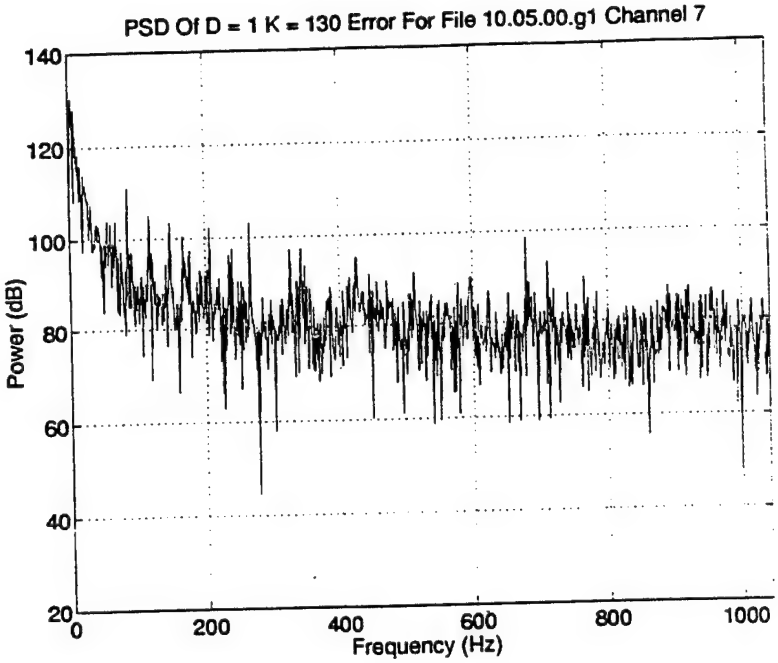


Figure 3: PSD of error curve for parameters d = 1, k = 130.

**Case 4 - d = 130, k = 1**

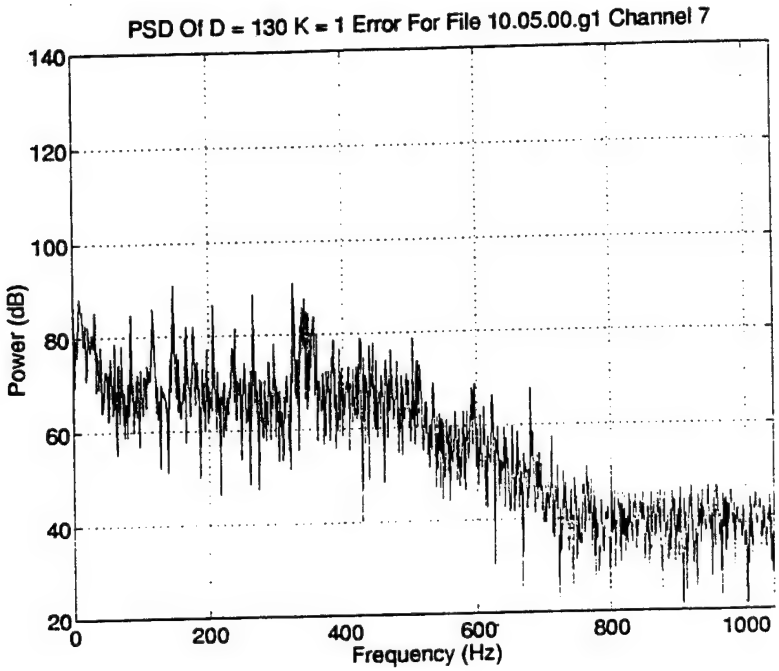


**Figure 4: PSD of error curve for parameters d = 130, k = 1.**

**Case 5 - d = 130, k = 130**

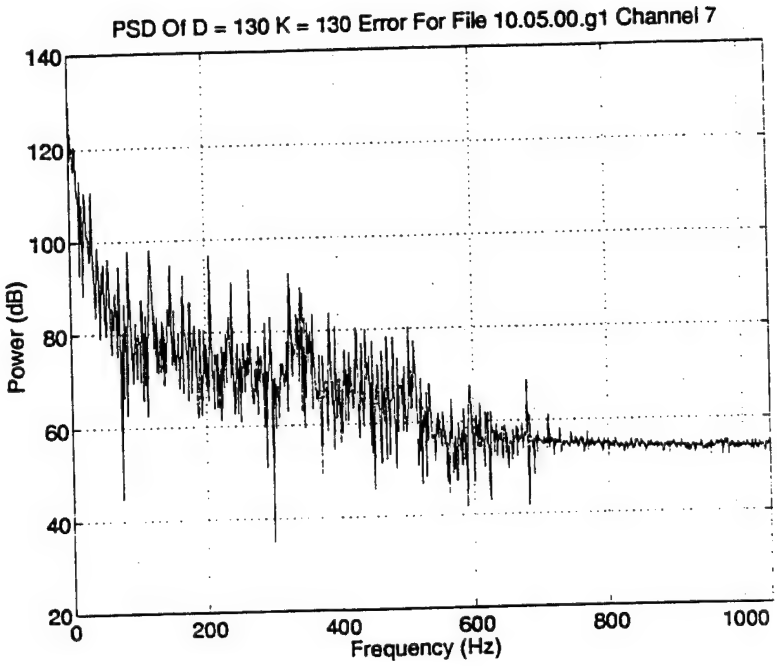


**Figure 5: PSD of error curve for parameters d = 130, k = 130.**

Ed.

SPCOT
Edward C. Real
PTP2-A001
885-5147
FAX 885-0631

MEMO: October 3, 1993

TO: C. Myers

FROM: E. Real

RE: Embedding dimension plots of residual error resulting from a 15 tap LS FIR filter.

CC: S. Lang

This memo contains percentage of joint false neighbor Vs. embedding dimension plots. This data was generated from residual error data resulting from a 15 tap least square (LS) FIR predictor filter (see October 1, 1993 memo to C. Myers from E. Real). The original data was taken from channel 7 of the NASA wind tunnel data outlined in the September 15 fax to Doug Mook from Henry Abarbanel of UC San Diego. The specifics of the data plotted are repeated in the table below for convenience. For more information on the LS filter used and the meaning of parameters, please see the October 1, 1993 memo.

| Parameter | Value | Comments |
|---|---|---|
| File Name | 10.05.00.g1 | From NASA wind tunnel data accompanying above fax. |
| Data Creation Date | July 9, 1993 | As specified in the extracted tar file date stamp. |
| Data Creation Time | 15:26 | ibid. |
| Location Of Sensor Array | Front center of canopy | 6" diameter circular sensor array (see fax). |
| Channel Used For Sensor Output | 7 | As specified by C. Myers. There are 8 channels total. |
| Group # Used | 1 | ibid. |
| Sample Rate | 2083.33 Hz | As given in the fax mentioned above. |
| FFT size used in PSD computation | 2048 | Approximately 1 Hz resolution. and approximately 1 second of data. |
| Starting Data Point | 1 | Beginning of data set. |
| FIR filter order used | 15 | All prediction error plots. |

**Table 1: Data Specifics**

**Embedding Dimension Plot for d = 1, k = 1:**

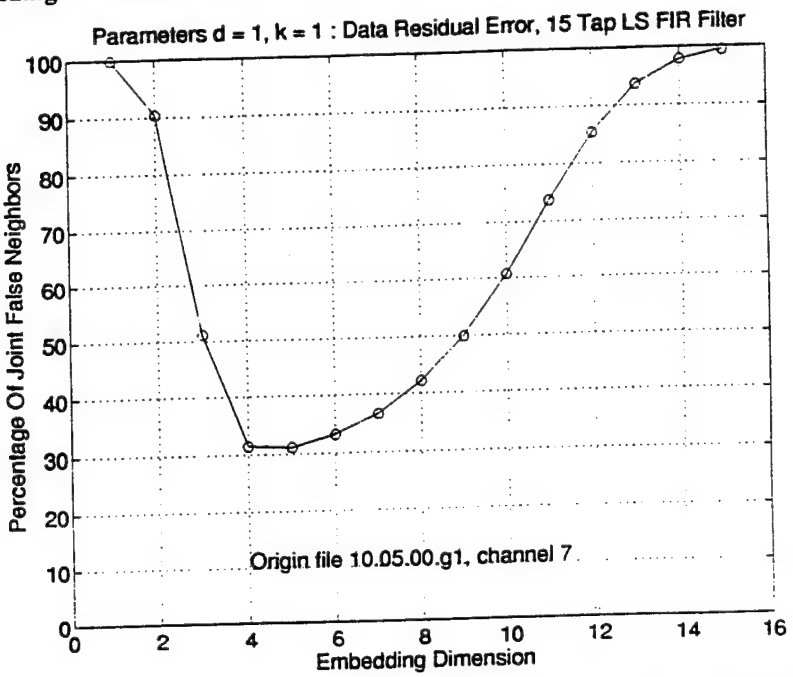


**Figure 1: Percentage Of Joint False Neighbors Vs. Embedding Dimension Vector Shift (d) = 1 Predictor Shift (k) = 1**

**Embedding Dimension Plot for d = 1, k = 130**

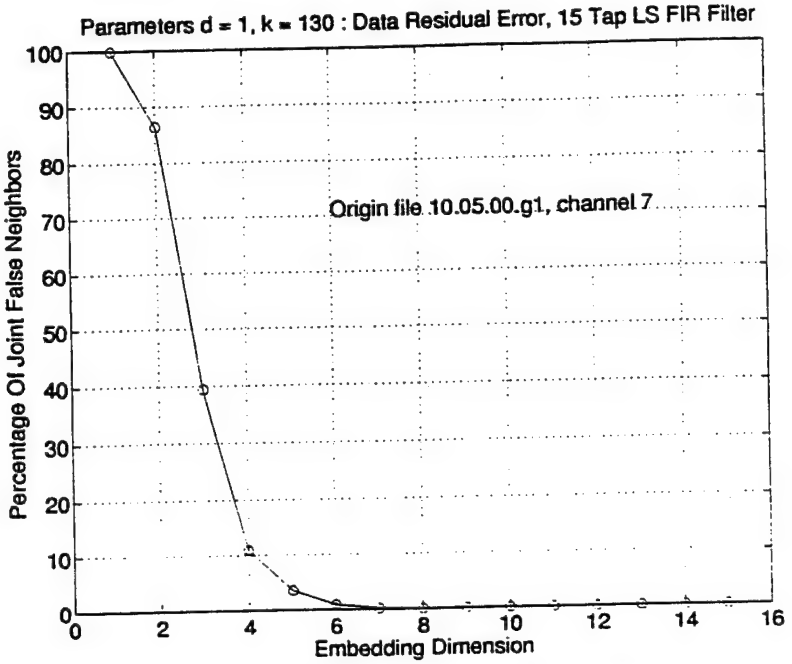


**Figure 2: Percentage Of Joint False Neighbors Vs. Embedding Dimension Vector Shift (d) = 1 Predictor Shift (k) = 130**

## Embedding Dimension Plot for d = 130, k = 1

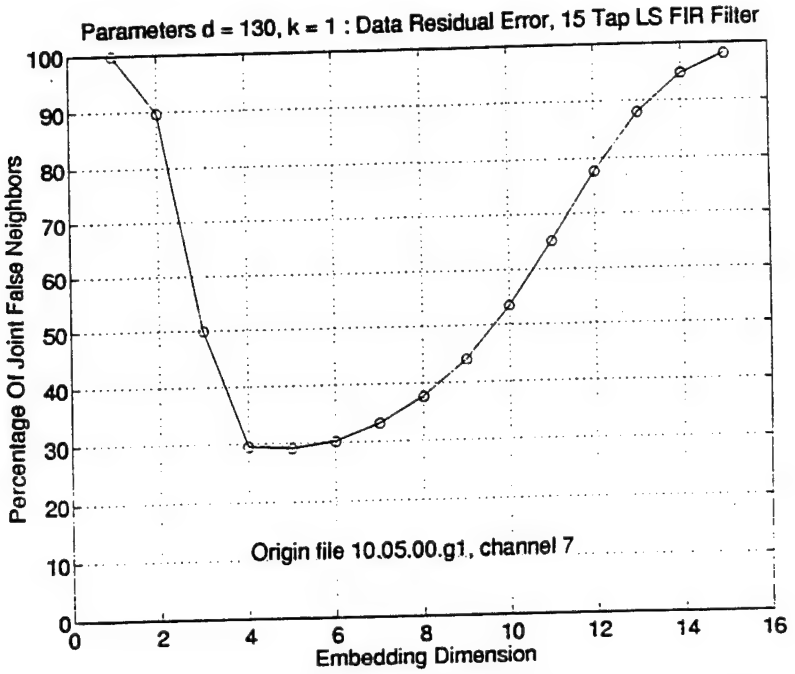


**Figure 3: Percentage Of Joint False Neighbors Vs. Embedding Dimension Vector Shift (d) = 130 Predictor Shift (k) = 1**

**Embedding Dimension Plot for d = 130, k = 130**

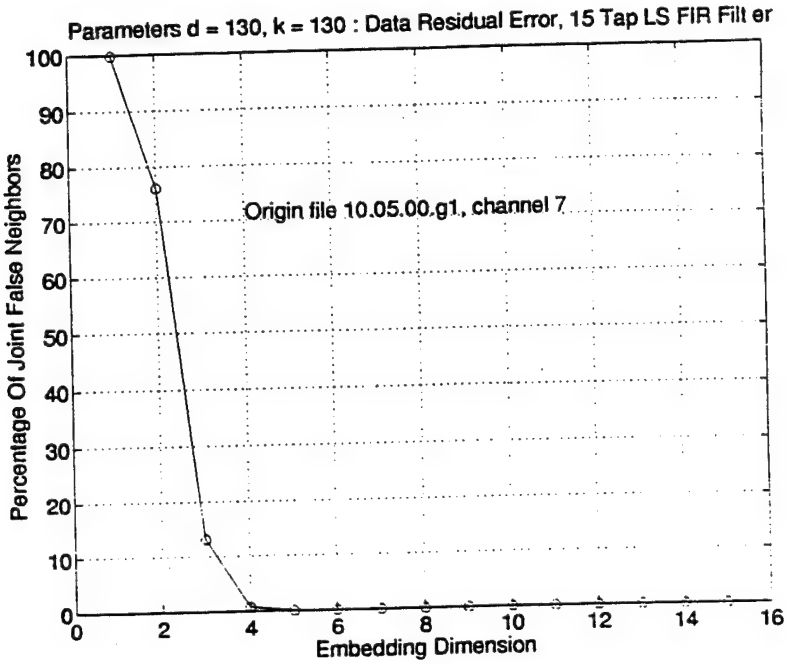


**Figure 4: Percentage Of Joint False Neighbors Vs. Embedding Dimension Vector Shift (d) = 130 Predictor Shift (k) = 130**

Ed.

SPCOT
Edward C. Real
PTP2-A001
885-5147
FAX 885-0631

MEMO: October 6, 1993

TO: C. Myers

FROM: E. Real

RE: PSD plots of residual error resulting from a 1 tap LS FIR filter.

CC: S. Lang

This memo shows residual error PSD plots resulting from a 1 tap least square (LS) FIR predictor filter (see October 1, 1993 memo to C. Myers from E. Real). The original data was taken from channel 7 of the NASA wind tunnel data outlined in the September 15 fax to Doug Mook from Henry Abarbanel of UC San Diego. The specifics of the data plotted are repeated in the table below for convenience. For more information on the LS filter

| Parameter | Value | Comments |
|---|---|---|
| File Name | 10.05.00.g1 | From NASA wind tunnel data accompanying above fax. |
| Data Creation Date | July 9, 1993 | As specified in the extracted tar file date stamp. |
| Data Creation Time | 15:26 | ibid. |
| Location Of Sensor Array | Front center of canopy | 6" diameter circular sensor array (see fax). |
| Channel Used For Sensor Output | 7 | As specified by C. Myers. There are 8 channels total. |
| Group # Used | 1 | ibid. |
| Sample Rate | 2083.33 Hz | As given in the fax mentioned above. |
| FFT size used in PSD computation | 2048 | Approximately 1 Hz resolution, and approximately 1 second of data. |
| Starting Data Point | 1 | Beginning of data set. |
| FIR filter order used | 1 | All prediction error plots. |

Table 1: Data Specifics

used and the meaning of parameters, please see the October 1, 1993 memo.

**PSD plot of original (unprocessed) data:**

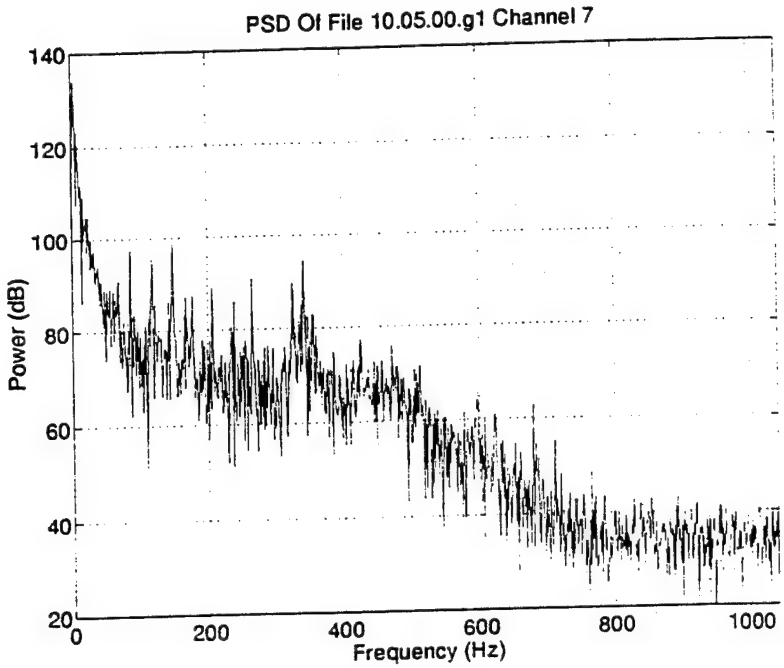


Figure 1: PSD of data from file 10.05.00.g1. channel 7

**PSD Plot for d = 1, k = 1**

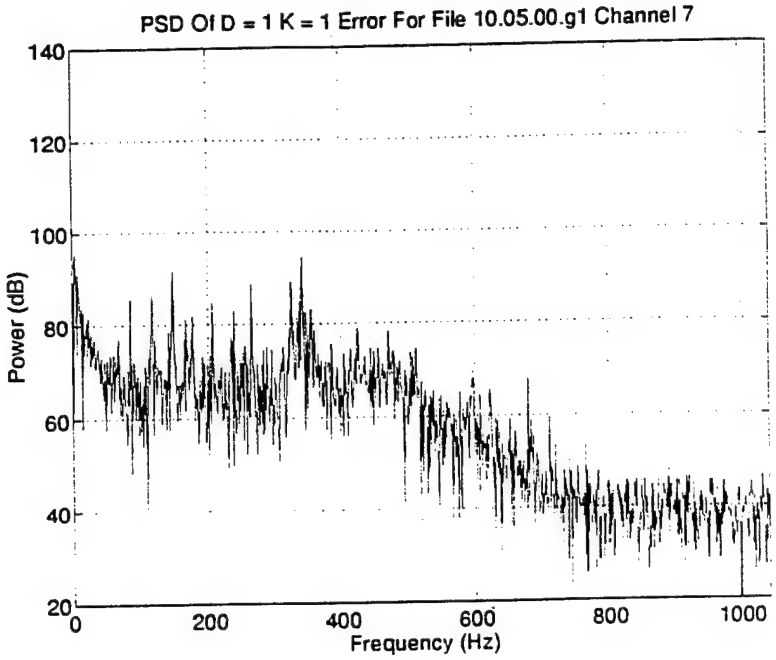


**Figure 2: PSD of residual error resulting from a 1 tap FIR filter Vector Shift (d) = 1 Predictor Shift (k) = 1**

**PSD Plot for d = 1, k = 130**

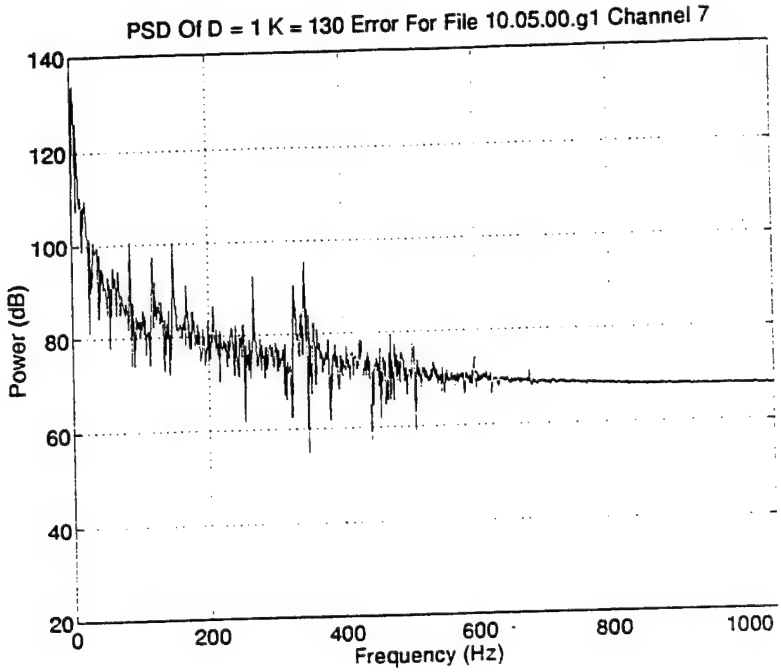


**Figure 3: PSD of residual error resulting from a 1 tap FIR filter Vector Shift (d) = 1 Predictor Shift (k) = 130**

**PSD Plot for d = 130, k = 1**

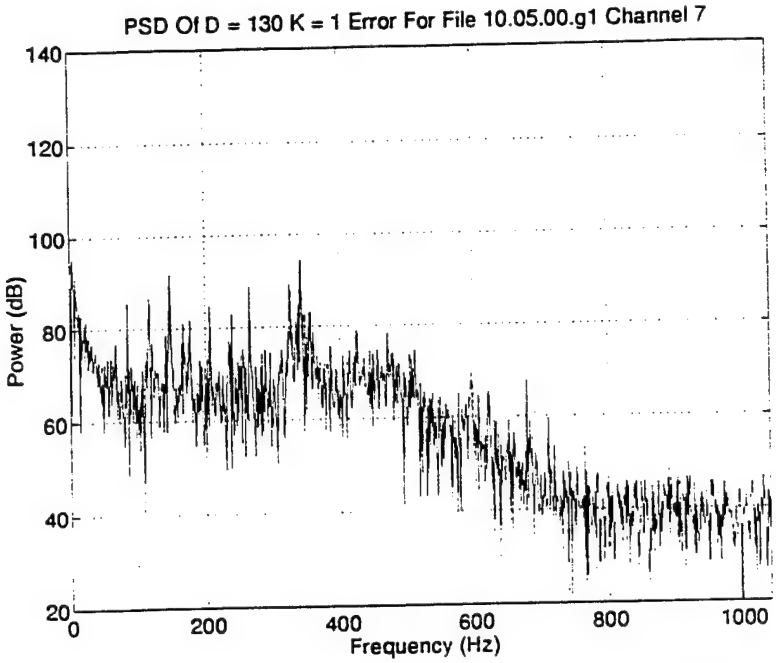


**Figure 4: PSD of residual error resulting from a 1 tap FIR filter Vector Shift (d) = 130 Predictor Shift (k) = 1**

**PSD Plot for d = 130, k = 130**

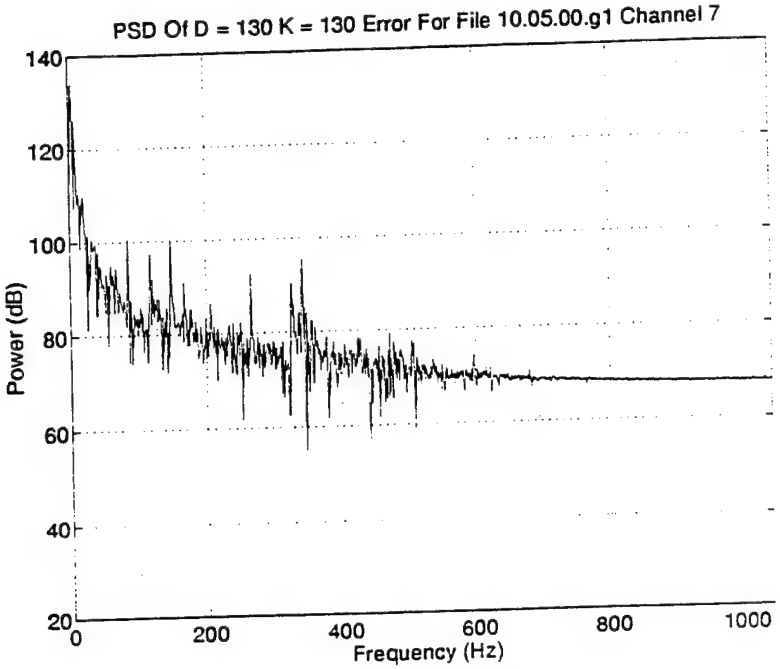


**Figure 5: PSD of residual error resulting from a 1 tap FIR filter Vector Shift (d) = 130 Predictor Shift (k) = 130**

Ed.

**SPCOT**

Edward C. Real

PTP2-A001

885-5147

FAX 885-0631

MEMO: October 7, 1993

TO: C. Myers

FROM: E. Real

RE: Embedding dimension plots of residual error resulting from a 1 tap LS FIR filter.

CC: S. Lang, W. Mistretta

This memo contains percentage of joint false neighbor Vs. embedding dimension plots. This data was generated from residual error data resulting from a 1 tap least square (LS) FIR predictor filter (see October 1, 1993 memo to C. Myers from E. Real). The original data was taken from channel 7 of the NASA wind tunnel data outlined in the September 15 fax to Doug Mook from Henry Abarbanel of UC San Diego. The specifics of the data plotted are repeated in the table below for convenience. For more information on the LS filter used and the meaning of parameters, please see the October 1, 1993 memo.

| Parameter | Value | Comments |
|---|---|---|
| File Name | 10.05.00.g1 | From NASA wind tunnel data accompanying above fax. |
| Data Creation Date | July 9, 1993 | As specified in the extracted tar file date stamp. |
| Data Creation Time | 15:26 | ibid. |
| Location Of Sensor Array | Front center of canopy | 6" diameter circular sensor array (see fax). |
| Channel Used For Sensor Output | 7 | As specified by C. Myers. There are 8 channels total. |
| Group # Used | 1 | ibid. |
| Sample Rate | 2083.33 Hz | As given in the fax mentioned above. |
| FFT size used in PSD computation | 2048 | Approximately 1 Hz resolution, and approximately 1 second of data. |
| Starting Data Point | 1 | Beginning of data set. |
| FIR filter order used | 1 | All prediction error plots. |

Table 1: Data Specifics

Note that for the single tap filter the vector shift parameter (d) is irrelevant since the data matrix contains only a single column. However, plots for the d = 1 and d = 130 case are included for completeness.

**Embedding Dimension Plot for d = 1, k = 1:**

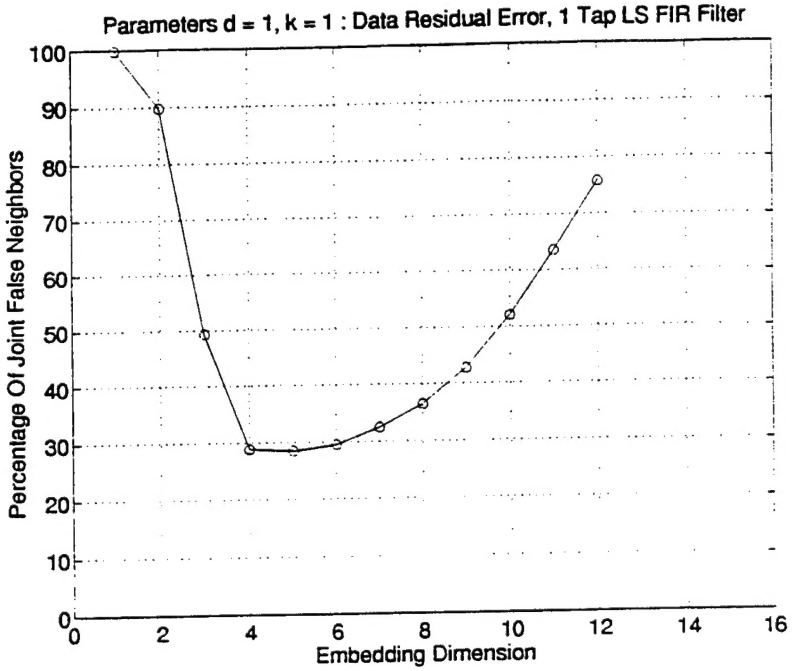


**Figure 1: Percentage Of Joint False Neighbors Vs. Embedding Dimension Vector Shift (d) = 1 Predictor Shift (k) = 1**

## Embedding Dimension Plot for d = 1, k = 130

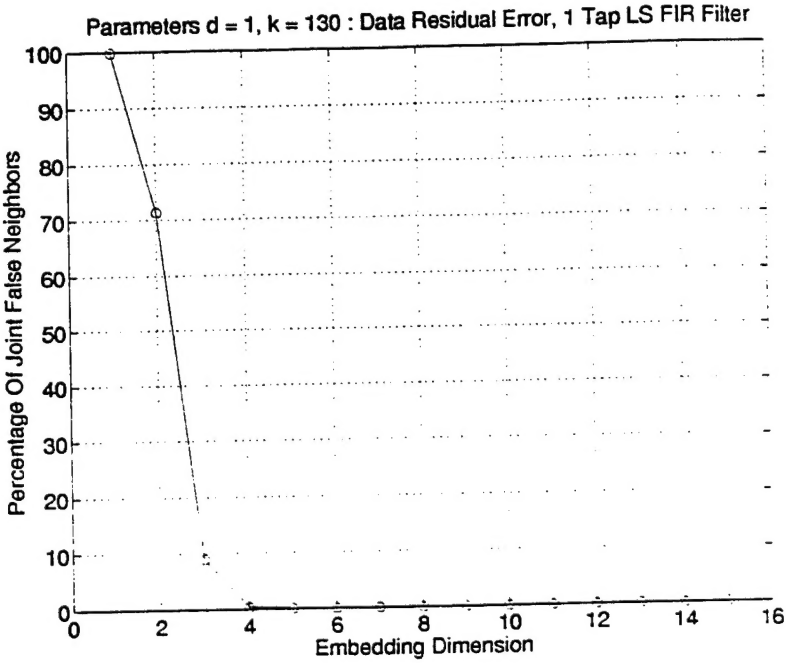


**Figure 2: Percentage Of Joint False Neighbors Vs. Embedding Dimension Vector Shift (d) = 1 Predictor Shift (k) = 130**

## Embedding Dimension Plot for d = 130, k = 1

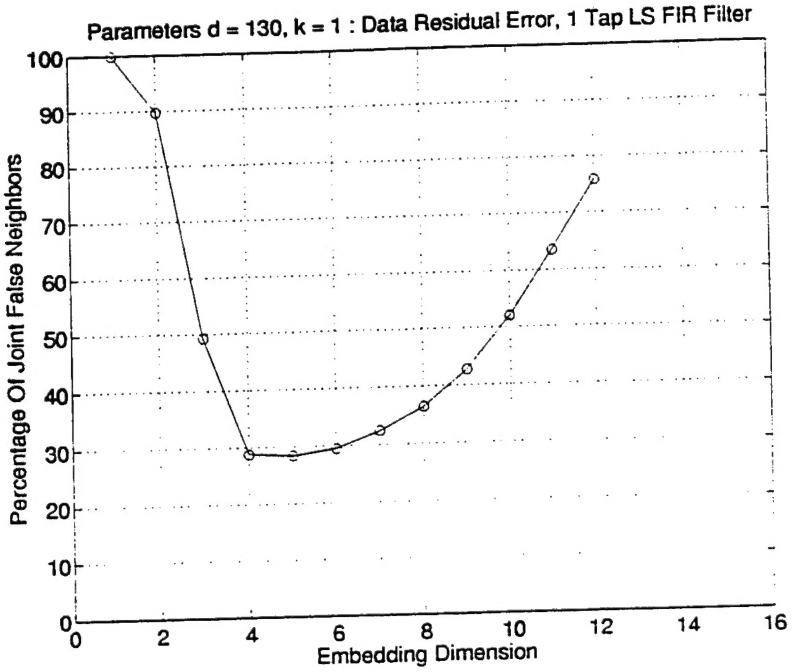


**Figure 3: Percentage Of Joint False Neighbors Vs. Embedding Dimension Vector Shift (d) = 130 Predictor Shift (k) = 1**

**Embedding Dimension Plot for d = 130, k = 130**

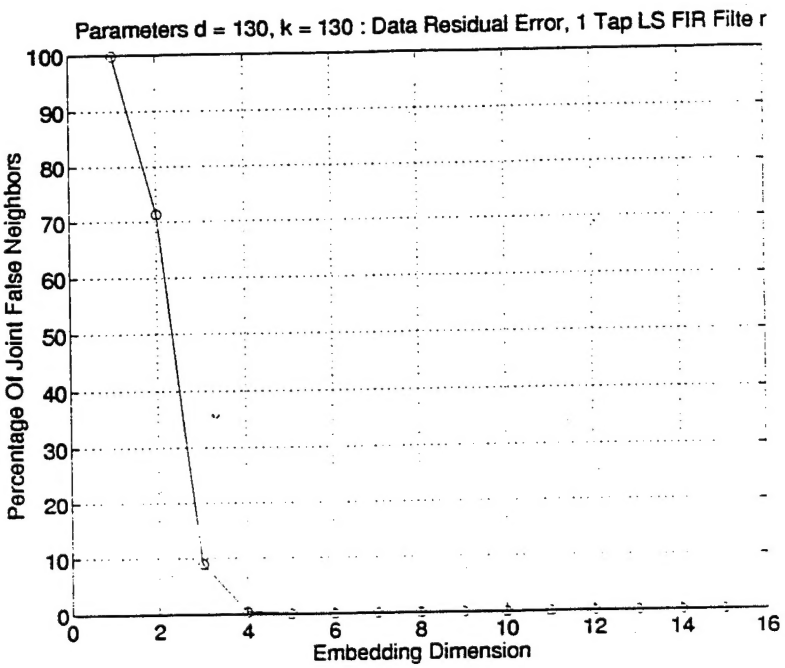


**Figure 4: Percentage Of Joint False Neighbors Vs. Embedding Dimension Vector Shift (d) = 130 Predictor Shift (k) = 130**

Ed.